# SEISMIC ANISOTROPY IN THE SURFACE LAYERS OF THE ROSS ICE SHELF, ANTARCTICA

By

James L. Fuchs

A THESIS

Submitted to
Michigan State University
in partial fulfillment of the requirements
for the degree of

MASTER OF SCIENCE

Department of Geology

1989

## ABSTRACT

# SEISMIC ANISOTROPY IN THE SURFACE LAYERS OF THE ROSS ICE SHELF, ANTARCTICA

By

James L. Fuchs

Seismic refraction surveys from the Ross Ice Shelf, Antarctica, are analyzed for the purpose of studying the effects of the near surface layering on the propagation of seismic waves.

Velocity anisotropy is observed for three types of seismic waves. The best indication of this anisotropy are the patterns which develop in the velocity surfaces with increasing depth. The correlation between energy radiation plots and the velocity surfaces add support to the presence of anisotropy.

A theoretical model, based on observable surface features of the study area, is developed and shown to be transversely isotropic. The transverse isotropy of the surface layers in the study area appears to be a form of structural anisotropy. This structural anisotropy is attributed to the interlayering of north-south oriented sastrugi and snow in the study area.

ACKNOWLEDGEMENTS

Special thanks are owed to Dr. Hugh Bennett for suggesting the idea behind this study, helping to see it through, and for braving Antarctic weather to obtain the data.

Many thanks are due to the following people and groups for the assistance provided:

To Mark Schoomaker for his invaluable computer programs and suggestions.

To Dr. Wilband for his aid in using the computer system and for serving on the thesis committee.

To Dr. Larson for his help with reference material and for also serving on the thesis committee.

To Dr. Fujita for helping critique thesis drafts.

To the National Science Foundation for providing the funds used to collect the data and support the research.

To my wife and parents who always supported my efforts to pursue an education.

TABLE OF CONTENTS

LIST OF TABLES

## LIST OF FIGURES

# Chapter 1

## INTRODUCTION

The purpose of this study is to determine if seismic anisotropy is present in the near surface layers of the Ross Ice Shelf, and to compare this anisotropy to the velocity anisotropy observed in deeper zones of the Ross Ice Shelf (Wanslow, 1981; Bennett et al., 1978; Bennett et al., 1979). A theory is developed to explain the anisotropy of the near surface layers.

In seismic exploration surveys it is usually assumed that the material through which seismic waves propagate is isotropic. However, it has been demonstrated by several authors that many surface rocks are anisotropic to some extent (Hagedoorn, 1954; Cholet & Richard, 1954; Uhrig & Van Melle, 1955; Krey & Helbig, 1956; Buchwald, 1959; Anderson, 1961; Backus, 1962; Sato & Lapwood, 1968; Nur & Simmons, 1969; Crampin, 1970; Nur, 1971; Tillman & Bennett, 1973; Daley & Hron, 1977; Crampin, 1977; Crampin & Bamford, 1977; Keith & Crampin, 1977; Crampin, 1978; Levin, 1978; Berryman, 1979).

The behavior of seismic waves in anisotropic material varies with the direction of propagation.

Variation of velocity is one of the anomalies associated with anisotropic material. Furthermore, the variation of velocity with direction must exhibit centrosymmetry if the material is anisotropic, since it is directly related to the effective elastic constants in a crystalline symmetry (Crampin, et al., 1977).

Anisotropy in its purest form is exhibited in single crystals (Anderson, 1961). In a seismic survey fairly uniform material would be best suited for the purpose of a detailed study of velocity anisotropy (Bennett, 1968). The Ross Ice Shelf provides a simple, monomineralic material in which to conduct this study. Anisotropy of ice has been verified in several studies (Bennett, 1968; Dewart, 1968; Bentley, 1972; Bennett et al., 1978,1979).

It is suspected that the near surface layers in the study area may exhibit some form of anisotropy due to observation of abundant sastrugi on the surface. Sastrugi are surface features that are observed on many ice shelfs throughout the world. They are wavelike ridges of extremely hard snow which are formed on a level surface by the action of the wind, and with axes parallel to the wind direction.

The seismic refraction method is used in this study since the reflection method can only be used to determine an average velocity for the entire thickness of the ice shelf. The refraction method yields a more detailed

velocity analysis.

In other studies anisotropy has been more apparent for shear waves than for compressional waves (Jolly, 1956; Levin, 1979). Therefore, it was expected that shear waves would yield the best results for analysis of anisotropy in this study also.

## Chapter 2

## LOCATION AND PARAMETERS OF STUDY AREA

The study area is located 18 kilometers due east of Minna Bluff, Antarctica, on the Ross Ice Shelf (78.40 N latitude, 167.10 E longitude) (Figure 1).

The area was chosen to test the effects of the shear zone, created by the movement of the ice shelf against Minna Bluff, on seismic wave propagation. The study area was located far enough east of Minna Bluff in an attempt to avoid zones of fractures near Minna Bluff. It has been shown that fractures can cause anisotropy (Nur, 1971)

The Ross Ice Shelf was discovered by Sir James Ross in 1841. It is the largest single sheet of floating ice in the world, comprising approximately 525,000 square kilometers. The ice shelf flows northward at an estimated rate of .2 - 1.5 kilometers per year. The ice shelf moves in response to the annual net accumulation of snow on the ice shelf itself, and to the flow of ice from the interior of the continent (Crary et al., 1962).

Sastrugi are observed at many places on the Ross Ice Shelf. The elongations of the sastrugi are predominantly north-south or northeast-southwest, and they are much more

pronounced near Minna Bluff than other areas of the shelf (Crary et al., 1962). The study area contained abundant north-south oriented ridges of sastrugi on the surface, with snow or hoarefrost between the hardened ridges (Communication with Dr. H.F. Bennett).

The annual snow accumulation is estimated at 20-23 centimeters. The density of the upper ten meters of the ice shelf ranges from 0.40 to 0.55 grams per cubic centimeter. The thickness of the ice shelf ranges from 250 to 700 meters. In the study area the shelf is approximately 320 meters thick as determined from reflection arrivals from the ice-water interface (Crary et al., 1962).

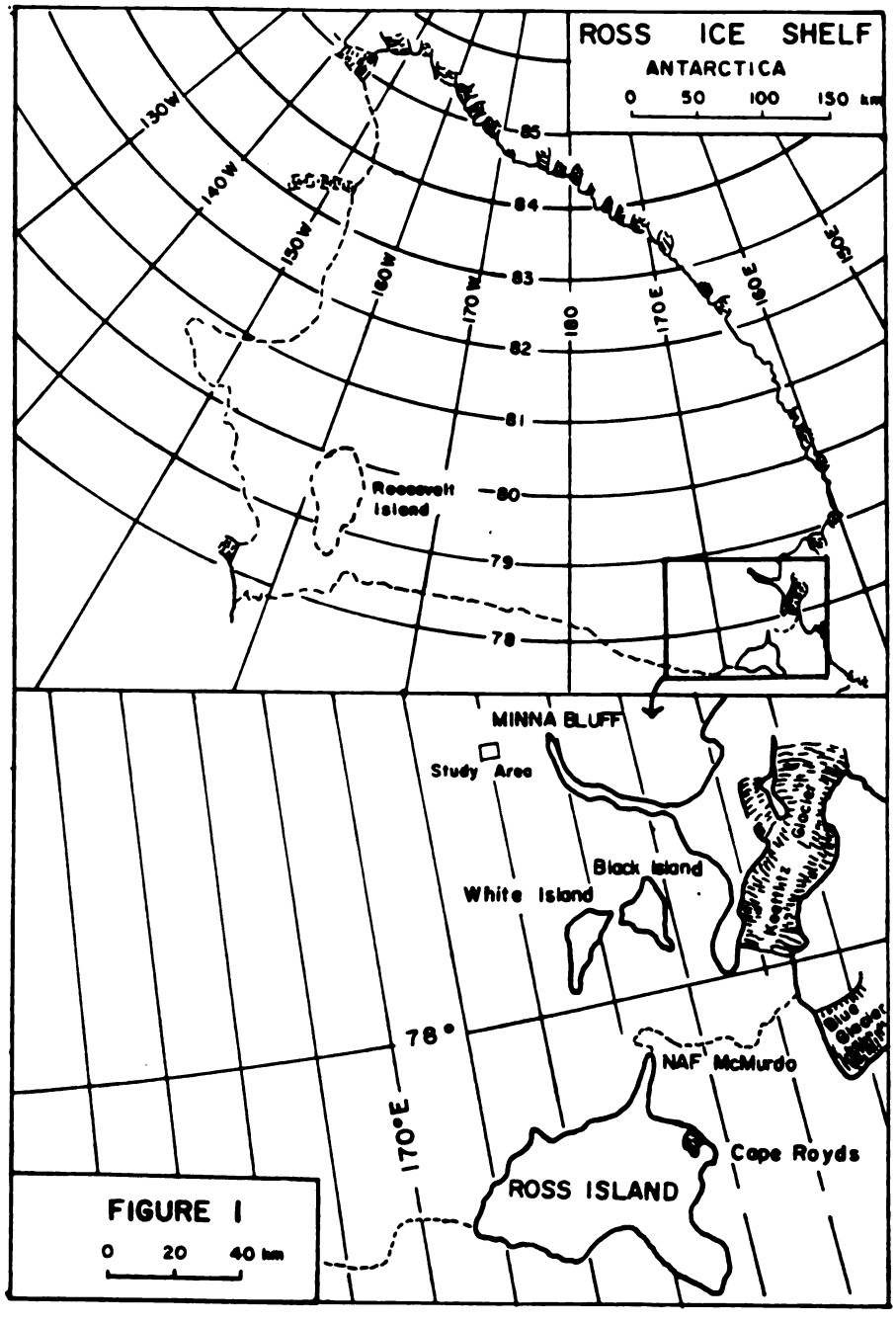


FIGURE 1: Map of the study area on the Ross Ice Shelf, Antarctica.

# Chapter 3

# FIELD METHODS

The seismic surveys were conducted by Bennett and others in the 1976-1977 austral summer. Compressional seismic waves (P waves) and two types of shear seismic waves (SH & SV waves) were generated and recorded. The format of the data consists of 24 traces that are digitally recorded on magnetic tape at a sampling interval of 2.083 milliseconds. This odd sampling interval is used because the maximum sampling rate of the equipment was 480 samples per second. The Nyquist frequency for the maximum sample rate is 240 Hertz. Recorded gains and filtering were controlled by analog amplifiers.

The data can be divided into two distinct sets of seismic lines. The first set are the long spread lines, which have source to geophone offsets ranging from 50 to 3300 feet. The second set are the short spread lines, which have offsets from 5 to 100 feet.

The long spread lines were used primarily for analysis of the deeper zones of the ice shelf. Since these were analyzed by others (Bennett, 1978,1979; Wanslow, 1981) further discussion will only consider the results of these analyses.

The short spread lines were used to analyze the near surface layers of the study area. The lines consist of 24 geophones that are divided into two sets of 12 geophones each. The two sets of geophones were oriented at an angle of 45 degrees to each other. The spacings of each group of 12 geophones were as follows: 5, 10, 15, 20, 30, 40, 50, 60, 70, 80, 90, and 100 feet, from source to receiver. Initially the spread was arranged with one set of 12 geophones oriented east-west (000), and the other set of 12 geophones oriented northeast-southwest (045). Separate events were then recorded for each type of seismic wave. The two sets of geophones were then rotated 45 degrees counterclockwise to obtain lines oriented north-south (090) and northeast-southwest (045). This procedure was repeated once more such that the final position of the spread was one set oriented north-south (090), and one set oriented northwest-southeast (135).

The source for the short spread data was a hammer and board. As a P wave source the hammer was manipulated so that it struck the board vertically, or perpendicular to the surface of the ground. As a shear wave source the hammer was manipulated so that it struck the board horizontally, or parallel to the ground. The orientation of the board was important for the SH and SV waves. The board was oriented such that first motions were parallel to the direction of the seismic line for SV waves, and perpendicular

to the direction of the seismic line for SH waves. Shear waves of opposite polarity were produced by changing the direction of the hammer blow by 180 degrees.

The orientation of the geophones for P waves is relatively unimportant as long as they are approximately vertical to the ground. However, the orientation of geophones for shear waves is extremely important in order to record the proper arrival with a significant amplitude. The geophones must always be oriented such that the plane which defines the movement of the coil within the geophone is parallel to the particle motion of the seismic wave. For SH waves the geophones were oriented in a way that they would detect the horizontal component of motion perpendicular to the azimuth of the seismic line. For the SV waves the geophones were oriented to detect the horizontal component of motion parallel to the azimuth of the seismic line.

# Chapter 4

## ANALYSIS METHODS

A series of computer programs developed by Mark Schoomaker are used to facilitate analysis of the data. The raw seismic data is stored on two nine track magnetic tapes (VRN-6746, VRN-6770) in the Michigan State University Computer Tape Library.

Separate events were removed from the main data tapes using the program Datasetup. The initial step was to make plots of the event using the program Pitasource. These plots are essentially the uninterpreted seismic records. Arrival times for each geophone can then be picked visually from the plots, and these arrival times are in turn plotted on time versus distance graphs.

Velocities were determined for the time picks by use of various curve fitting methods. The inverse of the slope of a particular portion of the curve is used to indicate the cross spread velocity. The methods of fitting various curves to the data will be discussed further in the data analysis section.

Depths of penetration were determined from the velocities and distances by use of the Wiechert, Herglotz, Bateman integral (Slichter, 1932; Officer, 1958).

Subsequent plots of the velocity surfaces at various depths are used to determine if velocity patterns are developing with increasing depth of penetration.

The programs Processor and Finale were used to determine energy radiation patterns. Processor is used interactively at a Tektronix terminal to extract various waveforms from individual traces of a specific event. Finale performs a fast Fourier transform on the extracted waveform, normalizes all waveforms of one event to a specified gain, plots the amplitude and phase spectrum for each waveform, and integrates the amplitude spectrum of the waveform within a given frequency range. The integrated values of each trace for one event are then normalized with respect to other events such that energy versus direction at a given distance can be compared.

# Chapter 5

# DATA ANALYSIS

## TIME PICKS

Time picks for P, SH, and SV waves from the short spread lines are listed in Appendix I, Tables 1-5. The tables for the SH and SV waves indicate picks were made for sources of opposite polarities. Therefore, there are two tables at each direction for each type of shear wave. The first refraction arrival is picked for all modes of seismic waves.

Time picks for the P waves (Table 1) were made from seismic records using vertically oriented geophones. The "first break" of the seismic trace is picked, and the first motion is always in the upward direction.

Time picks for the SH waves were made from seismic records using horizontally oriented geophones that were perpendicular to the seismic line. The "first break" of the seismic trace is again picked, as in the P wave records. However, one set of lines has the "first breaks" of the seismic traces in the upward direction, and the other set of lines has the "first breaks" in the downward direction. This is due to the reversal of source polarity. Seismic lines with "first breaks" in the upward direction

are denoted as having a positive (+) source (Table 2). Seismic lines with "first breaks" in the downward direction are denoted as having a negative (-) source (Table 3).

Time picks for the SV waves were made from seismic records using horizontally oriented geophones that were parallel to the azimuth of the seismic line. The SV wave events can be divided into two sets of seismic lines that had sources of opposite polarities. As in the case of the SH waves events with "first breaks" in the upward direction are denoted as having a positive (+) source (Table 4), and events with "first breaks" in the downward direction are denoted as having a negative source (-) (Table 5). There is no data listed for the SV(+) 135 degree direction seismic line because that event could not be located on the main data tapes.

## CURVE FITTING

Several methods of curve fitting were used to obtain velocities from the time distance data of the previous section. The two methods that gave the best results were a log curve and a power curve, with the former giving the superior fit.

The power curve used is a moving power curve. A moving power curve takes a specified number of points, fits a power curve to them, then the last data point is eliminated and a new data point is added. The formula for a power curve is:

$$T=ax^{b}$$

T= arrival time

X= distance from source to receiver

a & b = regression coefficients

Once the regression coefficients are determined the velocity may be obtained by transforming the equation into the form below:

$$\frac{dX}{dT} = (abX^{b-1})^{-1}$$

The number of data points used to fit the power curve must be great enough so the velocity will always increase for points farther from the source. This becomes a necessary condition upon examination of the Wiechert, Herglotz,

Bateman integral, which is used to determine depths of penetration. This will be explained further in the Depth of Penetration section.

The moving power curve for the P waves required a seven point moving curve for the best fit. The statistics for the power curve fits of the P wave data are listed in Appendix II, Tables 7-10. The curves defined by the statistics are plotted with the original time versus distance data in Figures 2-5.

The moving power curves for the SH waves required a seven point moving curve for the best fit. The data that is used is the average of the SH wave picks of opposite polarity (Appendix I, Tables 6). The average times are used becauses the values are close to each other. Statistics for the power curves of the SH data are listed in Appendix II, Tables 11-14. The curves defined by the statistics are plotted with the original data in Figures 6-9.

The moving power curve for the SV wave data required a seven point moving curve for the best fit. Unlike the SH wave data the SV data of opposite polarity was not averaged because the values varied by a considerable amount, making the SV data suspect. Therefore, the SV data of opposite polarity are analyzed separately. The statistics for the power curve fit of the SV data are listed in Appendix II, Tables 15-21. The curves defined by the statistics are plotted with the original data in Figures 10-16.

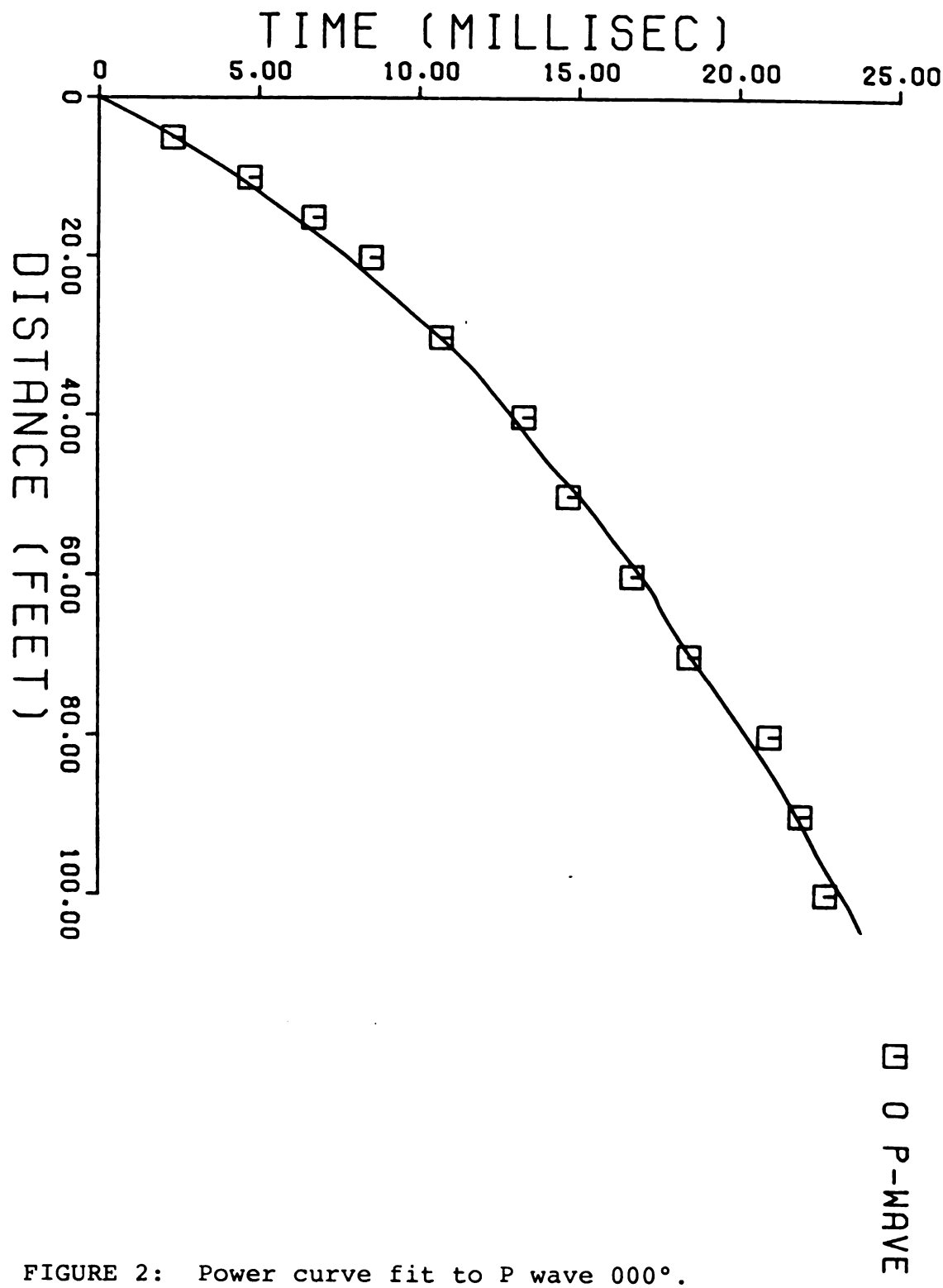


FIGURE 2: Power curve fit to P wave 000°.

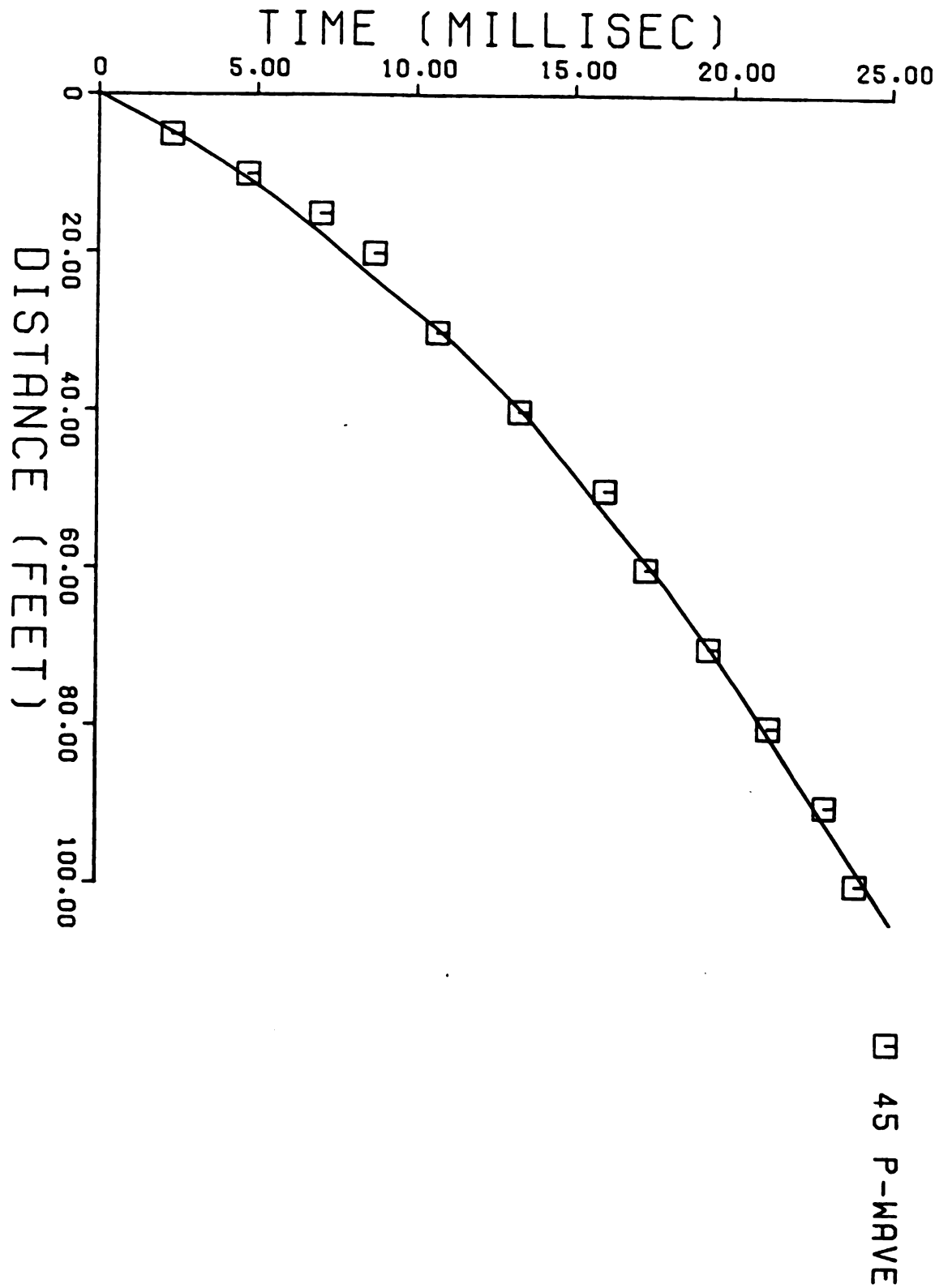


FIGURE 3: Power curve fit to P wave 045°.

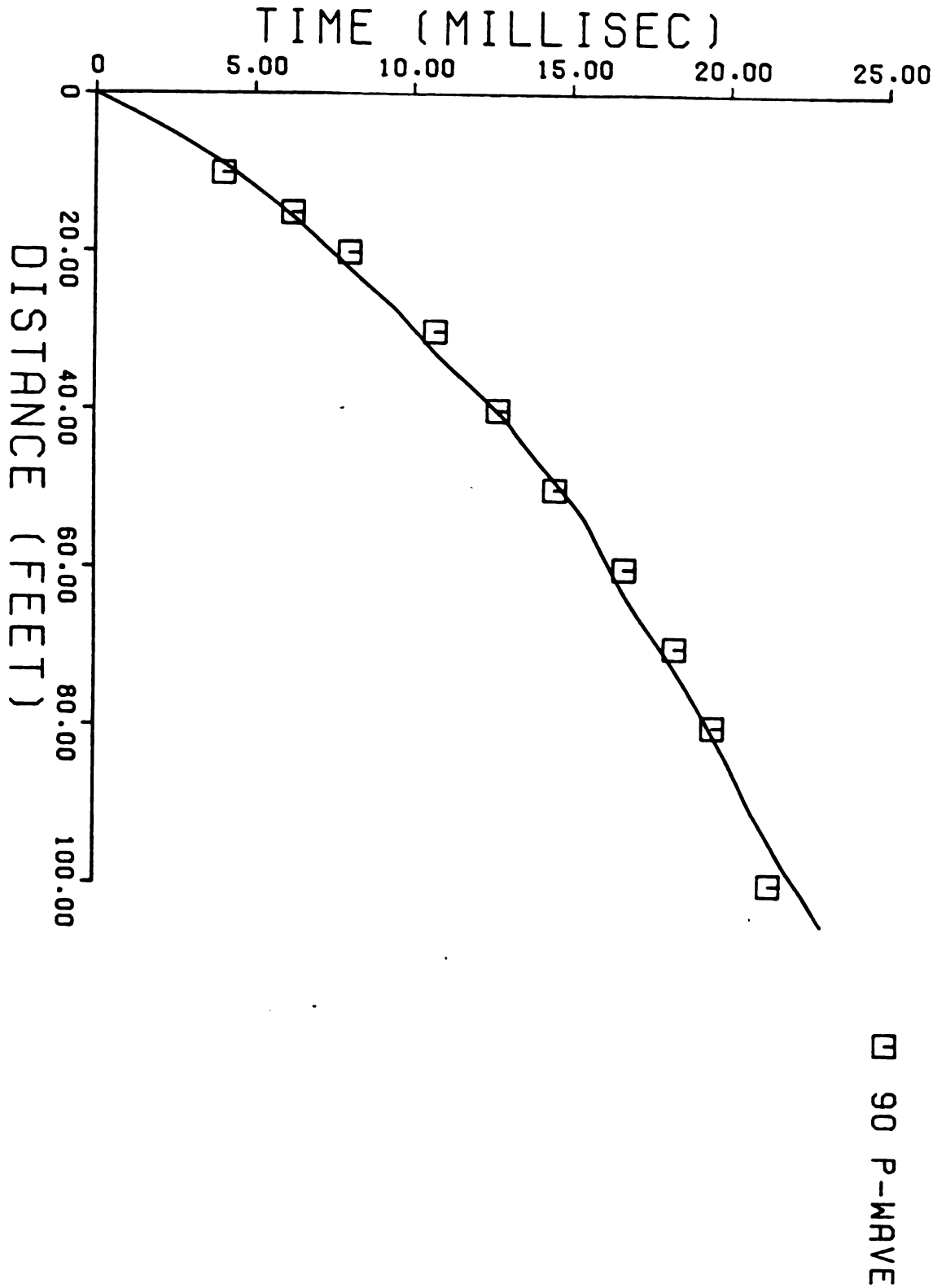


FIGURE 4: Power curve fit to P wave 090.

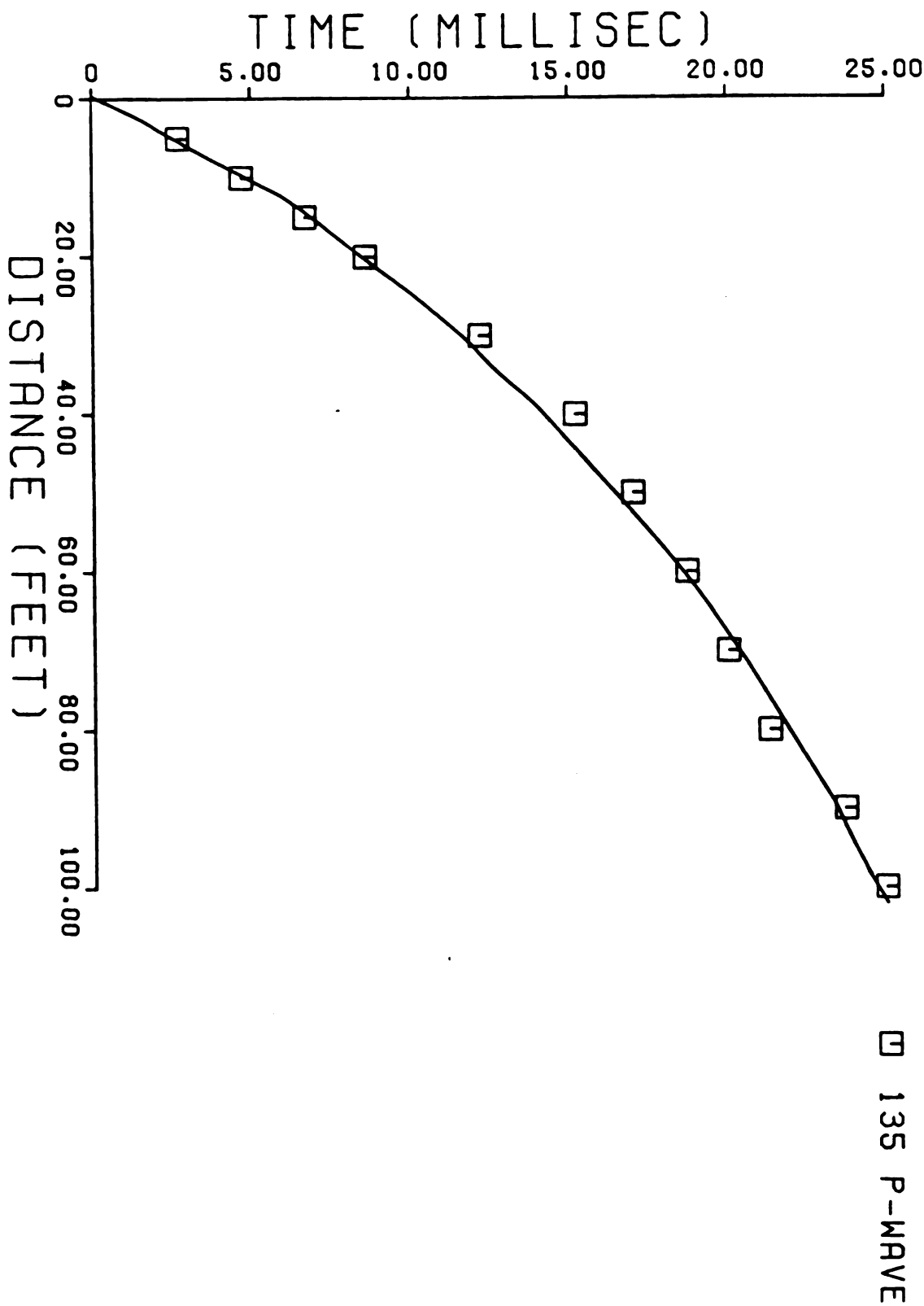


FIGURE 5: Power curve fit to P wave 135.

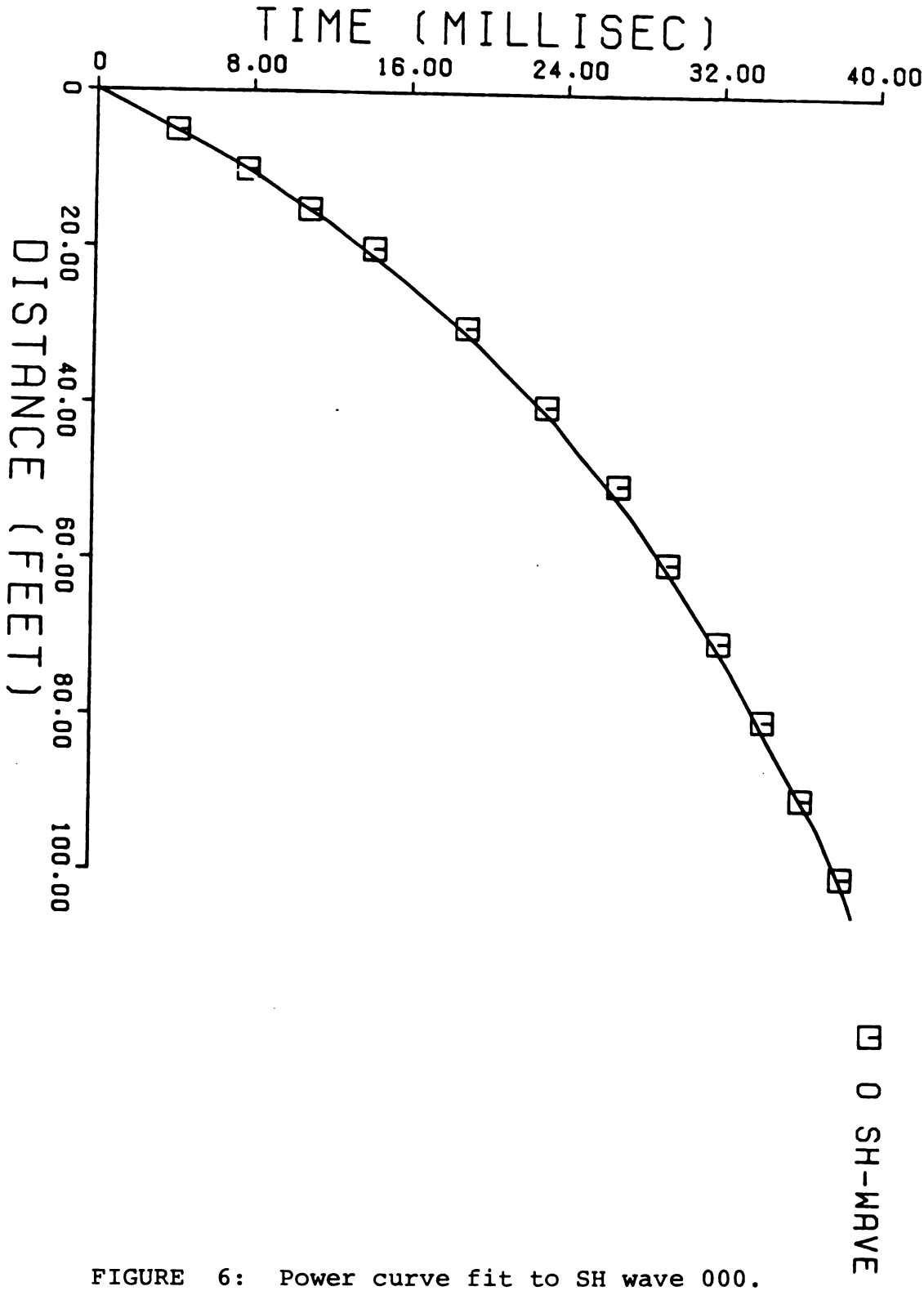


FIGURE 6: Power curve fit to SH wave 000.

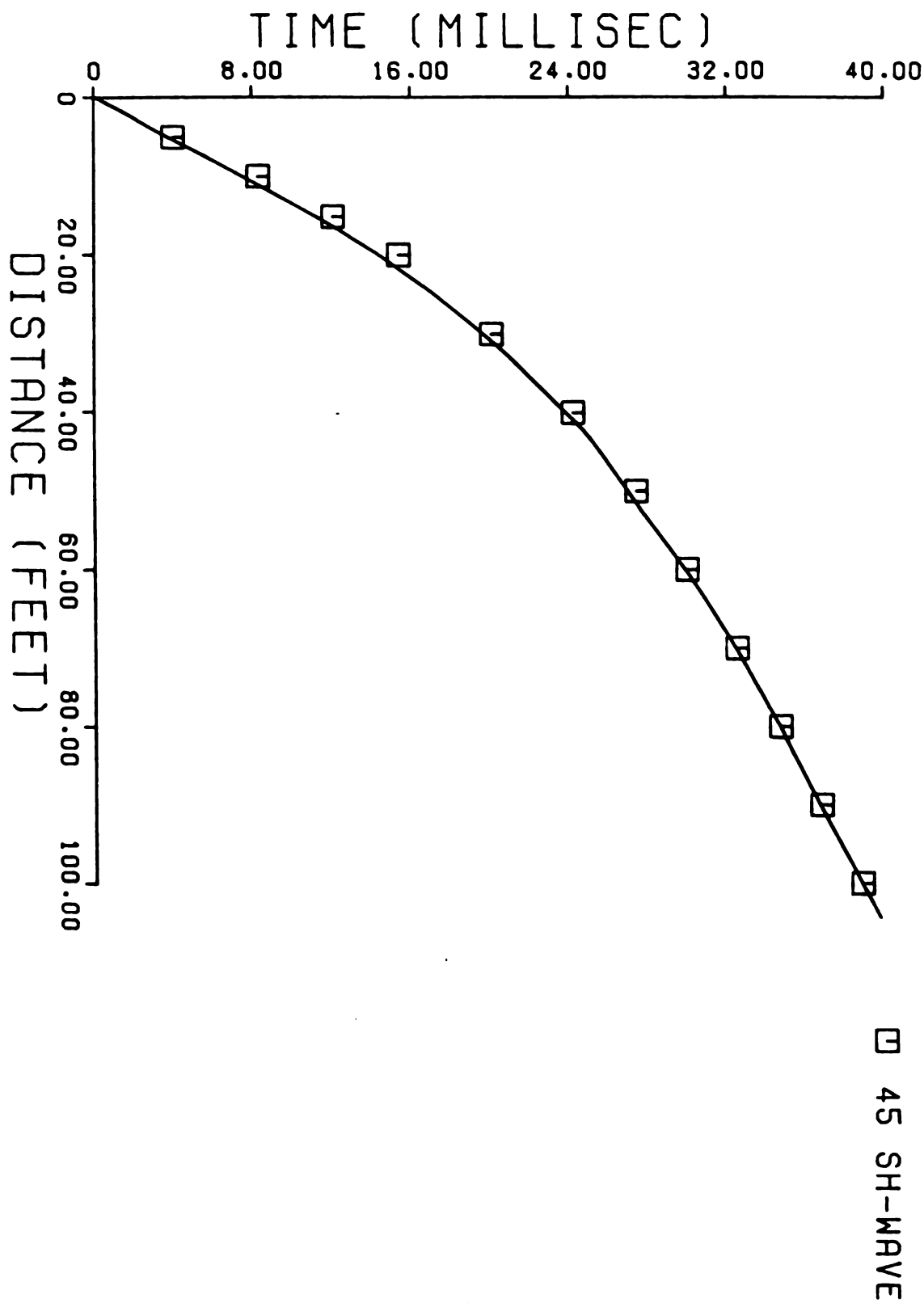


FIGURE 7: Power curve fit to SH wave 045.

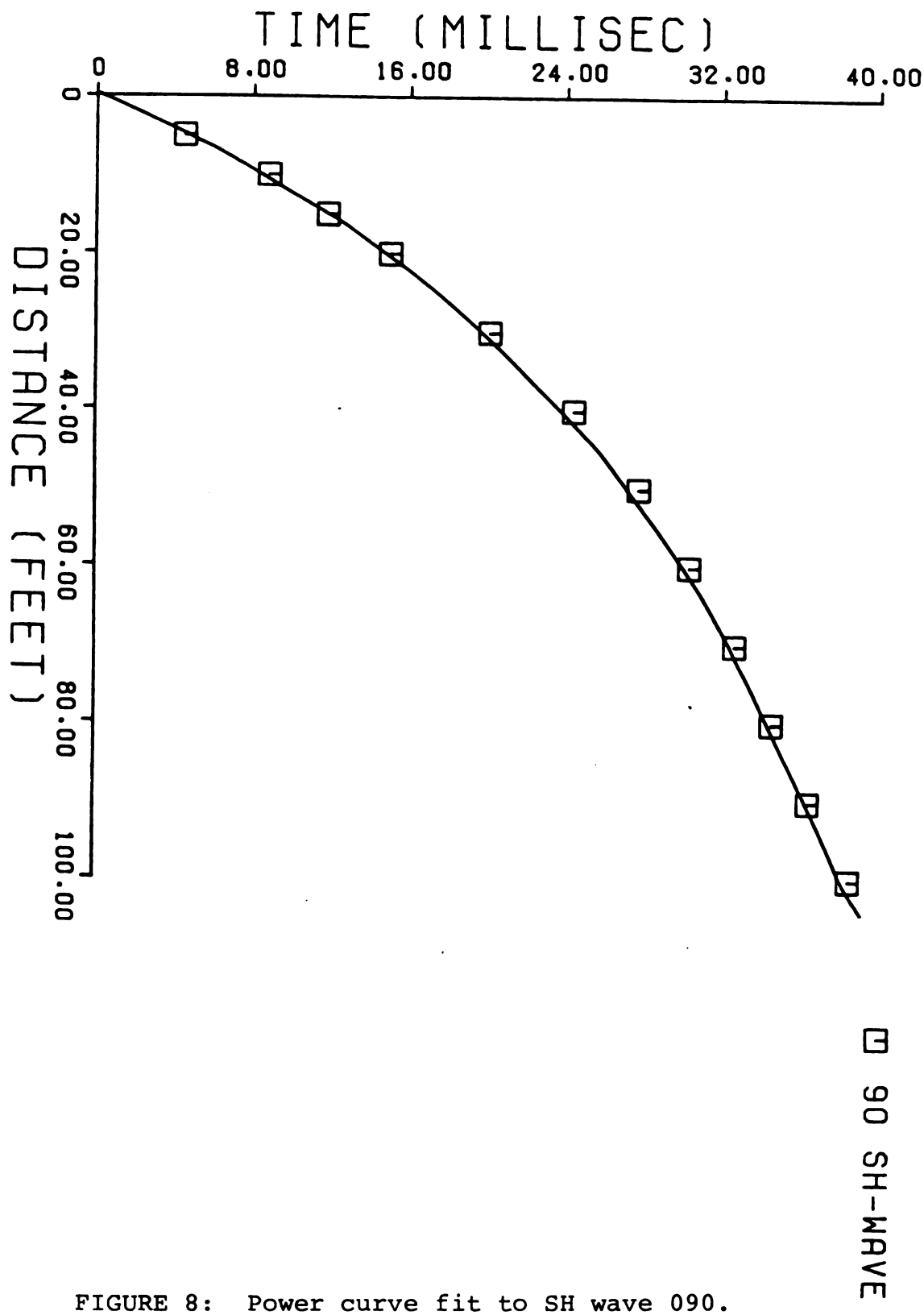


FIGURE 8: Power curve fit to SH wave 090.

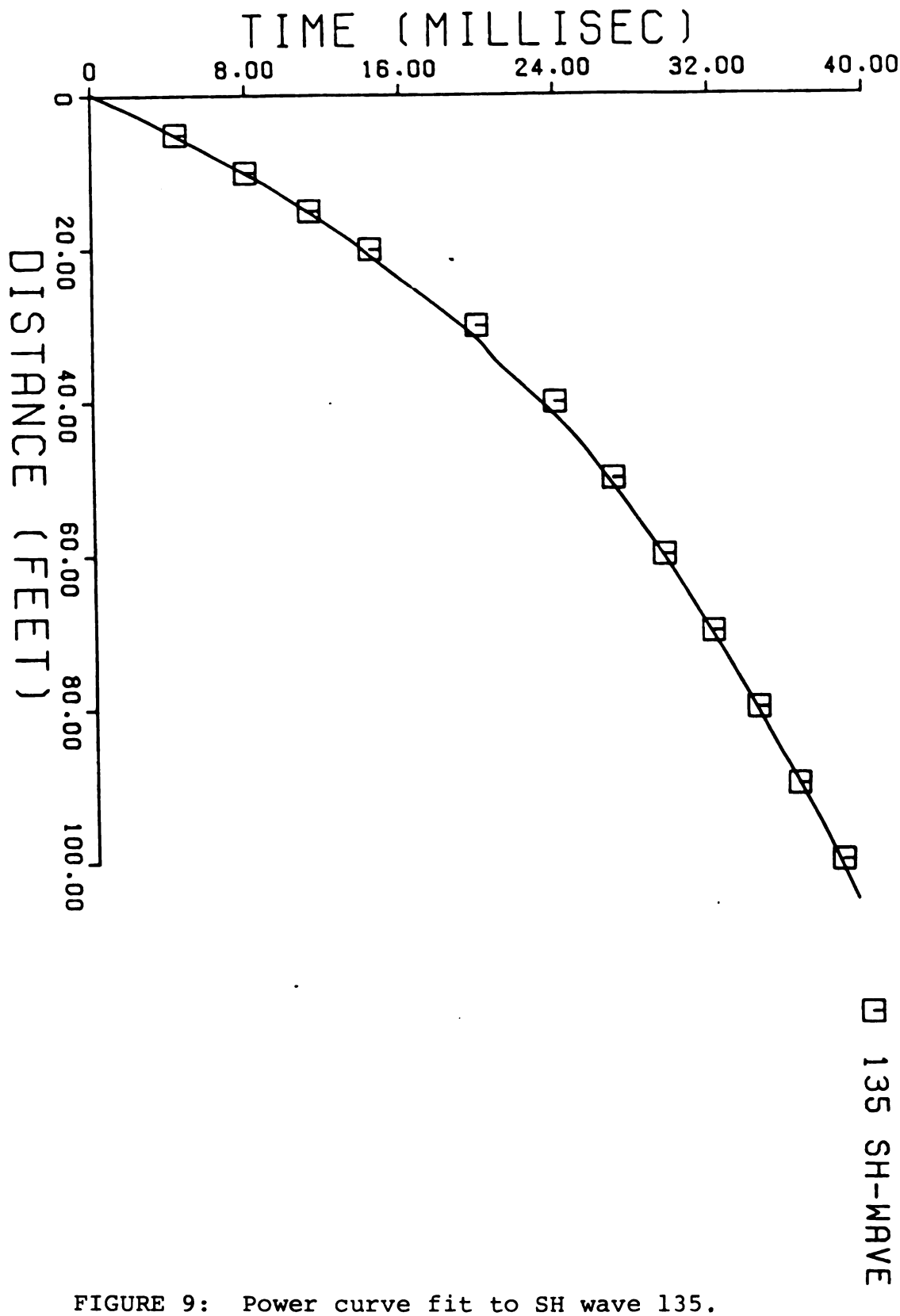


FIGURE 9: Power curve fit to SH wave 135.

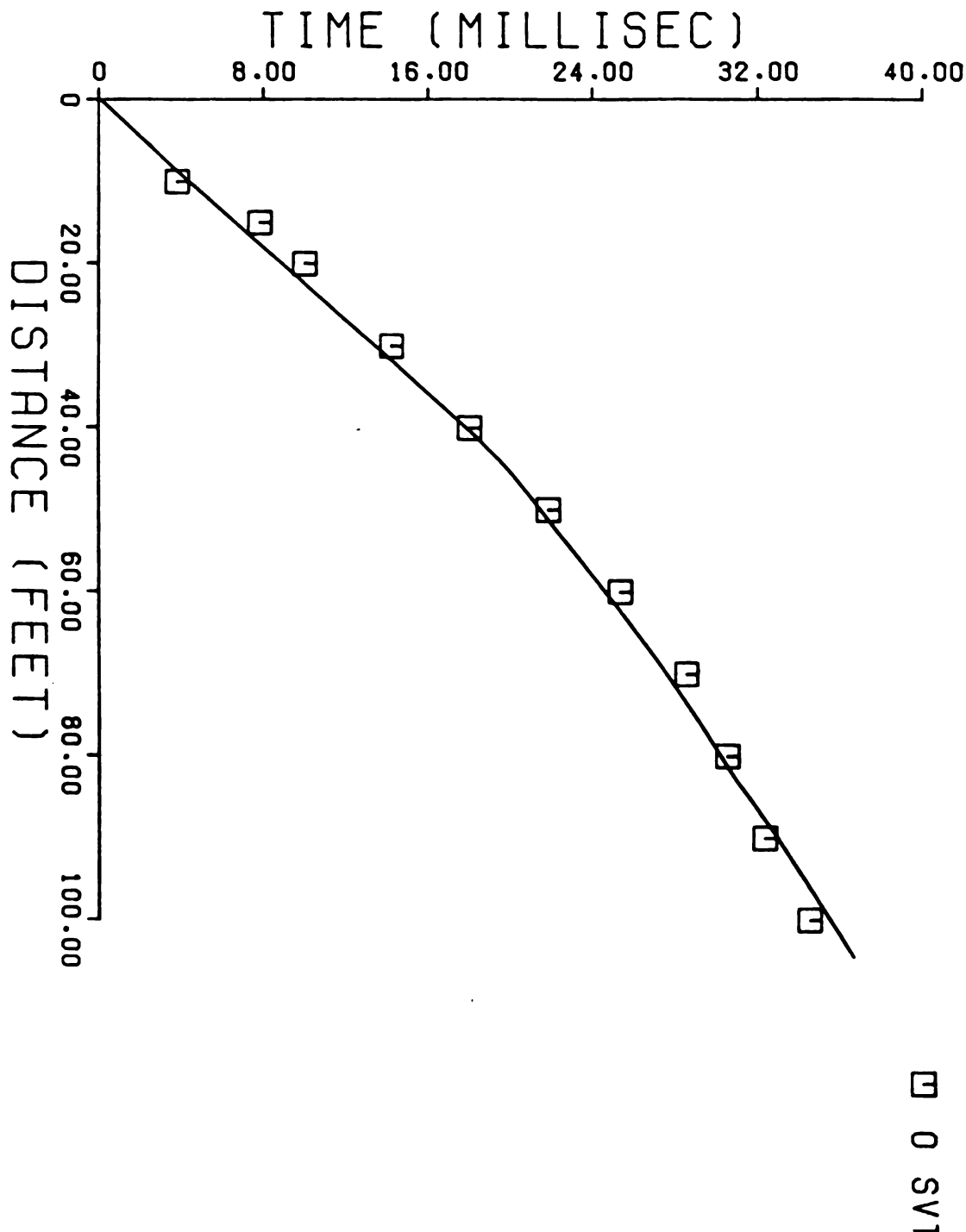


FIGURE 10: Power curve fit to SV(+) wave 000.

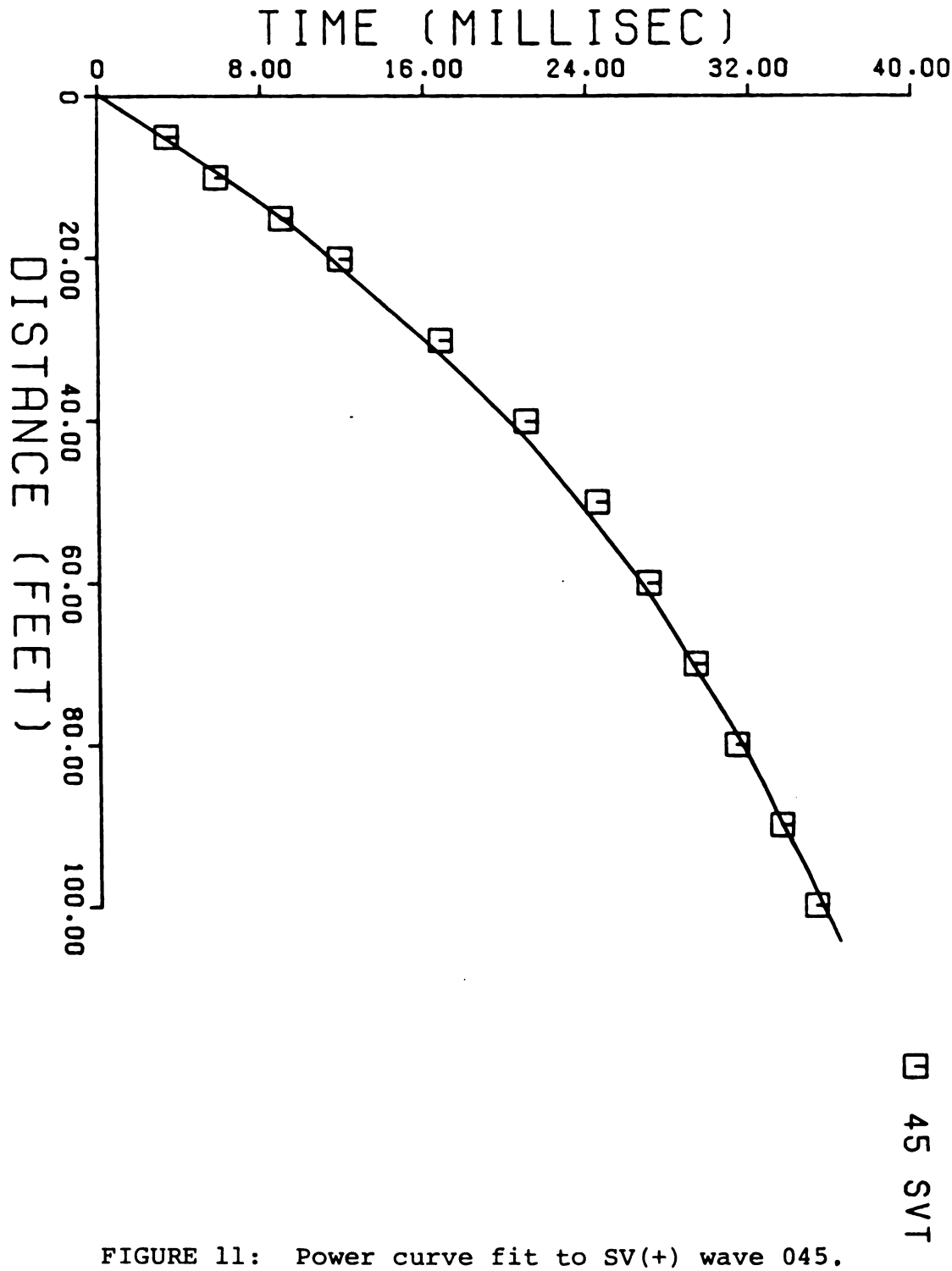


FIGURE 11: Power curve fit to SV(+) wave 045.

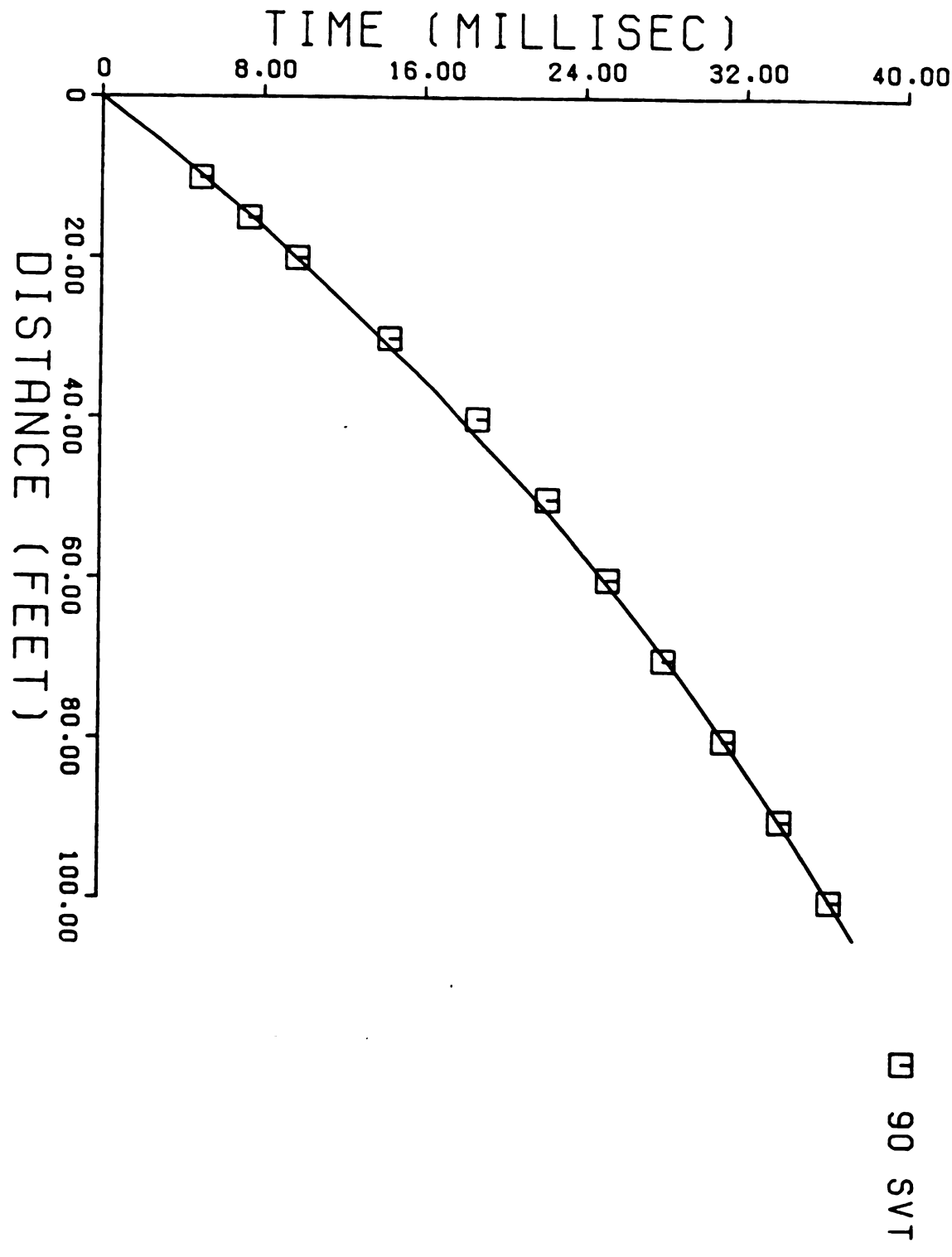


FIGURE 12: Power curve fit to SV(+) wave 090.

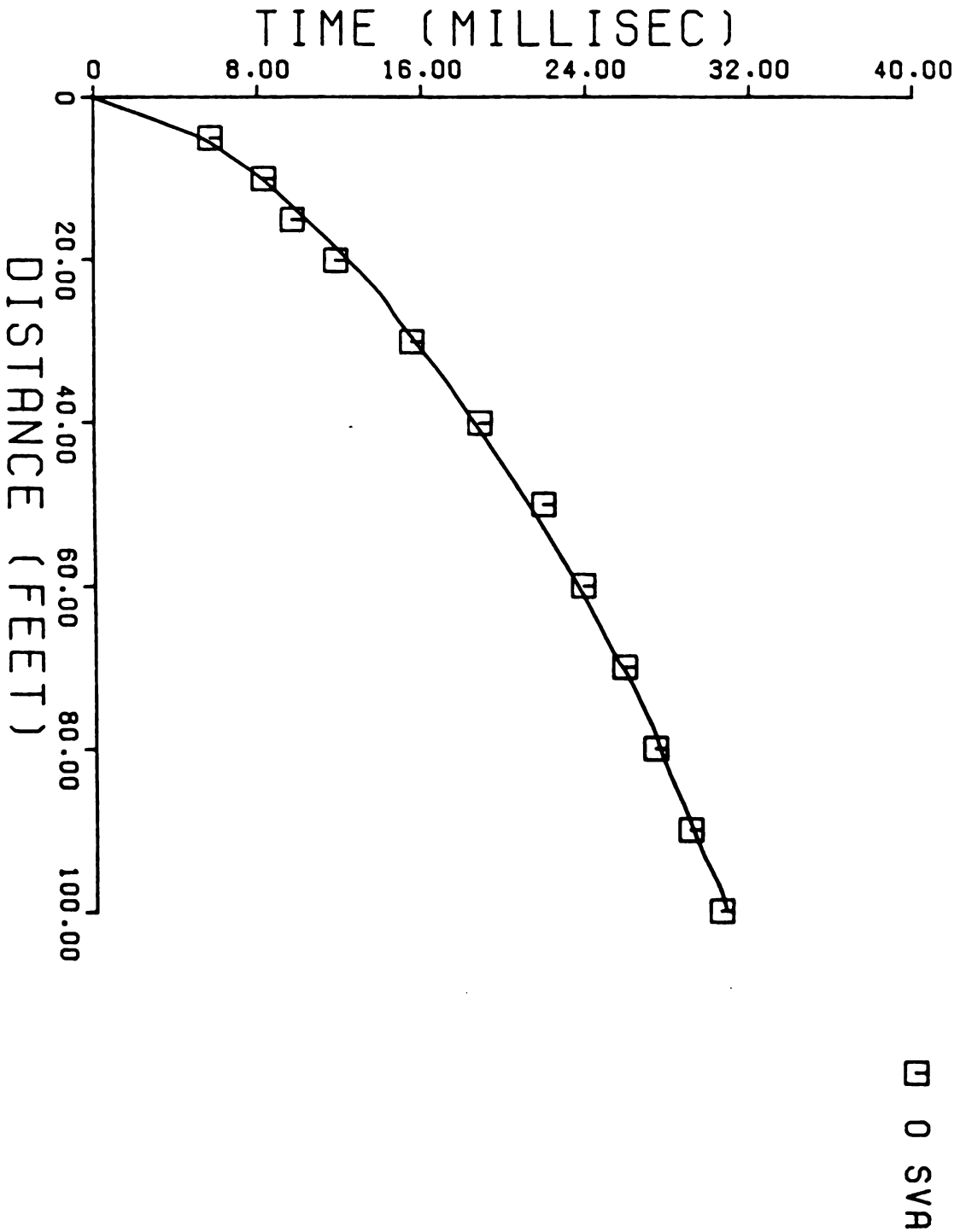


FIGURE 13: Power curve fit to SV(-) wave 000.

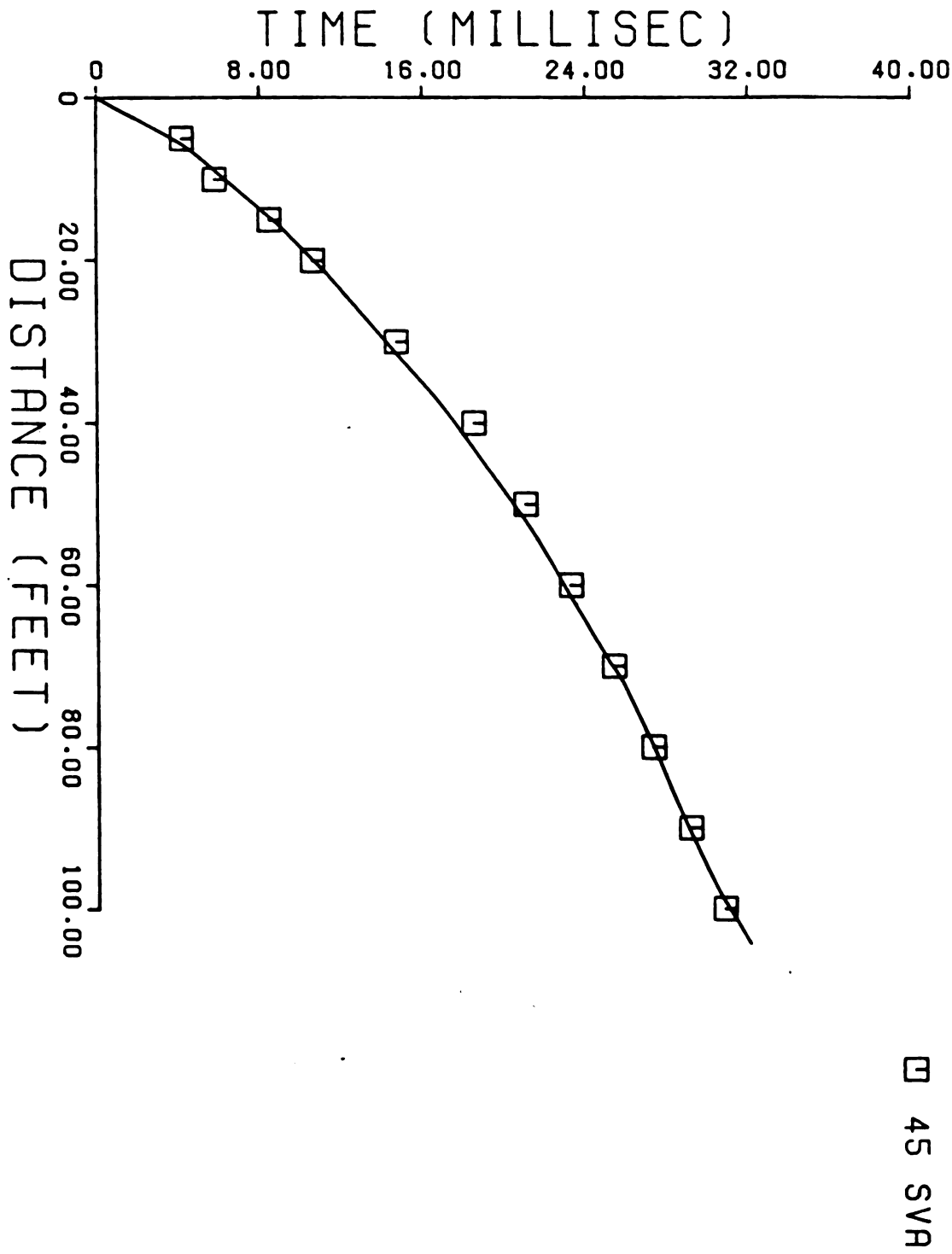


FIGURE 14: Power curve fit to SV(-) wave 045.

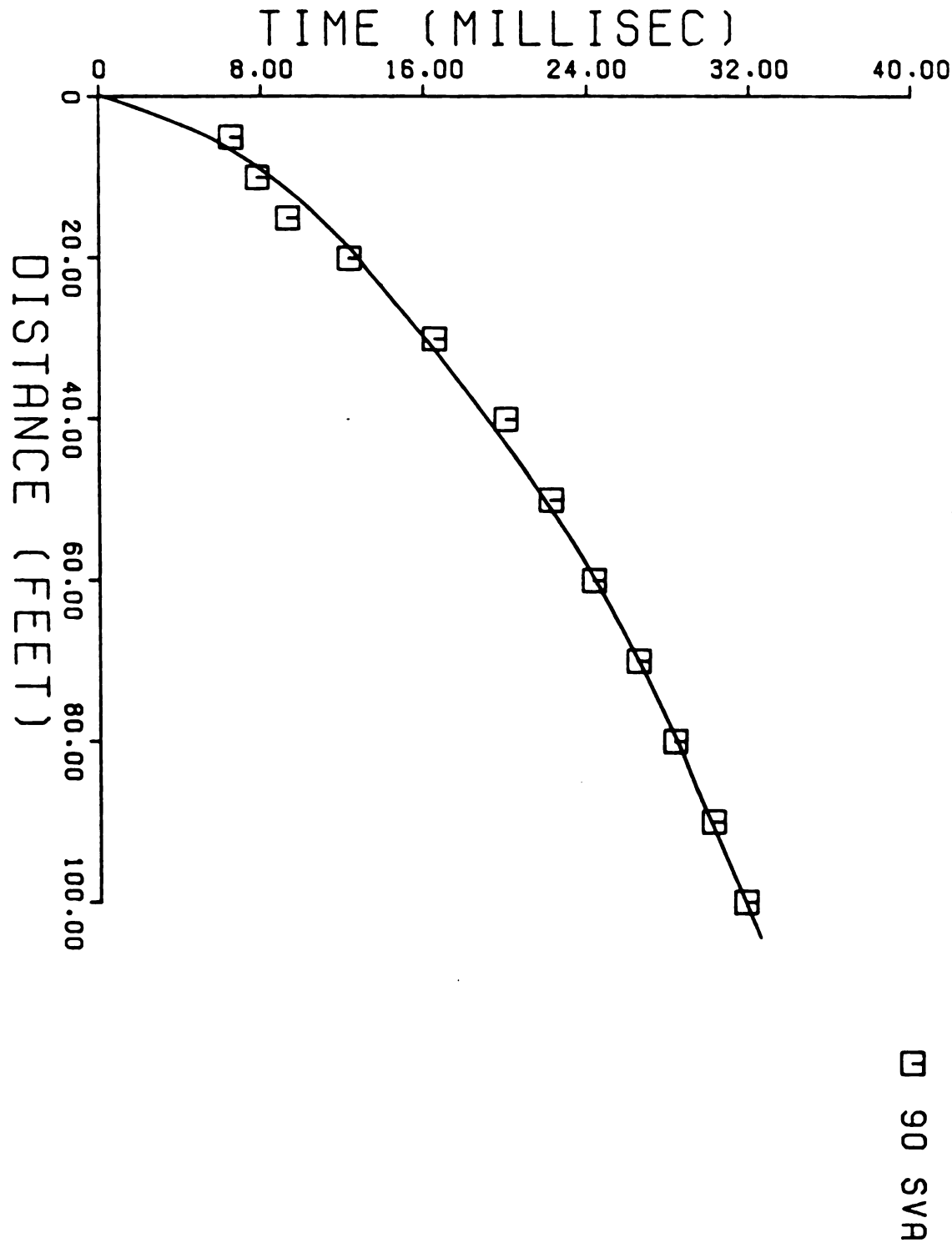


FIGURE 15: Power curve fit to SV(-) wave 090.

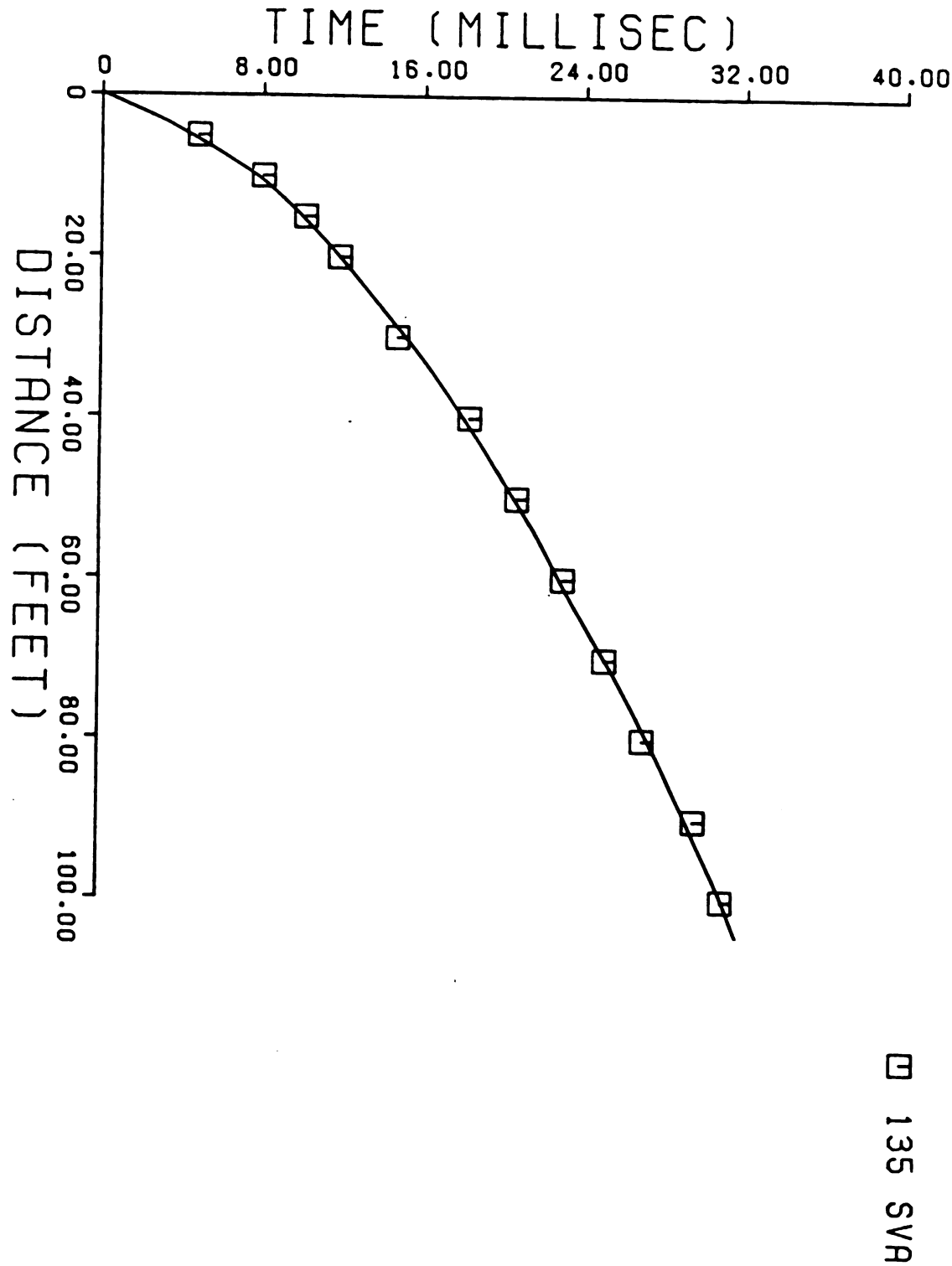


FIGURE 16: Power curve fit to SV(-) wave 135.

The best fit to the time versus distance data was obtained by using a log curve. The formula for the log curve used is as follows:

$$T = a + b\,(\ln\,(x + c))$$

T= arrival time

X= distance from source to receiver

a & b = regression coeffients

c= constant

The constant, c, is used in the equation because when X=0, T must also equal zero. However, for the usual log curve equation, T=a+b(lnX), T= -inf when X=0, hence the introduction of the constant c. Once a, b, and c are determined, velocities may be obtained by transforming the equation to the following form:

$$\frac{dX}{dT} = \frac{X + c}{b}$$

The statistics of the log curve fit for the P wave data in Appendix I, Table 1, is listed in Appendix II, Table 22. The log curves defined by the statistics with the original data superimposed are plotted in Figures 17-20.

The statistics for the log curve fits for the average SH wave data is listed in Appendix II, Table 23. The curves defined by the statistics with the original data superimposed are plotted in Figures 21-24.

The statistics of the log curve fits for the SV wave data in Appendix I, Tables 4-5, are listed in Appendix II, Table 24. The curves defined by the statistics with the

original data superimposed are plotted in Figures 25-31.

Examination of the plots of all types of seismic waves, and of the correlation coefficients, reveals that the log curves provide the best fit to the seismic data. Furthermore, the log curves are preferred since only one set of regression coefficients are required, creating one smooth curve.

The time versus distance data for all directions are plotted for each type of seismic wave in FIgures 32-35. The P wave data in Figure 32 shows that for the last data points at 80, 90 and 100 feet the 090 direction has the smallest arrival time followed by the 000, 045, and 135 directions respectively. This indicates that the 090 direction should have the highest velocity for P waves.

The SH and SV plots in Figures 33-35 are more difficult to analyze in this manner because the arrival times group together more closely than the P wave arrival times.

One observation that can be made from these graphs is that if the difference in the time of P wave arrivals is caused by anisotropy, then apparently the P waves exhibit a greater percent anisotropy than the shear waves. This is contrary to the results found by others (Levin, 1979).

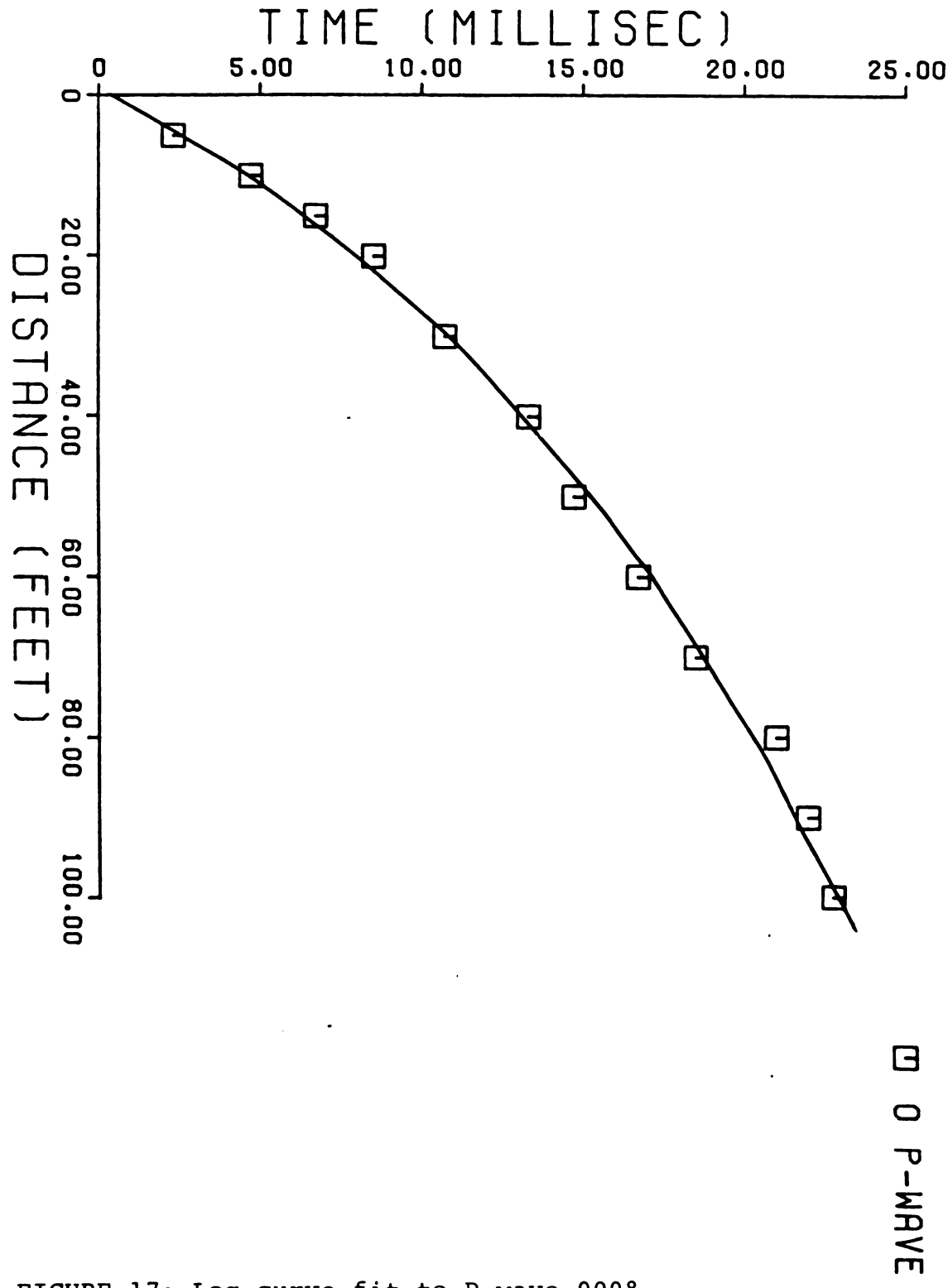


FIGURE 17: Log curve fit to P wave 000°.

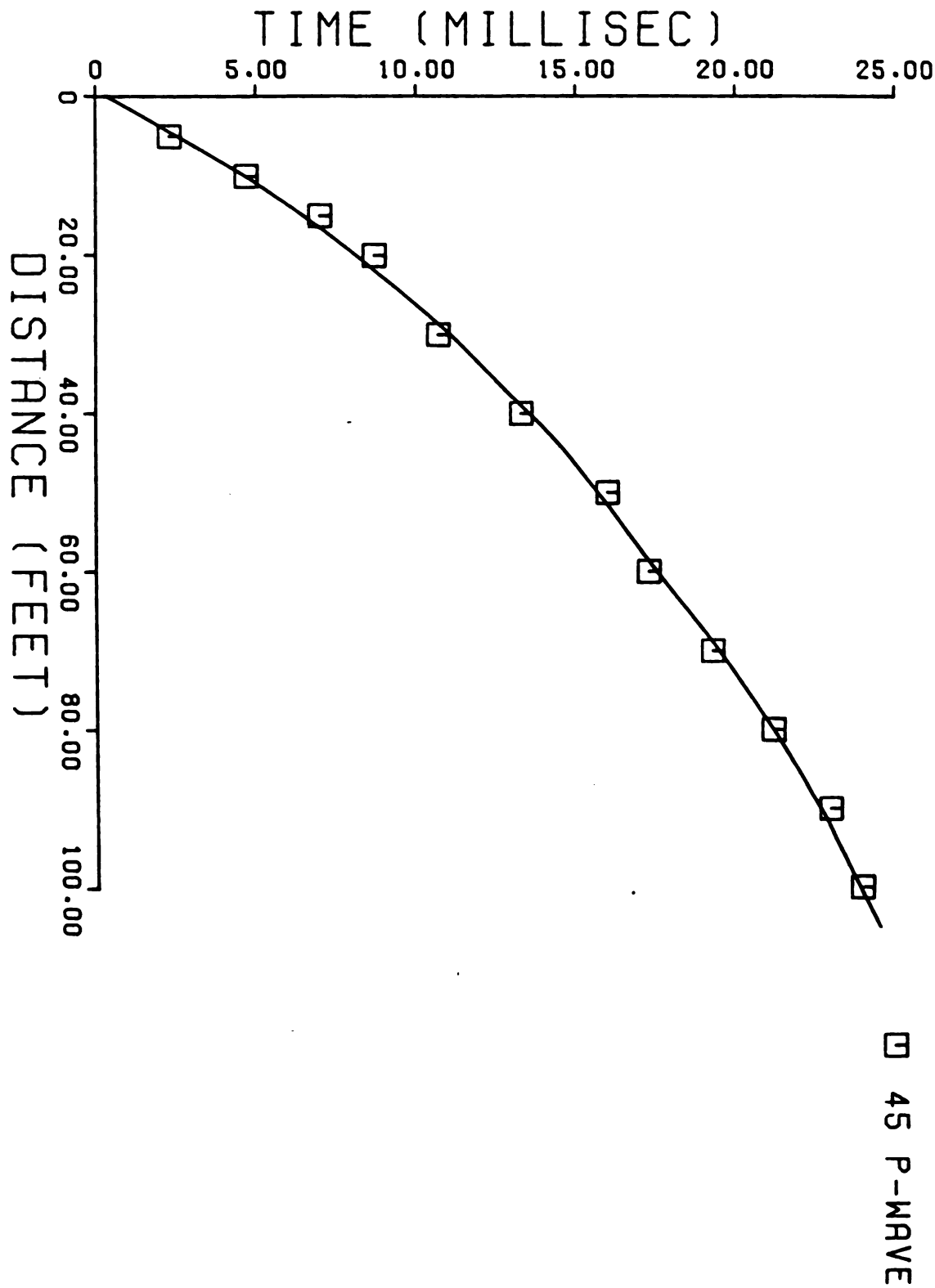


FIGURE 18: Log curve fit to P wave 045°.

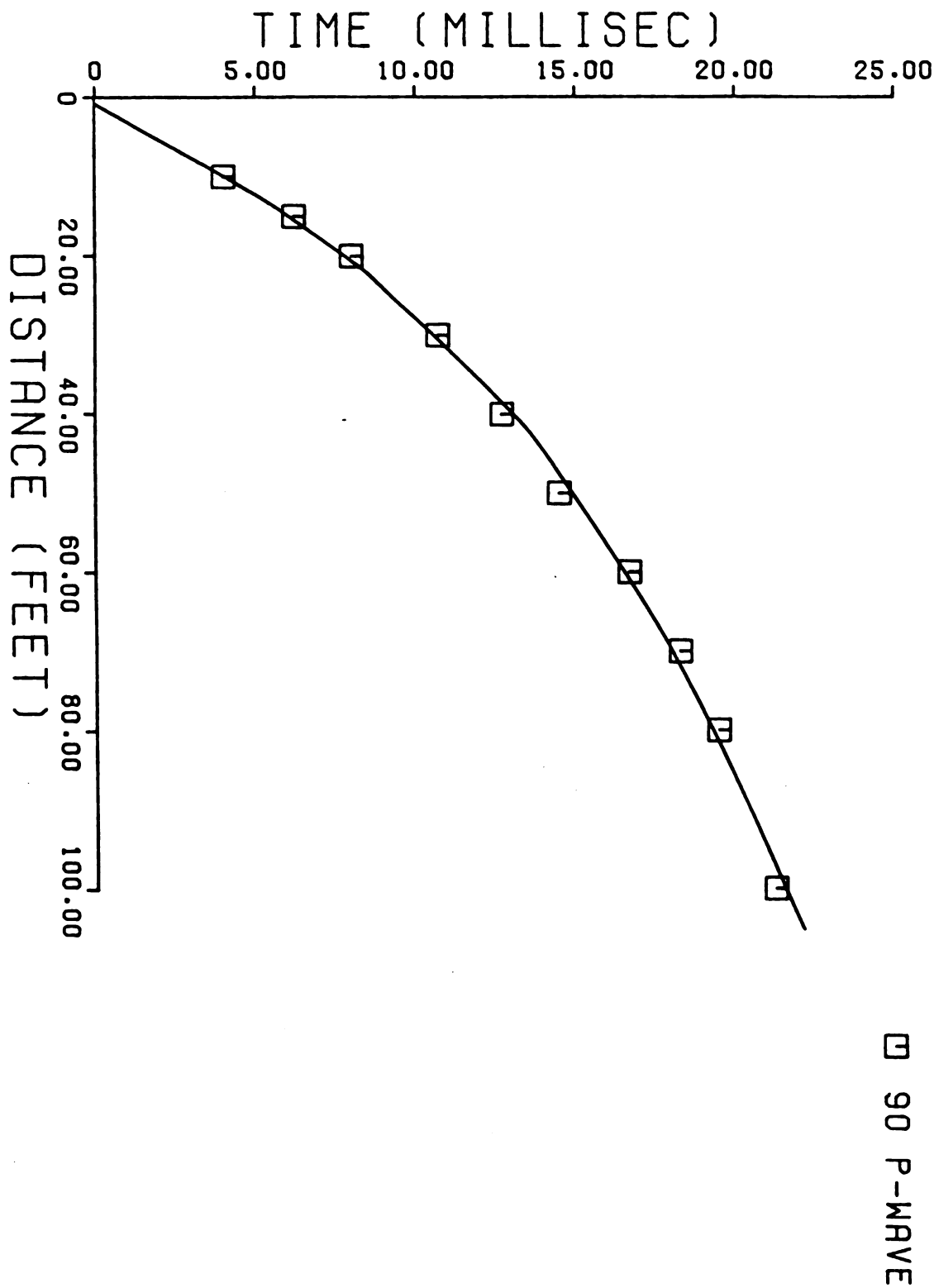


FIGURE 19: Log curve fit to P wave 090°.

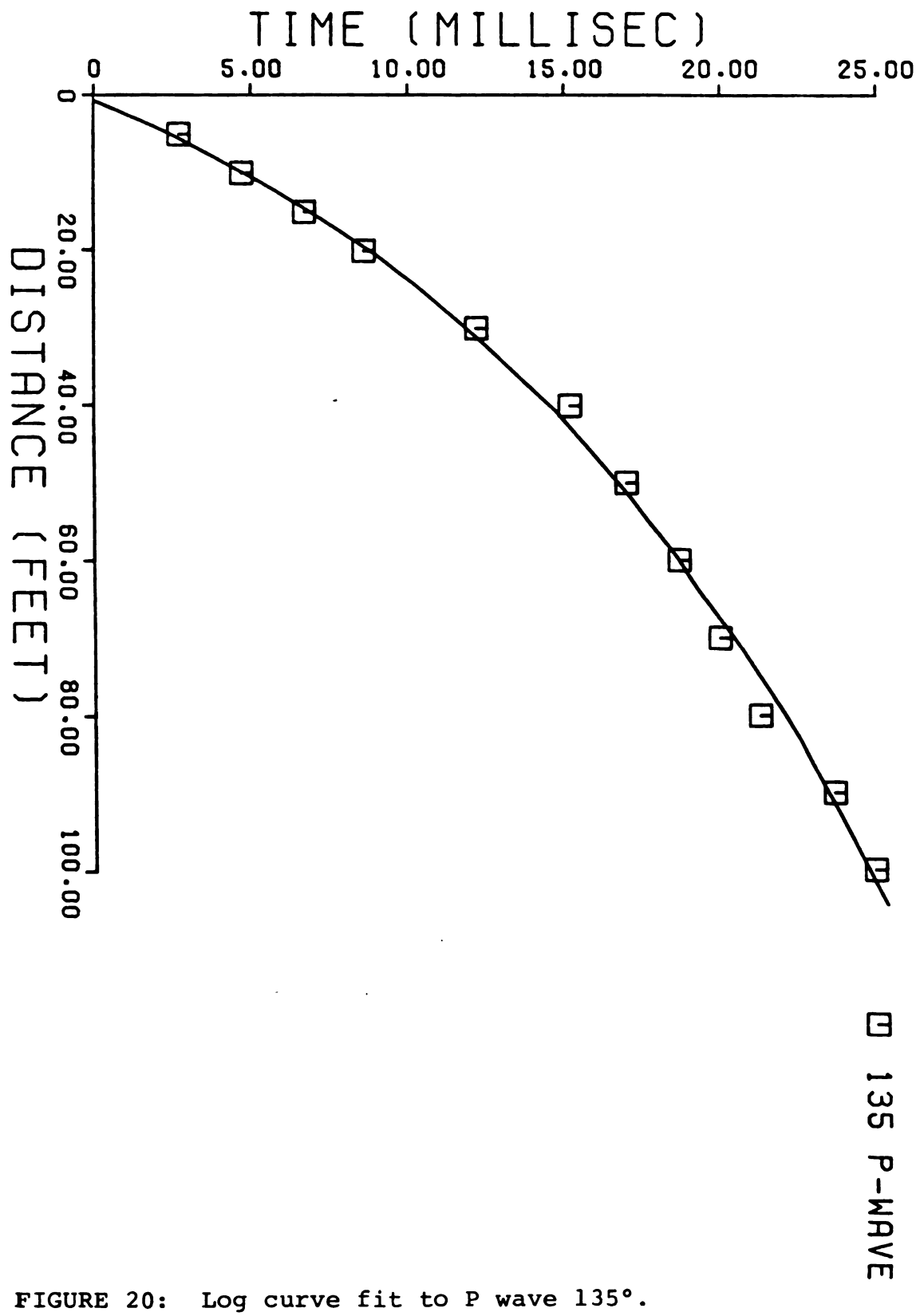


FIGURE 20: Log curve fit to P wave 135°.

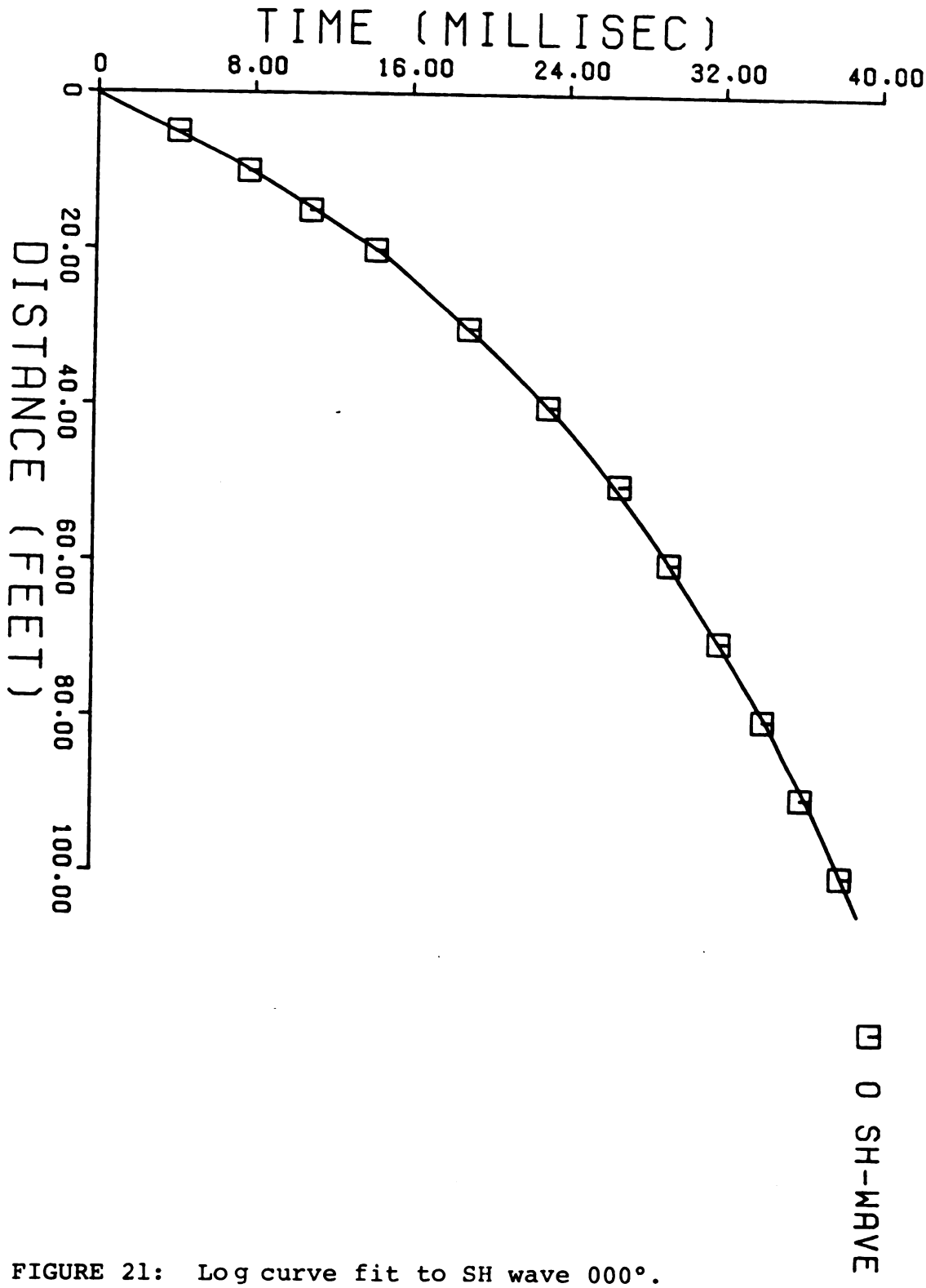


FIGURE 21: Log curve fit to SH wave 000°.

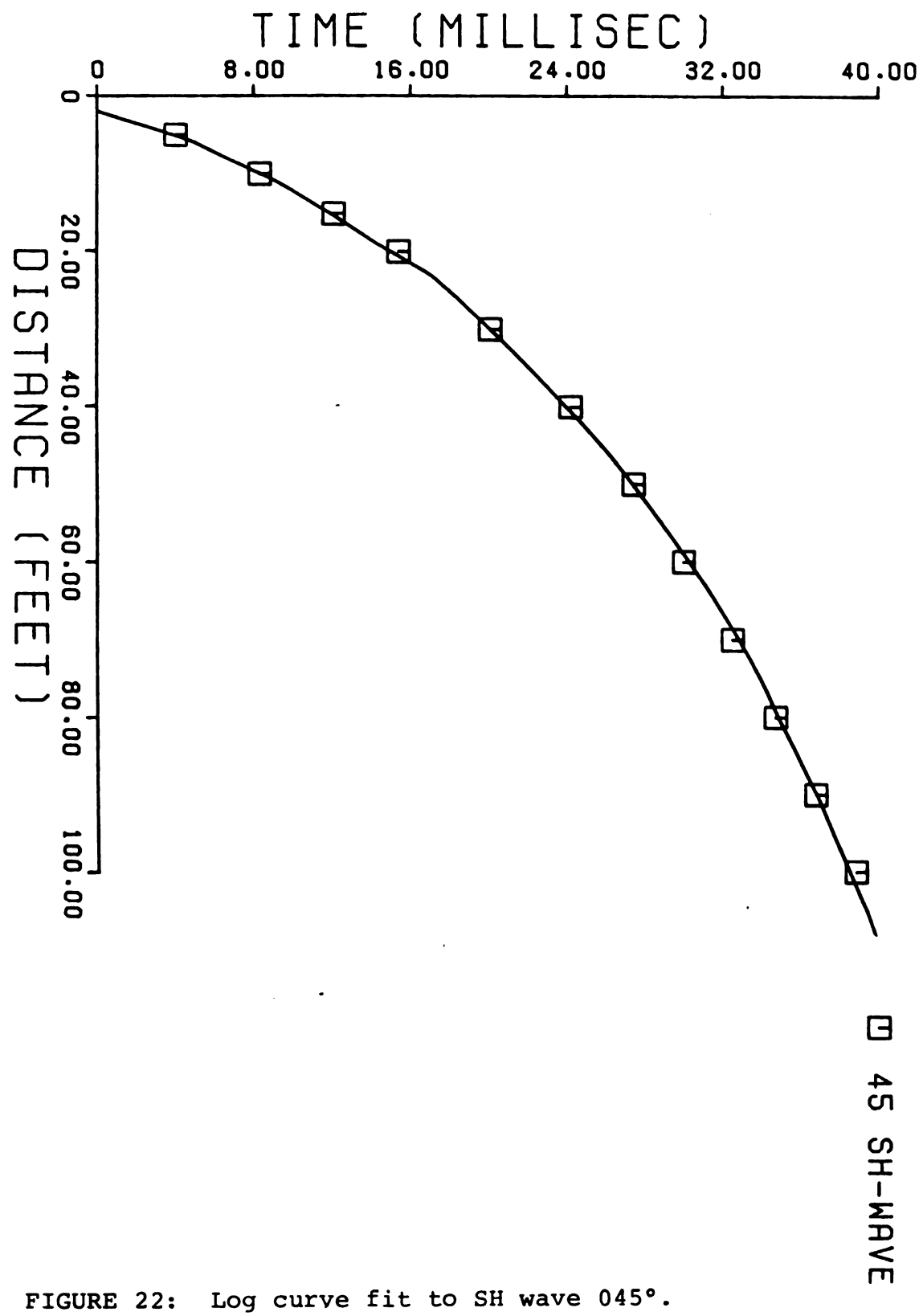


FIGURE 22: Log curve fit to SH wave 045°.

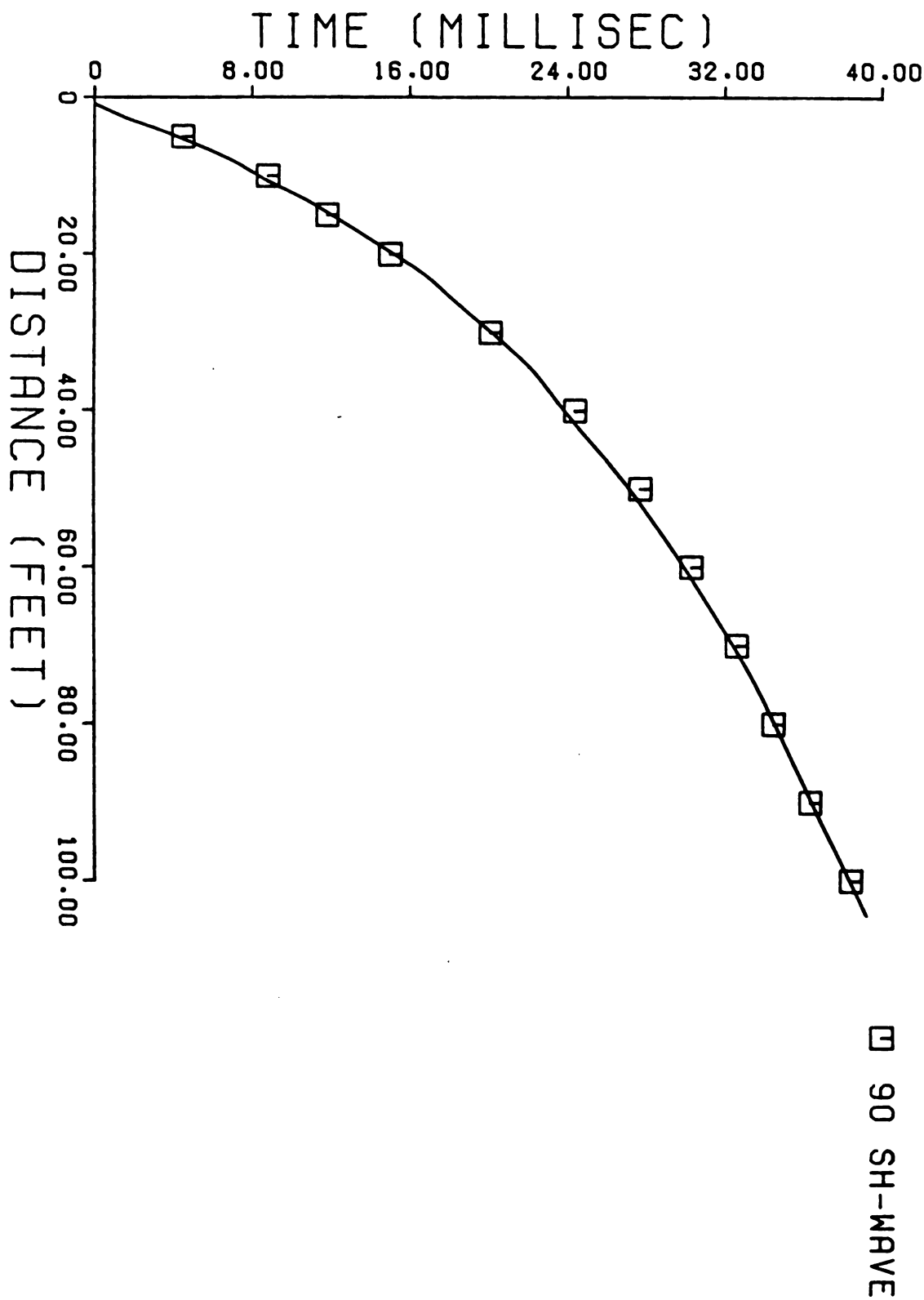


FIGURE 23: Log curve fit to SH wave 090°.

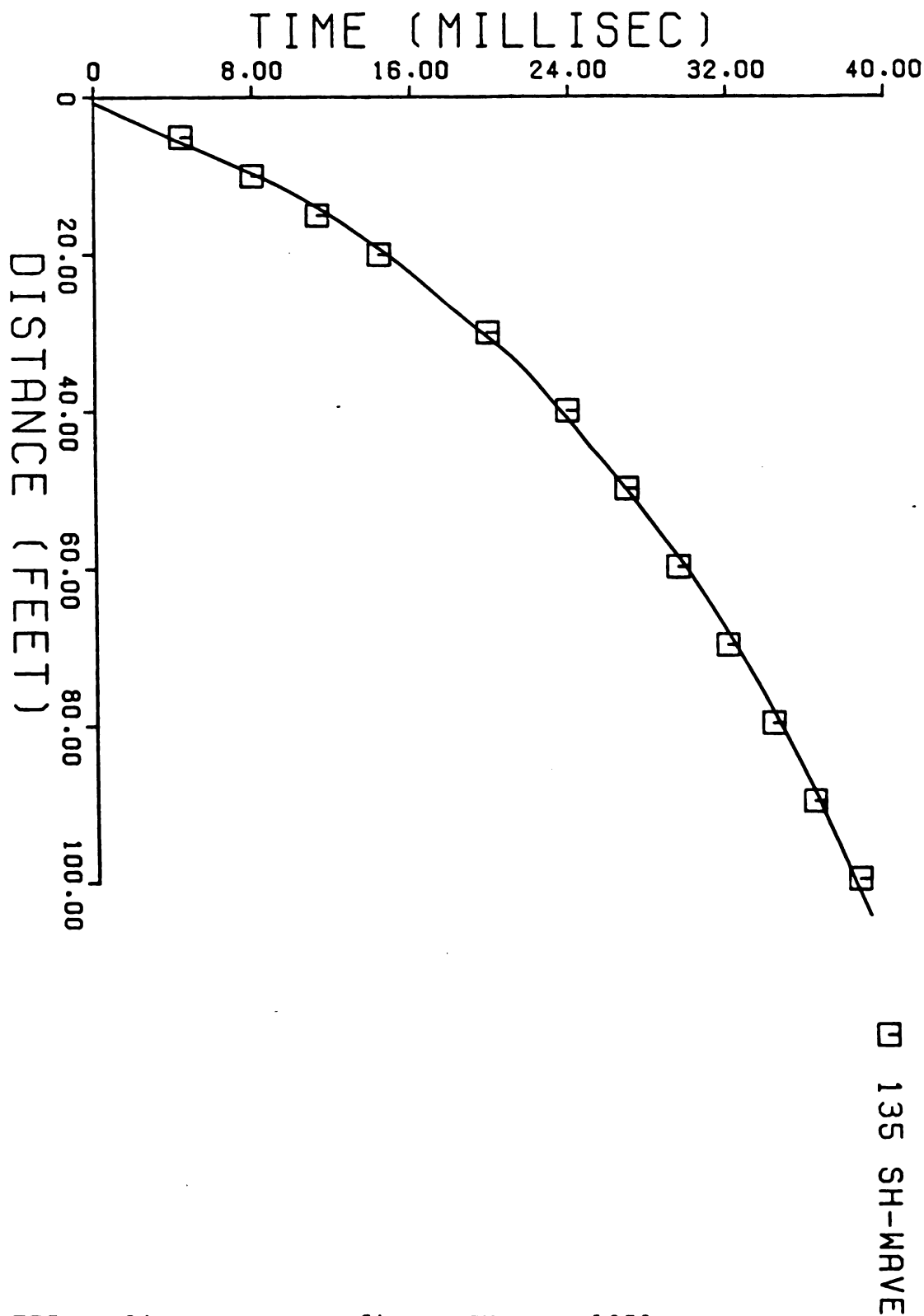


FIGURE 24: Log curve fit to SH wave 135°.

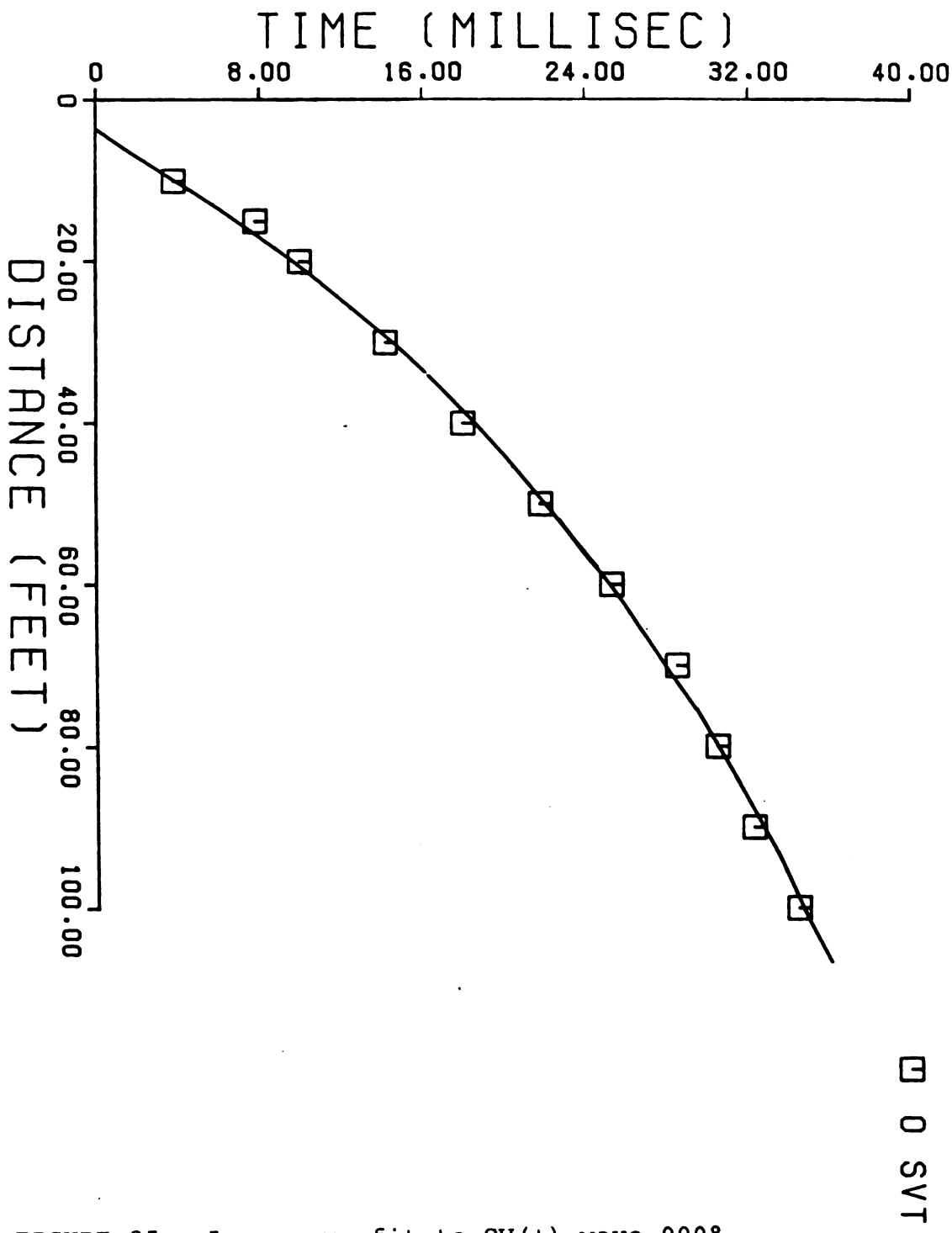


FIGURE 25: Log curve fit to SV(+) wave 000°.

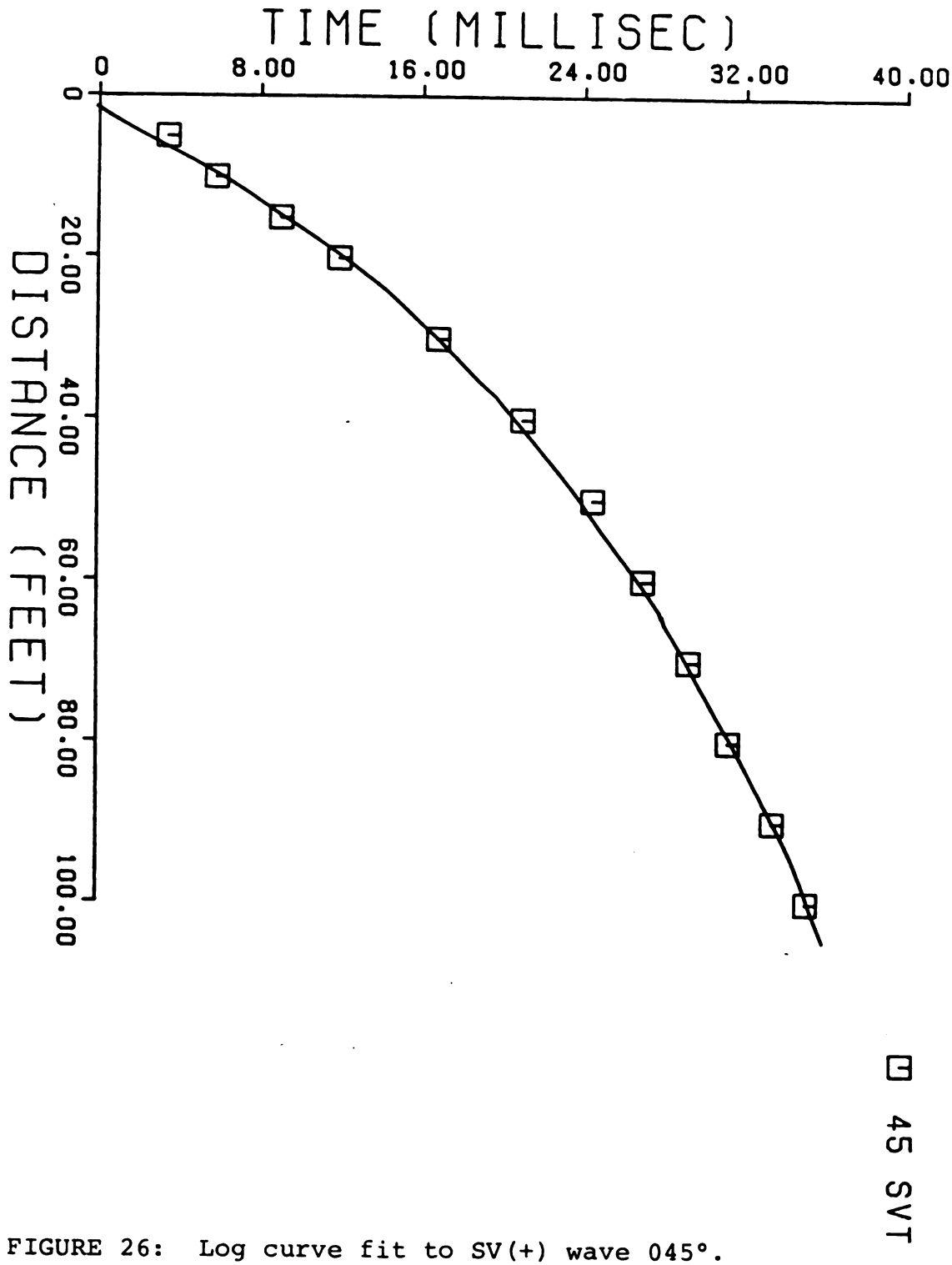


FIGURE 26: Log curve fit to SV(+) wave 045°.

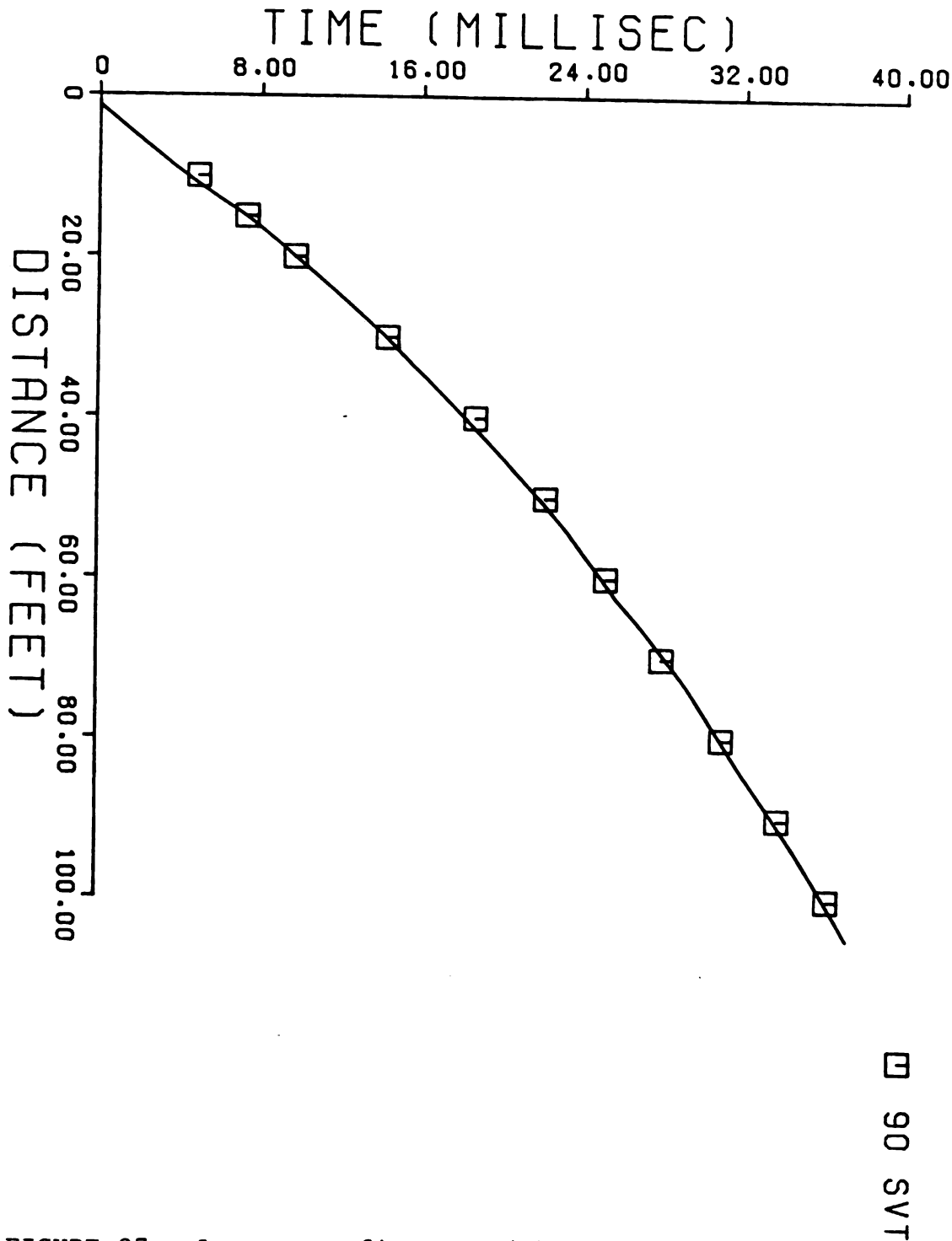


FIGURE 27: Log curve fit to SV(+) wave 090°.

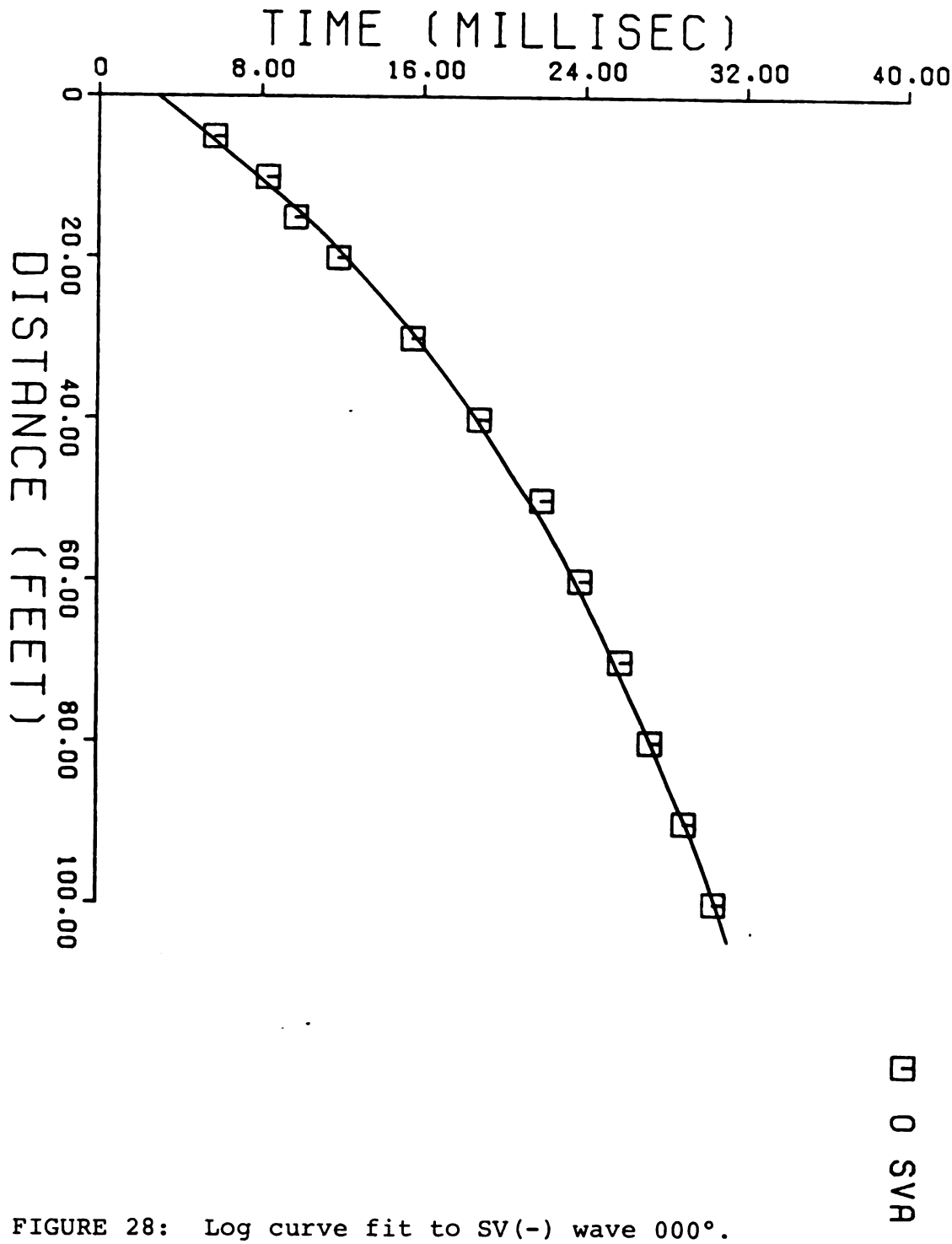


FIGURE 28: Log curve fit to SV(-) wave 000°.

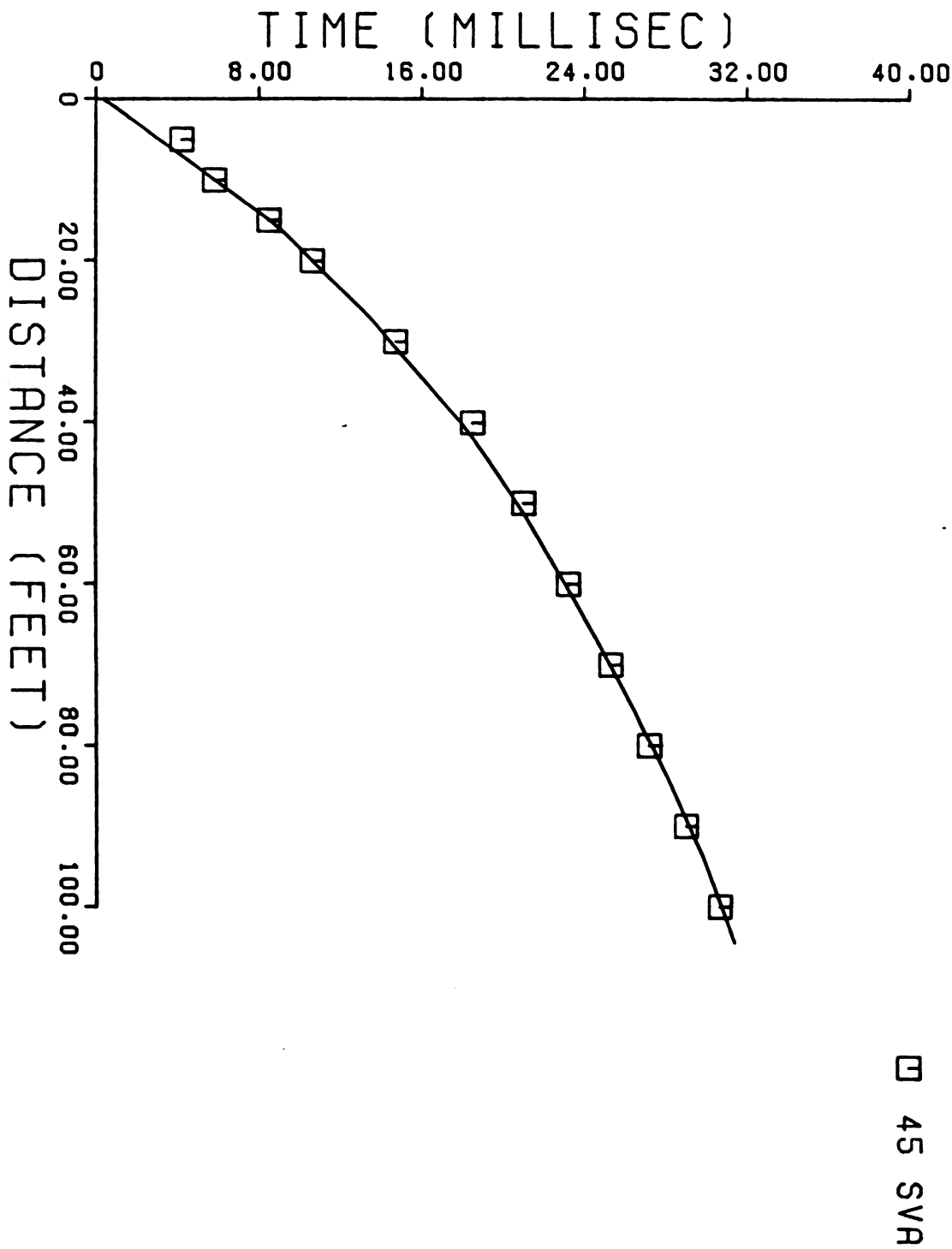


FIGURE 29: Log curve fit to SV(-) wave 045°.

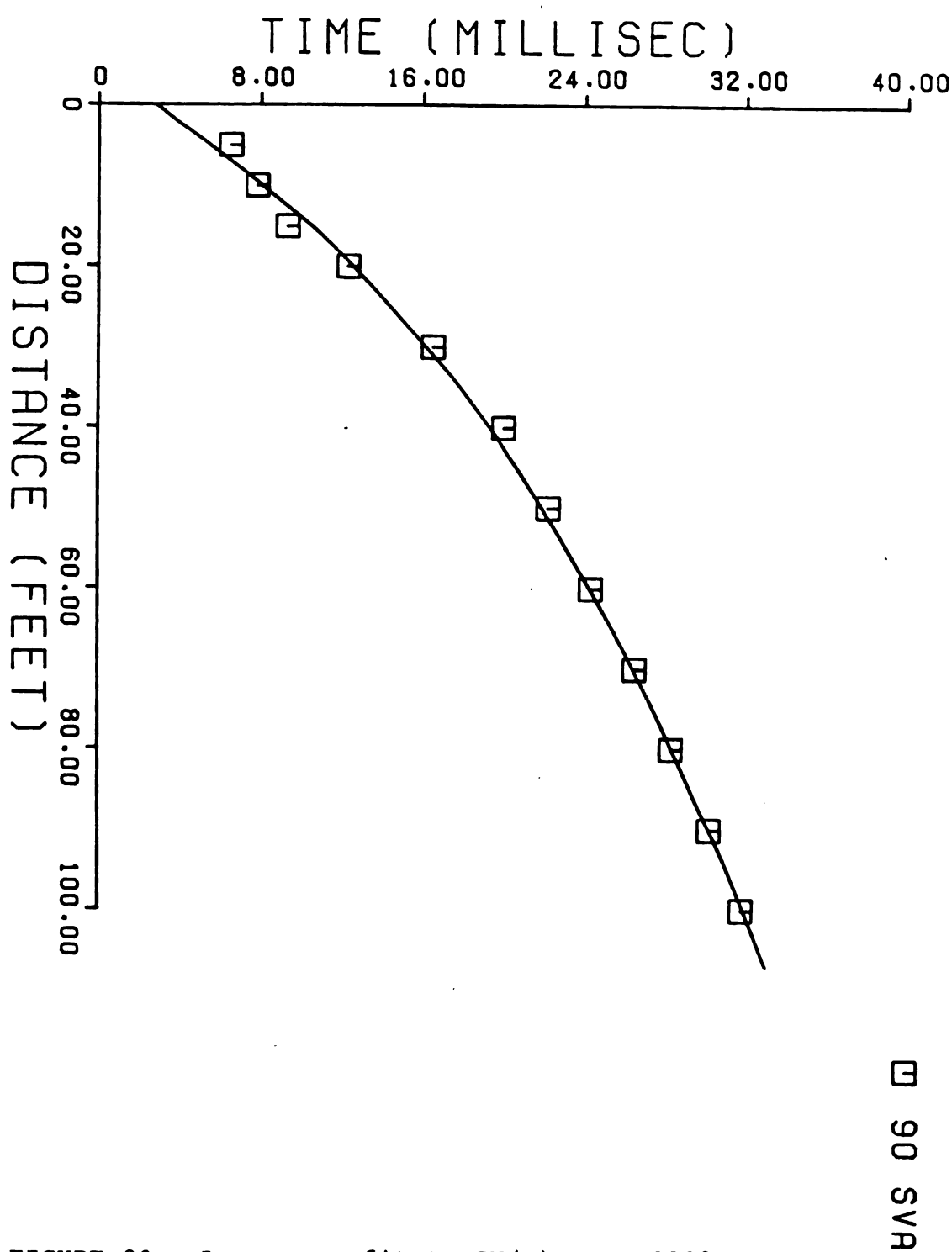


FIGURE 30: Log curve fit to SV(-) wave 090°.

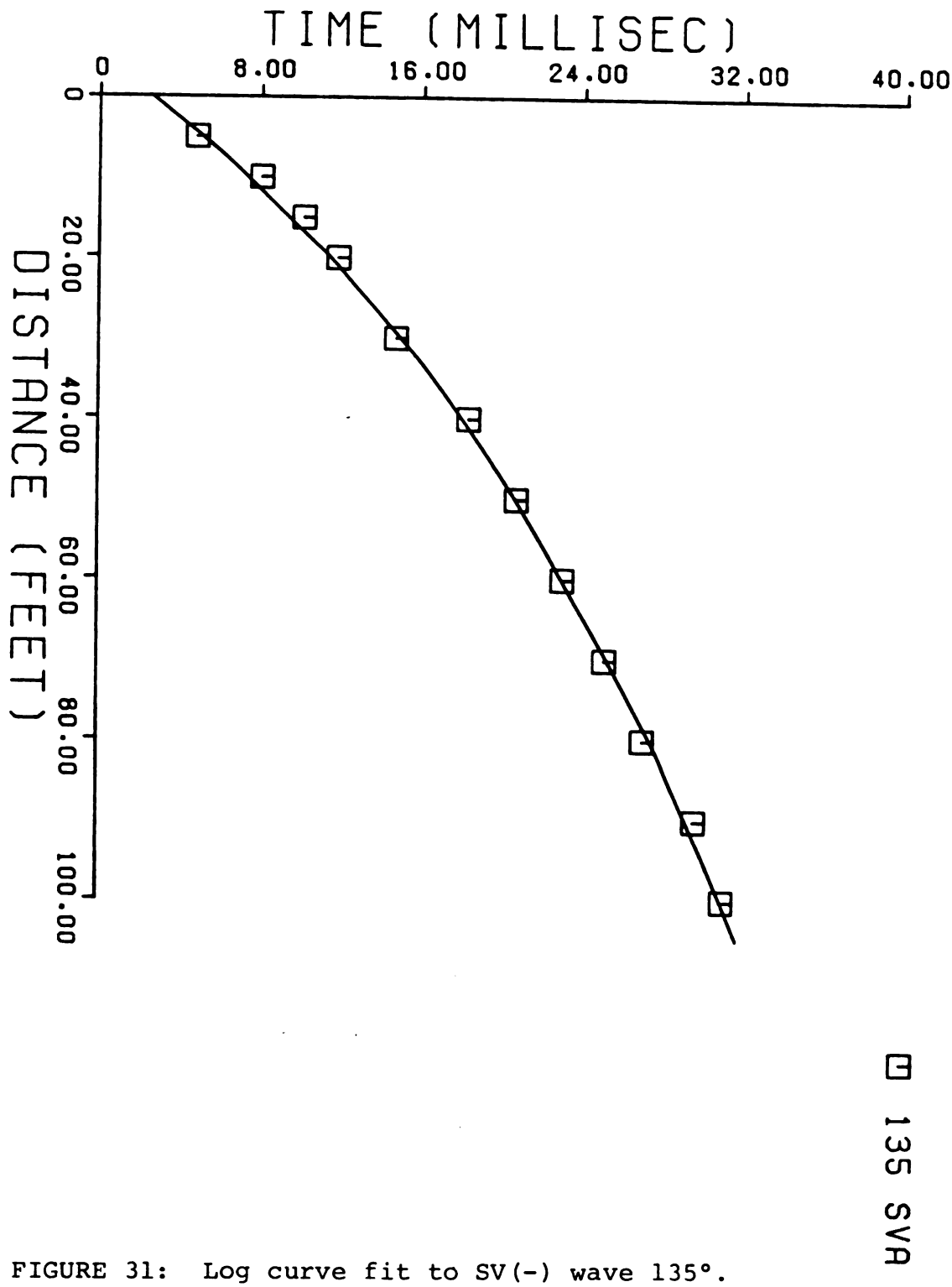


FIGURE 31: Log curve fit to SV(-) wave 135°.

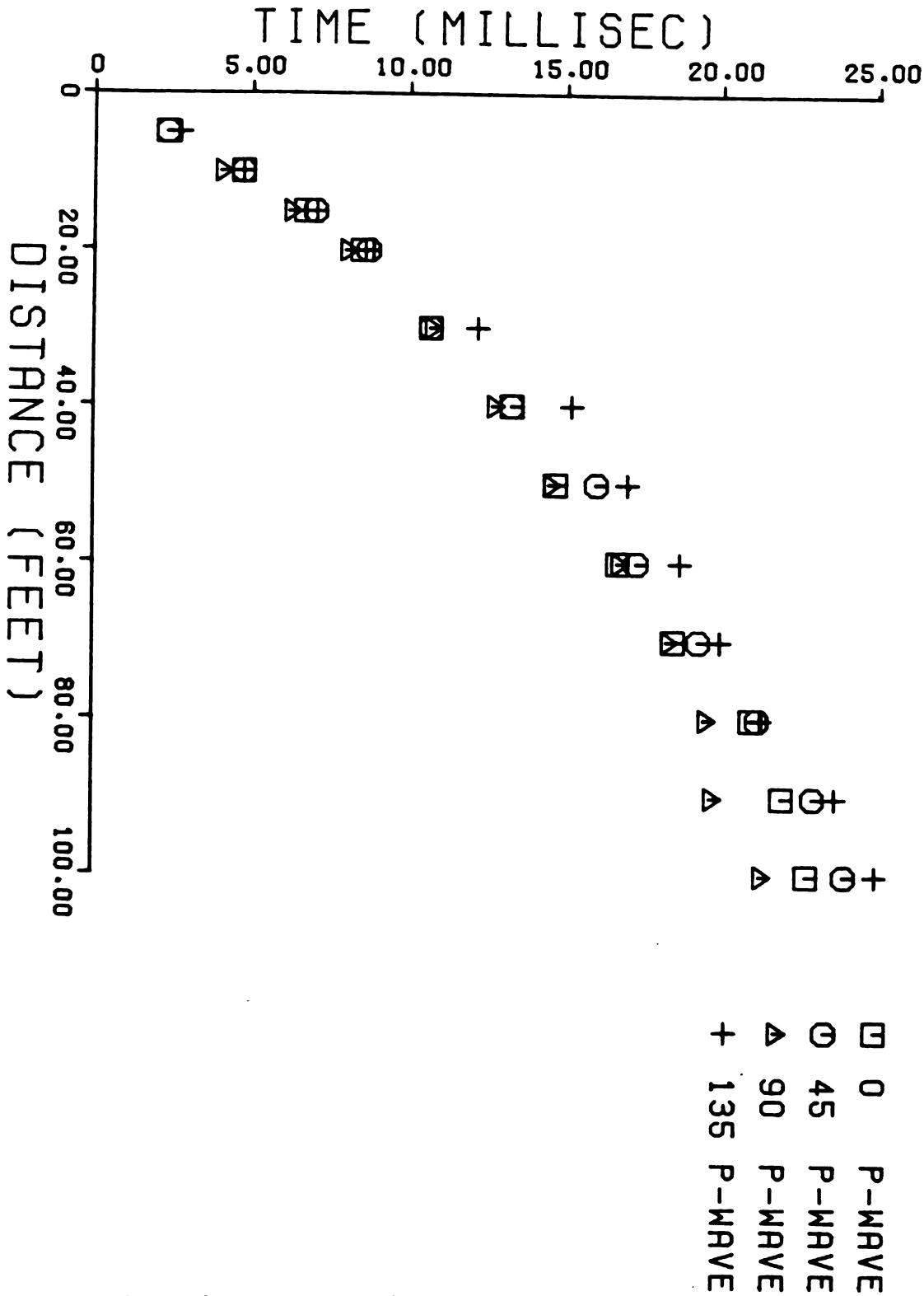


FIGURE 32: Time versus distance plots P waves.

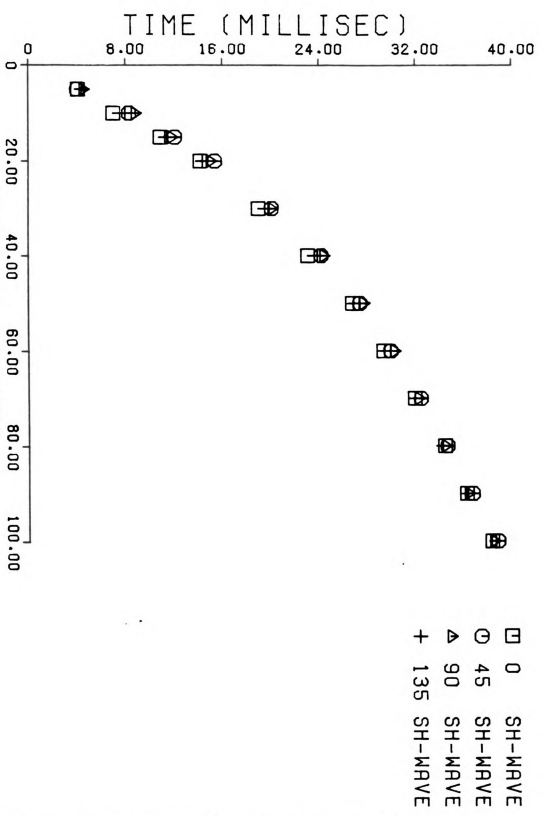


FIGURE 33: Time versus distance plots SH waves.

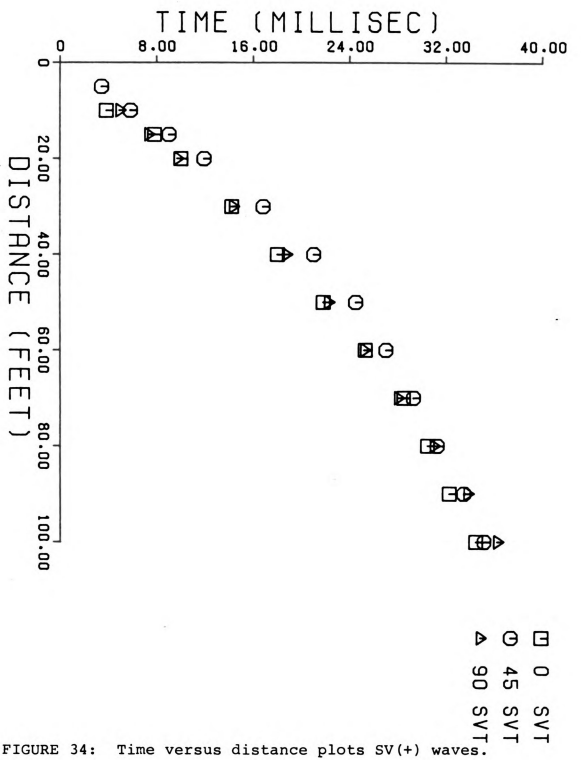


FIGURE 34: Time versus distance plots SV(+) waves.

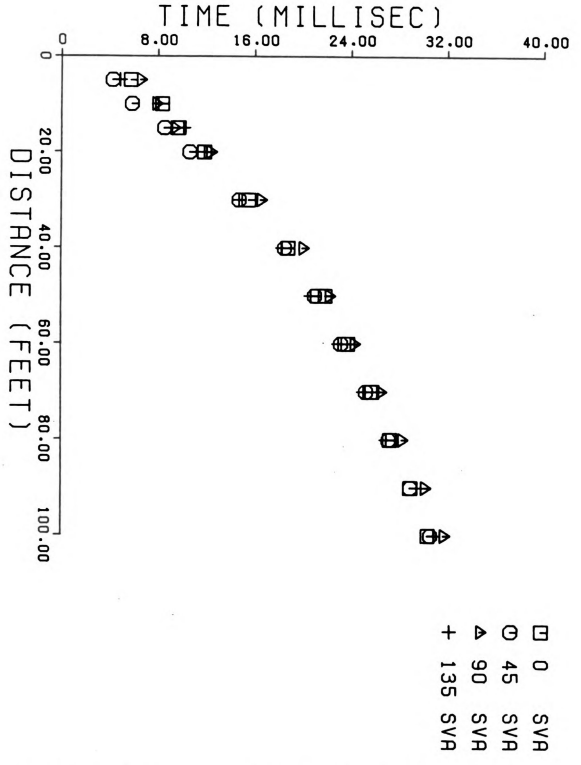


FIGURE 35: Time versus distance plots SV(-) waves.

## DEPTH OF PENETRATION

The depth of penetration for each type of seismic wave in the various directions is needed to determine velocity surfaces. The velocity surface is a diagrammatic representation of velocity versus azimuth for a given depth. The depths of penetration can be determined if the velocities and source to receiver offsets are known by applying the Wiechert, Herglotz, Bateman (WHB) integral. The WHB integral as derived from Officer (1958) is as follows:

$$Z = \frac{1}{\pi} \int_0^y \cosh^{-1}\left(\frac{V_L}{V_i}\right) dX$$

Z= depth at which velocity V is reached = depth of penetration of ray from origin to distance X

y= distance from source to receiver where V is determined

$V_L$ = velocity determined at X distance from the source

$V_i$ = velocity determined at $X_i$ distance between the source and X

A necessary condition that is imposed by this equation is that the velocity always increases at distances farther from the source. This may be determined by examination of the WHB integral. If $\frac{V_L}{V_i} < 1$, then $\cosh^{-1}\frac{V_L}{V_i}$ is undefined. The assumption of there being no velocity reversal

present seems valid for an ice shelf since the material is monominerallic and the increase of overburden with depth causes compaction which will continuously increase velocity until a maximum velocity is obtained. The depths of penetration were determined for the velocities obtained from the log curves since they provided the best fit and do not have to be forced to show no velocity reversals.

The velocities defined by the log curve fits were obtained by applying the statistics in Appendix II, Tables 22-24 to the transformed log curve equation:

$$\frac{dX}{dT} = \frac{X + c}{b}$$

The log curve velocities are listed with the appropriate depths of penetration in Appendix II, Tables 25-39.

The velocities obtained from the SV(-) data exceed the values obtained in other analysis that are much deeper in the study area. Bennett et al., (1979), determined a maximum shear wave velocity of 2073 $\pm$ 34 meters per second at a depth of 70 meters in the ice shelf. The SV(-) velocity obtains a maximum of 2100 meters per second at a depth of 11 meters in this analysis. Therefore, the SV(-) data that was picked from the seismic records is apparently another type of arrival. A PS seismic wave conversion is a possibility that might explain the high velocity observed. The SV(-) data must be rejected as being true SV wave arrivals, and the SV(+) data must be considered as the only

true SV wave arrivals in this study.

Velocity versus depth, in all four directions is plotted for each type of seismic wave in Figures 36-39.

Examination of the P wave velocity versus depth plot (Figure 36) reveal that for the last three stations the 090 direction has the highest velocity for a given depth. This observation is consistent with the time versus distance plot for P waves in Figure 32.

Examination of the SH wave velocity versus depth plot (Figure 37) shows that the data groups too closely to determine any maximum velocity direction.

THe SV(+) waves velocity versus depth plot (Figure 38) reveal the 045 direction as having the maximum velocity for a given depth.

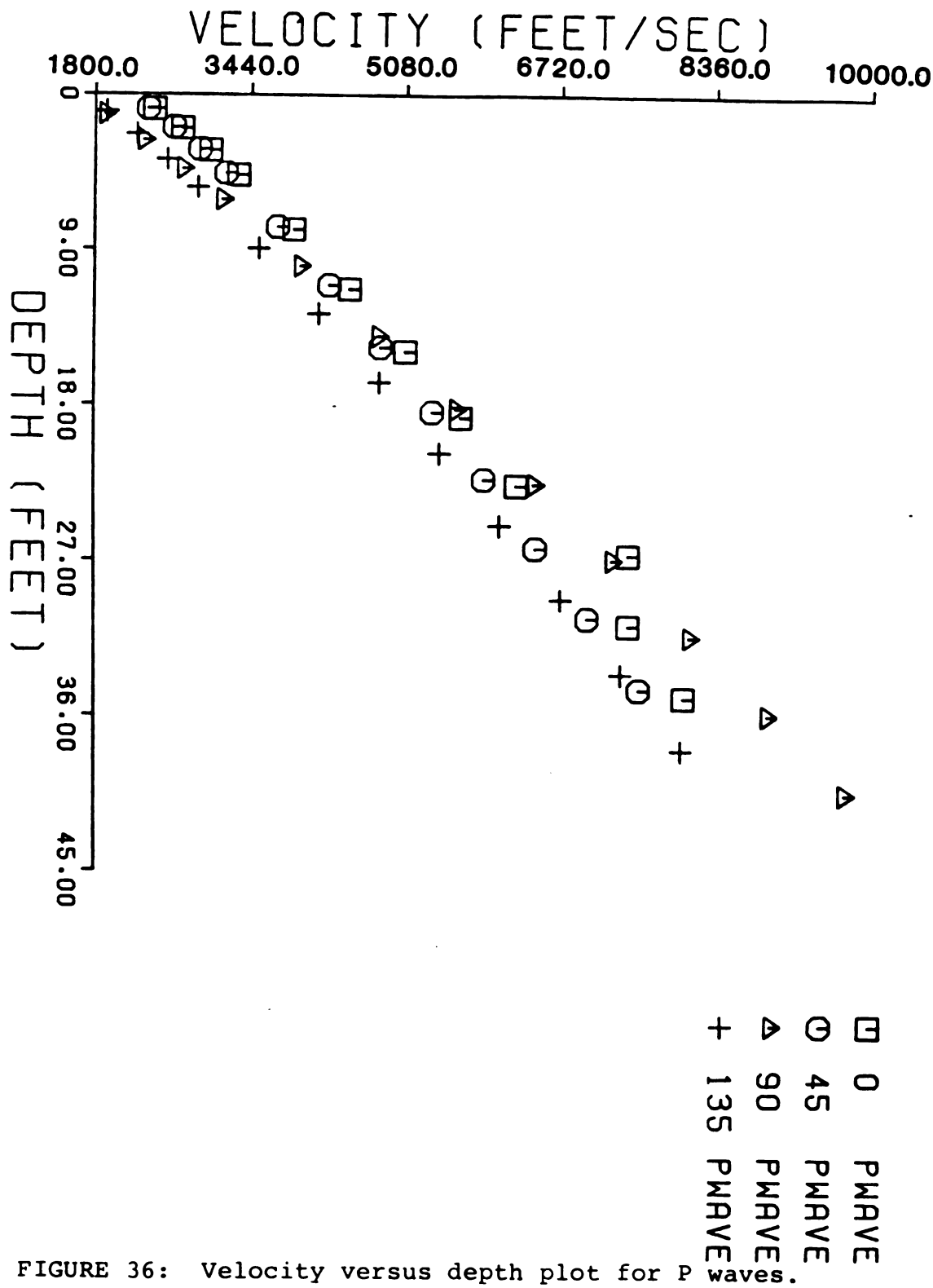


FIGURE 36: Velocity versus depth plot for P waves.

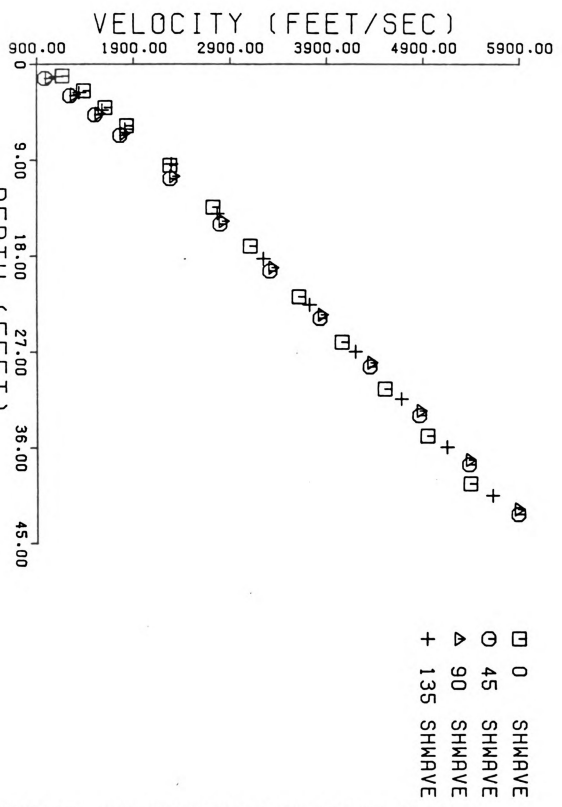


FIGURE 37: Velocity versus depth plot for SH waves.

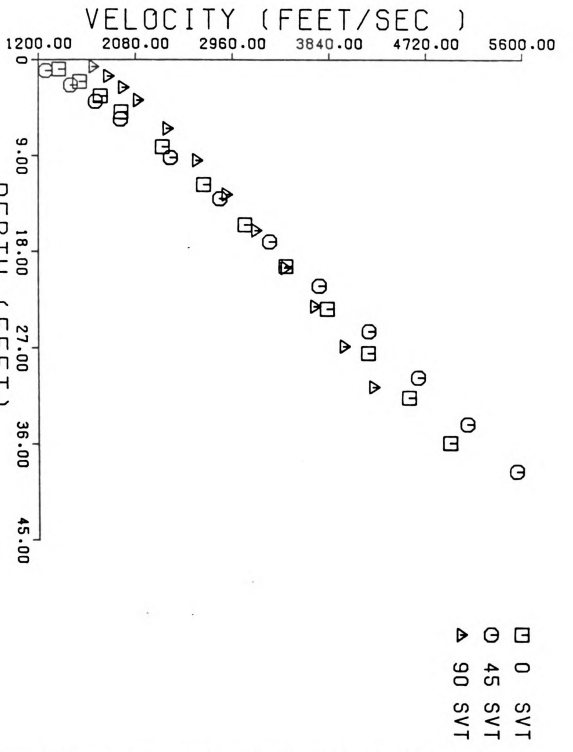


FIGURE 38: Velocity verus depth plot for SV(+) waves.

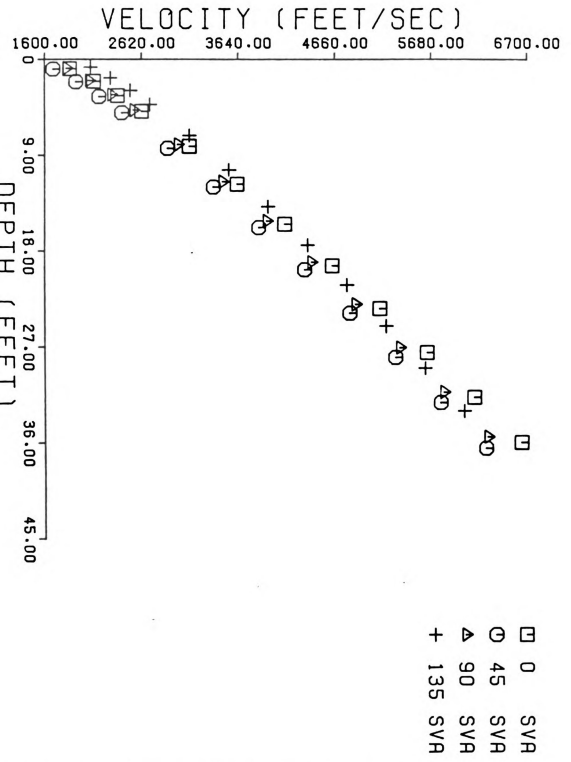


FIGURE 39: Velocity versus depth plot for SV(-) waves.

## VELOCITY SURFACES

As stated previously a velocity surface, as used here, is a diagrammatic representation of the variation of velocity versus azimuth at a particular depth. Plots of the velocity surfaces at depth intervals of 5 feet, from a depth of 5 to 40 feet, are shown for each type of seismic wave (Figures 40-43). Velocity surfaces were determined at 5 feet depth intervals to observe if a pattern of velocity anisotropy is developing with increasing depth.

Examination of the P wave velocity surfaces (Figure 40) reveal a pattern that develops from the 15 feet depth to the 40 feet depth. At a depth of 15 feet the velocity surface indicates the 000 direction to be the fastest velocity direction, but the velocity in the 090 direction has significantly increased from the 10 feet depth. The percent of velocity anisotropy is defined by the following equation:

$$\% \text{ Anisotropy} = \frac{2(\text{Vmax} - \text{Vmin})}{\text{Vmax} + \text{Vmin}}$$

The velocity surfaces at a 15 feet depth has 8.6% velocity anisotropy. The percent velocity anisotropy at the 20 feet depth is 11.9%, at the 25 feet depth is 12.1%, at the 30 feet depth is 13.6%, at the 35 feet depth is 14.5%, and at the 40 feet depth is 15.6%. Velocity anisotropy increases

continuously from 8.6% at a 15 feet depth to 15.6% at a 40 feet depth. The 090 direction (North-south) is the maximum velocity direction, the 045 and 135 directions are the minimum velocity directions, and the 000 direction is the intermediate velocity direction. The 15% difference in velocity and the centrosymmetry indicated by the proximity of velocities in the 045 and 135 directions are suggestive of velocity anisotropy.

Examination of the SH wave velocity surfaces (Figure 41) reveal a pattern that begins to develop at a deeper depth, and is not as pronounced as the pattern developed by the P waves. At a depth of 5 feet the maximum velocity direction for the SH waves is 000, and the percent anisotropy is 11%. This high value is presumed to be due to local heterogeneity of the shallow portion of the near surface layers. The percent anisotropy decreases from the 5 feet depth to the 25 feet depth. At the 30 feet depth a pattern begins to emerge in the velocity surface with 090 again being the maximum velocity direction, 045 and 135 being intermediate velocity directions, and 000 being the minimum velocity direction. This pattern is enhanced at the 35 and 40 feet depth velocity surfaces, with anisotropy increasing. The velocity anisotropy is 2.6% at the 30 feet depth, 3.5% at the 35 feet depth, and 3.9 % at the 40 feet depth. The difference in velocity is not as great for the SH waves as for the P waves. However,

it should be noted that the 045 and 135 directions are again very close in value indicating the probable existence of centrosymmetry in the velocity distribution.

Examination of the velocity surfaces of the SV(+) waves (Figure 42) reveal a pattern that begins developing at the 20 feet depth, and continues to the 40 feet depth. The 045 direction is the maximum velocity direction, the 000 direction is the intermediate velocity direction, and the 090 direction is the direction of minimum velocity. Percent anisotropy increase from 3.8% at a 20 feet depth, to 15.6% at a 40 feet depth. The 135 direction has no information since the raw records were not obtainable for that event. The lack of data in the 135 direction is the reason why centrosymmetry is not observable in the SV(+) velocity surfaces.

The SV(-) wave velocity surfaces are plotted in Figure 43. It is important to remember that although this data is being referred to as SV waves, it is apparently another type of arrival. The percent anisotropy of the SV(-) velocity surfaces almost continuously decreases from 15% at the 5 feet depth, to 7.2% at the 40 feet depth. This pattern is contrary to the patterns observed for the other three types of seismic waves. Note that there is no correlation between the SV(-) and the SV(+) velocity surfaces. This further supports the observation that the SV(-) waves are really another type of seismic arrival.

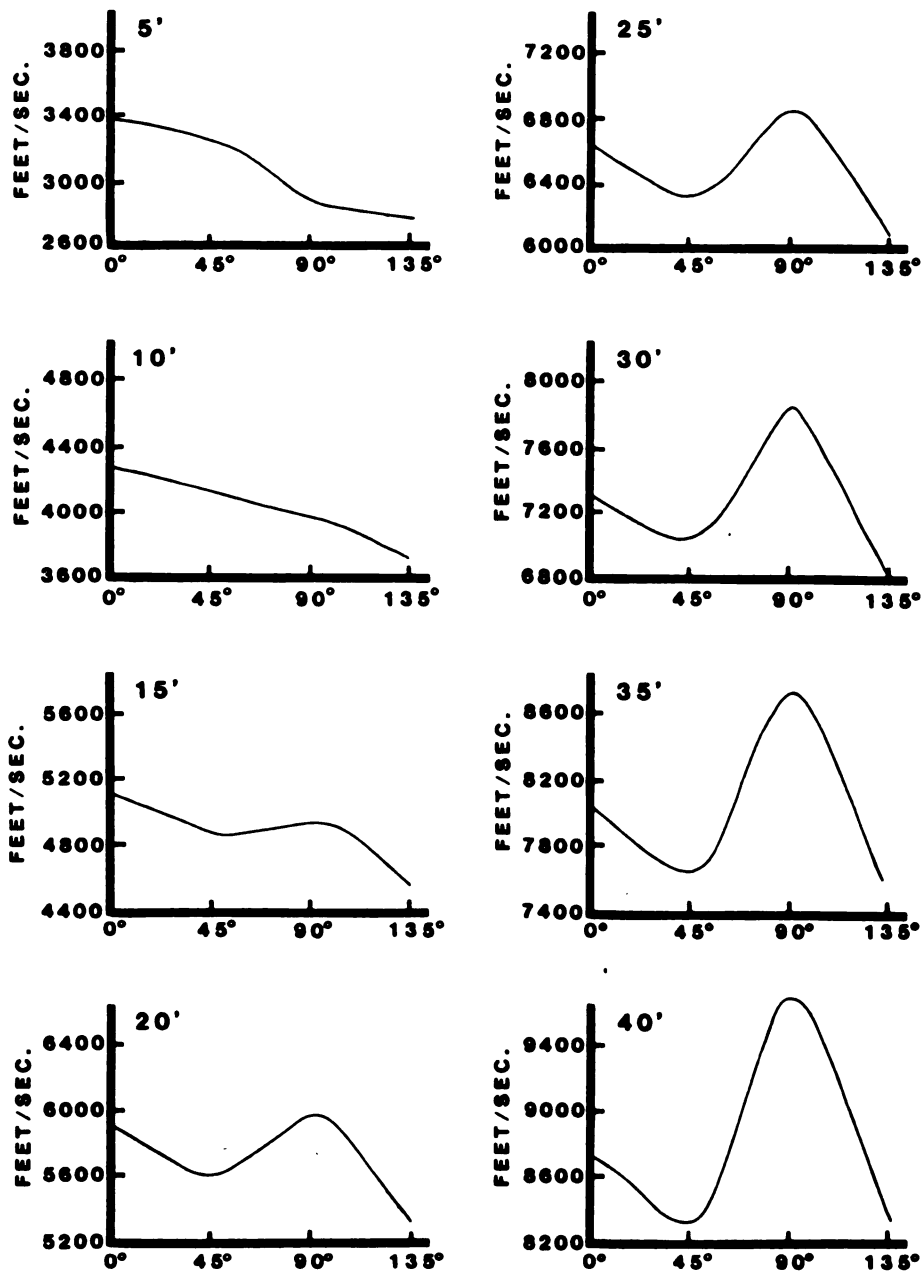


FIGURE 40: Velocity surfaces for P waves.

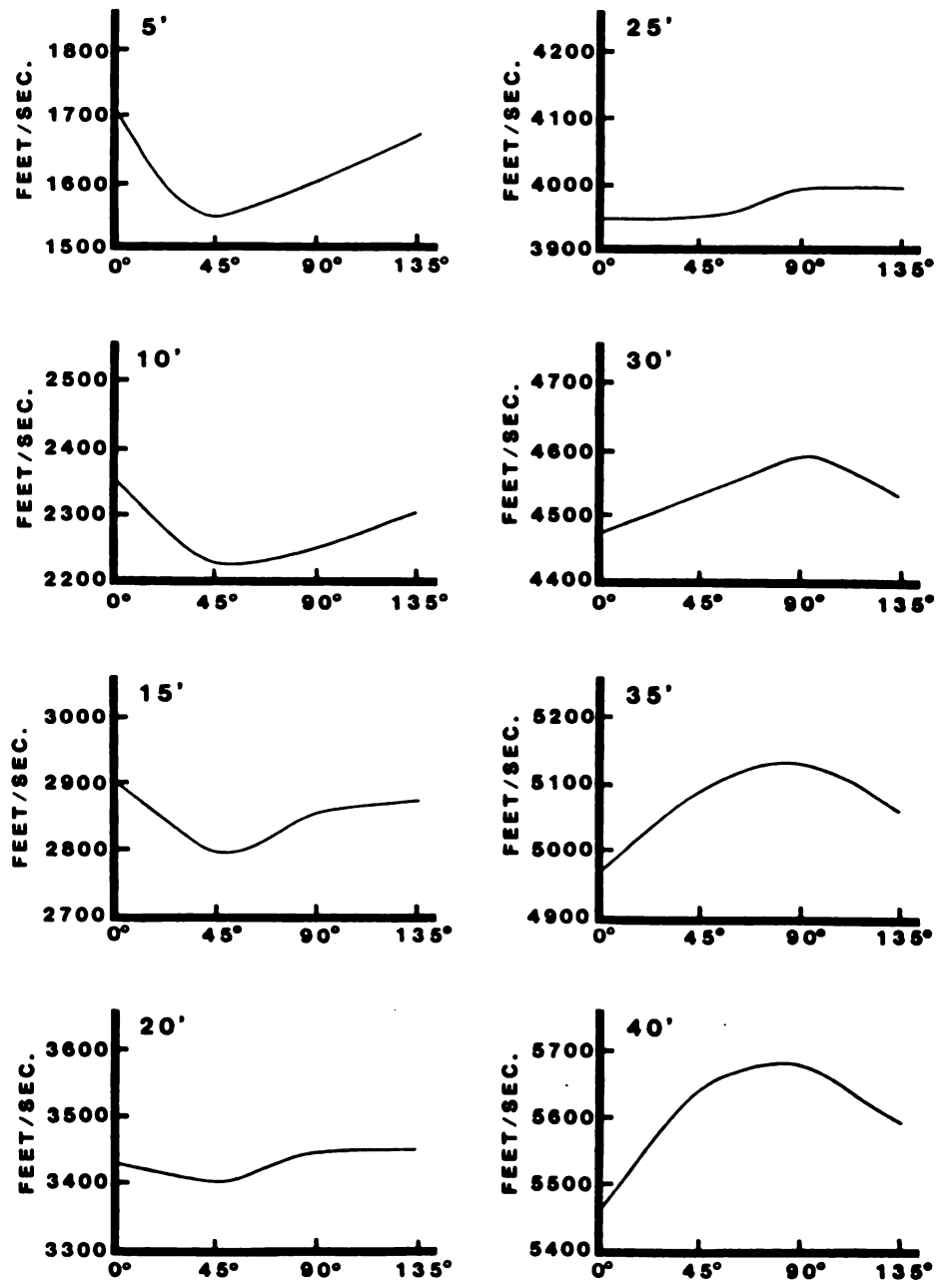


FIGURE 41: Velocity surfaces for SH waves.

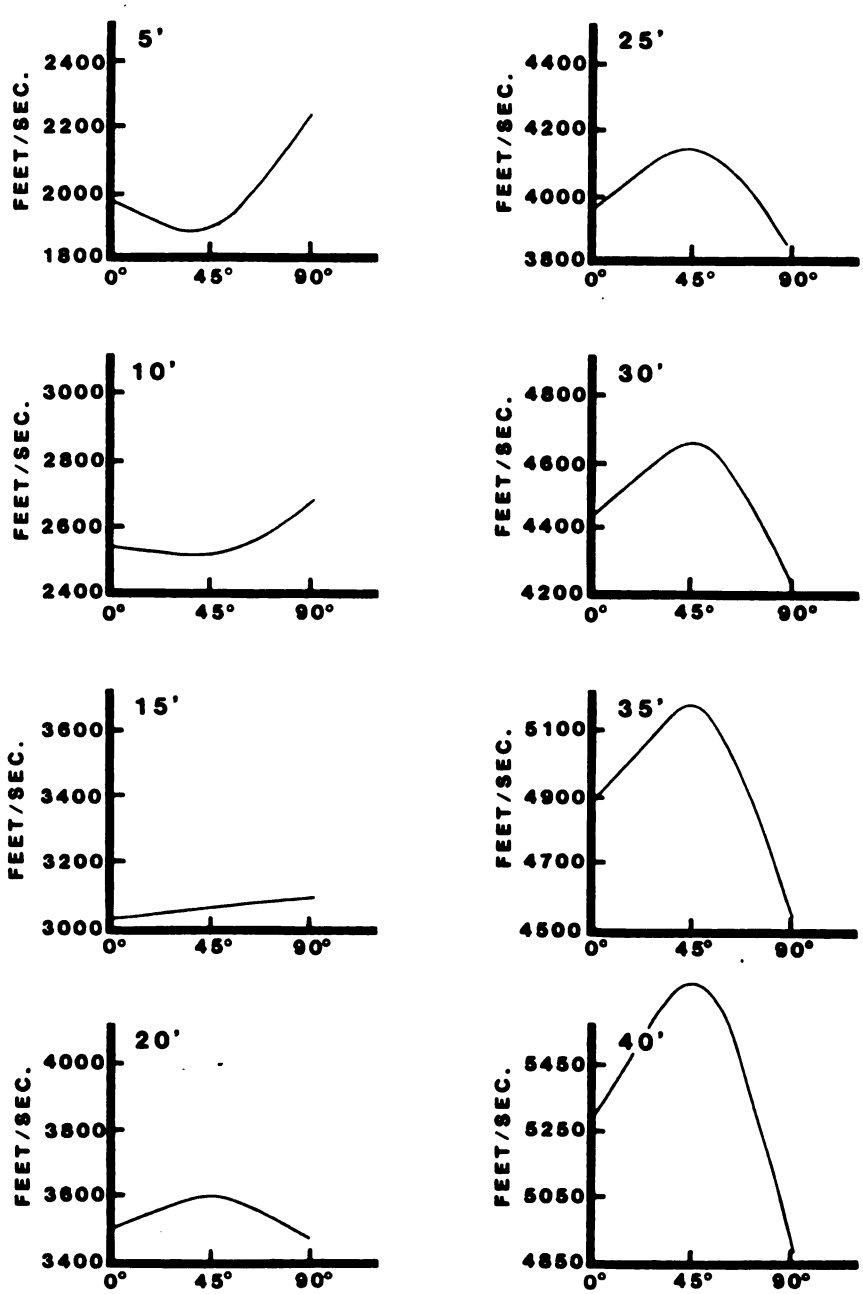


FIGURE 42: Velocity surfaces for SV(+) waves.

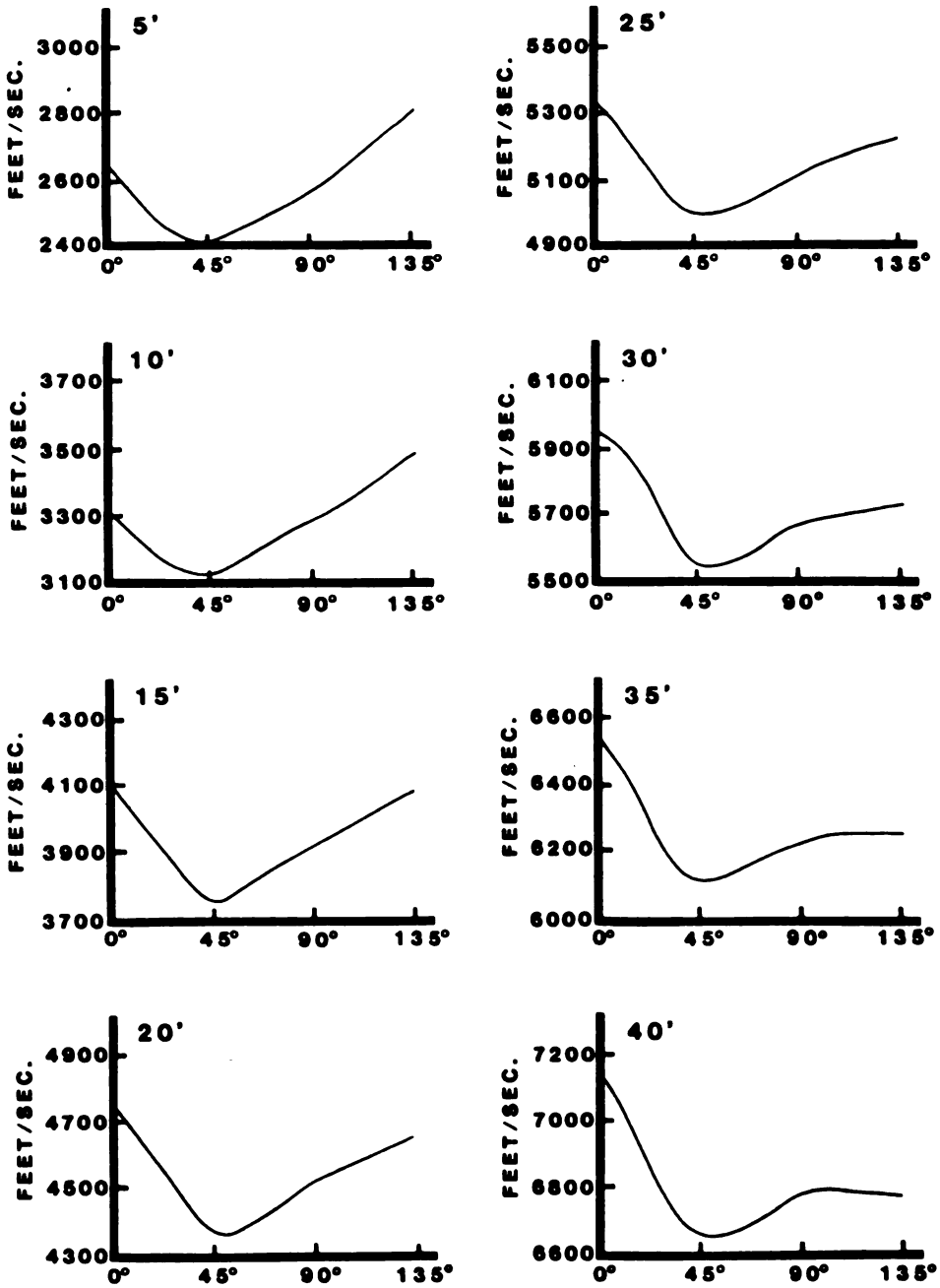


FIGURE 43: Velocity surfaces for SV(-) waves.

In the Anisotropic Model section an attempt is made to match the observed velocity surfaces with velocity surfaces determined for a theoretical model.

## ENERGY RADIATION

Anisotropic media will radiate a uniform stress in a non-uniform manner, and this energy radiation pattern will correspond to the wave surface for this media (Bennett, 1968). Furthermore, it has been shown that for the transversely isotropic single ice crystal, the wave and velocity surfaces are almost identical for P and SH waves, and vary by 6% at most for SV waves (Bennett, 1968). Therefore, if the near surface layers of the ice shelf are truely anisotropic the energy radiation pattern should bare a resemblance to the observed velocity surfaces. If the near surface layers are not anisotropic, but instead exhibit velocity variations due to directional heterogeneity, then the energy radiation patterns should not resemble the velocity surfaces.

Analysis of the seismic events of the long spread surveys, which analyze the deeper zones of the study area, were undertaken in another study (Wanslow, 1981). These results indicate that the directions of maximum energy radiation for SH waves were 045, 135, 225 and 315. These directions correspond to the maximum velocity directions of the SH waves determined by others (Bennett et al., 1979).

The short spread seismic events in this study were

analyzed to determine energy radiation patterns by using a series of programs developed by Mark Schoomaker in 1978-1979.

Waveforms are first removed from specific traces of a seismic event by using the Tektronix program Processor. The waveform removed starts at the beginning of the first arrival for each trace. The program Finale is then used on the extracted waveform to perform a fast Fourier transform. The program then plots the amplitude and phase spectrum for each waveform. The plot of the amplitude spectrum is used to determine the frequency band over which the waveform is to be integrated. This frequency band is then fed back into the Finale program and the waveforms are integrated within the specified limits. Logarithms of the integrated values of energy are listed in Appendix IV, Tables 40-41.

Logs of the integrated values of energy are plotted versus distance (Figures 44-45). Energy radiation data was not determined for the SV waves. The log of the energy values is used since there is sometimes a difference of four orders of magnitude between energy arrivals at 10 feet and at 100 feet.

Examination of the P wave energy radiation plots (Figure 44) reveal that 090 is the direction of maximum energy radiation from 60 to 100 feet. This corresponds to the maximum velocity direction for P waves as defined by the velocity surfaces.

Examination of the SH wave energy radiation plots (Figure 45) reveal that the 045, 090, and 135 directions, from 60 to 100 feet, are grouped together, having higher energy radiation values than the 000 direction. This observation is consistent with the velocity surfaces of SH waves which show a minimum velocity at the 000 direction, with the other three directions falling within 100 feet per second of each other.

The correlation between the determined energy radiation patterns and the velocity surfaces indicate that the near surface layers of the ice shelf in the study area are demonstrating some form of seismic anisotropy as opposed to having directional heterogeneity alone.

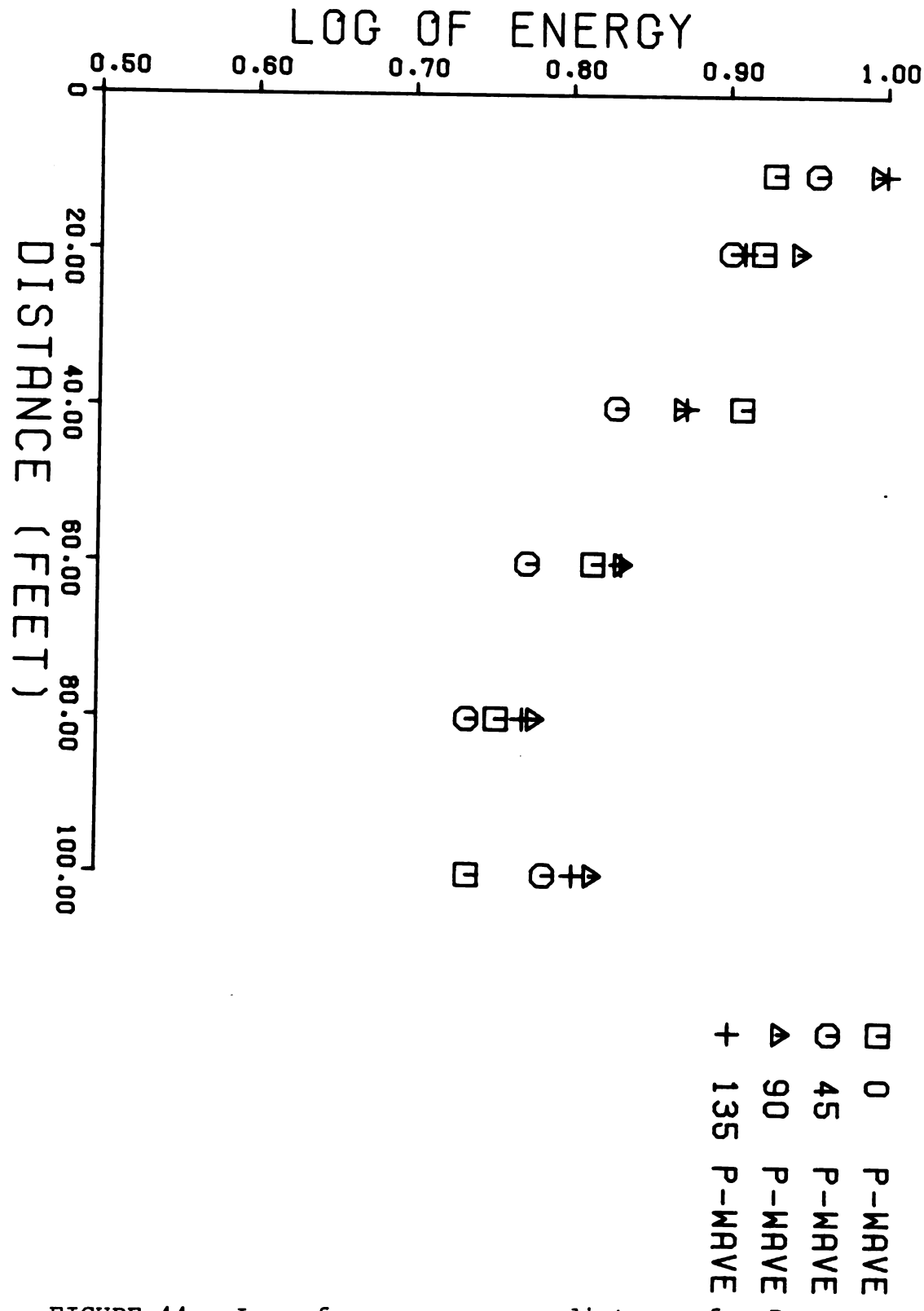


FIGURE 44: Log of energy versus distance for P waves.

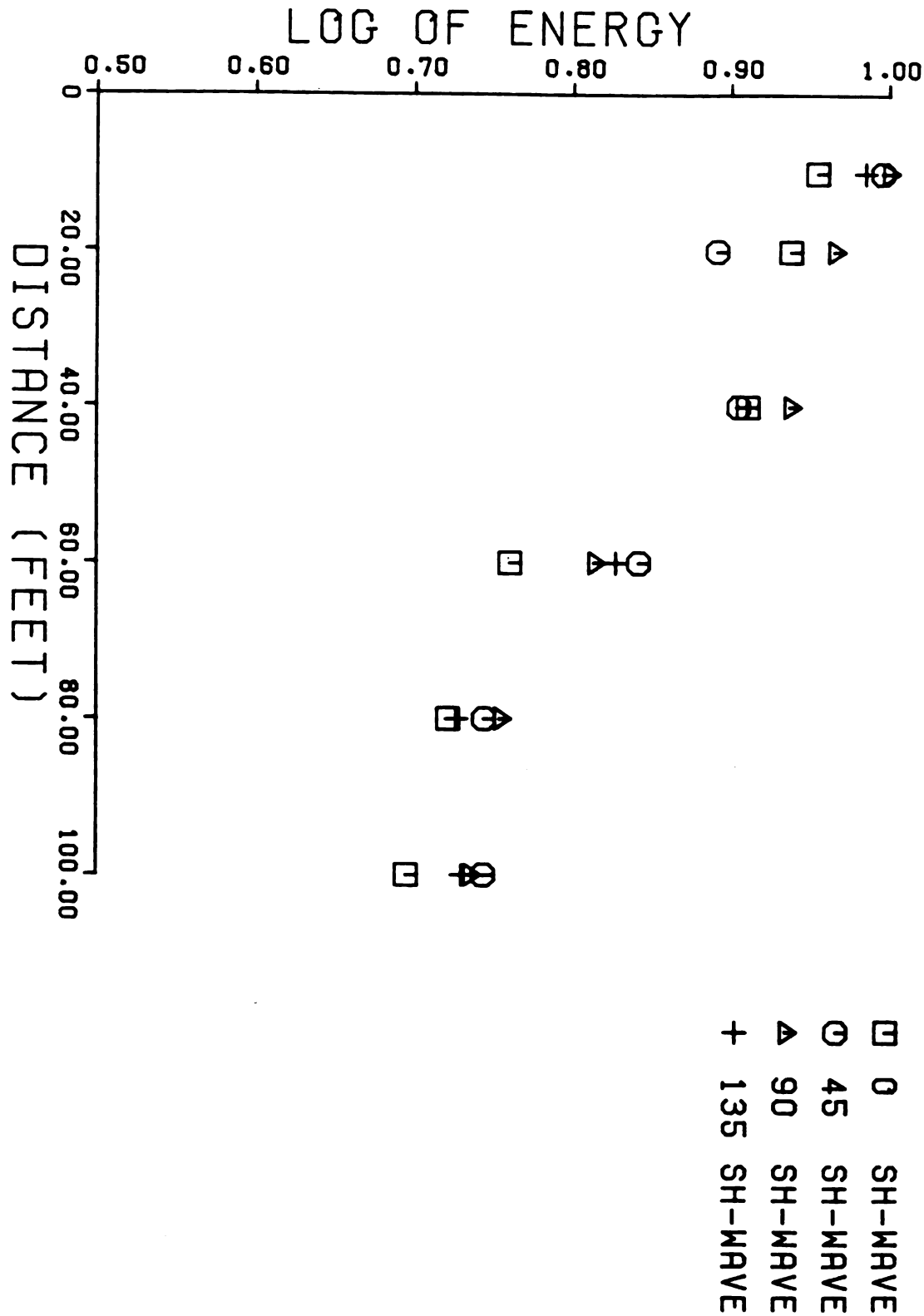


FIGURE 45: Log of energy versus distance for SH waves.

# Chapter 6

## COMPARISON TO DEEPER ANISOTROPY

In order to determine if the anisotropy that is being observed in the near surface layers is the same as the anisotropy observed in the deeper zones of the ice shelf a comparison of the short and long spread analyses was made.

The long spread seismic lines contain data from the deeper zones of the ice shelf in the study area and were analyzed by Bennett and others. The results of their studies indicate that P wave velocities varied with direction but displayed no centrosymmetry. The SH wave velocities showed centrosymmetry and were grouped in two orthogonal sets. One set had SH velocities of 1853 $\pm$ 28 meters per second in the north, south, east, and west directions. The other set had SH velocities of 2073 $\pm$ 34 meters per second in the 45 degree directions. This data was interpreted as being consistent with a model having a strong ice crystal C-axis oriented in an east-west horizontal direction.

Further study of the long spread lines revealed energy radiation patterns consistent with the analysis of the SH waves (Communication with Mark Schoomaker).

A major difference that can be found between the

analyses of the long and short spread seismic lines is the P wave information. In the short spread analysis of this study the P wave velocities not only showed a variation with direction, but also showed some degree of centrosymmetry. A complete 360 degree short spread seismic survey might have developed this centrosymmetry further. This difference between the P waves of the two surveys suggests that some form of anisotropy other than crystal orientation is occurring in the near surface layers. This is consistent with the idea that the upper firn layers of ice shelfs usually exhibit a random orientation of the ice crystals which compose them (Bennett, 1968).

Comparison of the SH wave analyses show some correlation in that the 045 and 135 directions of the short spread seismic lines are high in velocity and approximately the same. However, the 090 direction of the short spread lines is the maximum velocity direction and is not so in the long spread lines.

Furthermore, the P wave velocity anisotropy observed in this study is 15.6%. The P wave velocity anisotropy of a single ice crystal is only about 7% (Bennett, 1968). This observation adds more support to the idea that the anisotropy of the surface layers in the study are is not due to any orientation of the ice crystals.

# Chapter 7

## ANISOTROPIC MODEL

In the method of Postma (1955) a theoretical model was derived jointly by myself and Dr. H.F. Bennett that explains the anisotropy observed in the near surface layers. Postma showed that "a periodic structure of alternating plane, parallel, isotropic, and homogeneous elastic layers can be replaced by a homogeneous, transversely isotropic material, as far as it's gross-scale elastic behavior is concerned". Postma achieved this result by deriving the elastic moduli for the equivalent transversely isotropic material, from the elastic properties and thicknesses of the two individual isotropic layers. This derivation was performed by applying stress-strain relationships.

The model developed in this study is similar to Postma's model. The theoretical model consists of a combination of two separate materials as shown in Figure 46. Each material is isotropic unto itself, but has elastic properties which differ from the other. The model is based on the presence of oriented sastrugi interlayered with snow in the study area. The ridges of sastrugi have been hardened into an ice-like material by wind action and have greater velocities than the snow in betweeen the ridges. It is

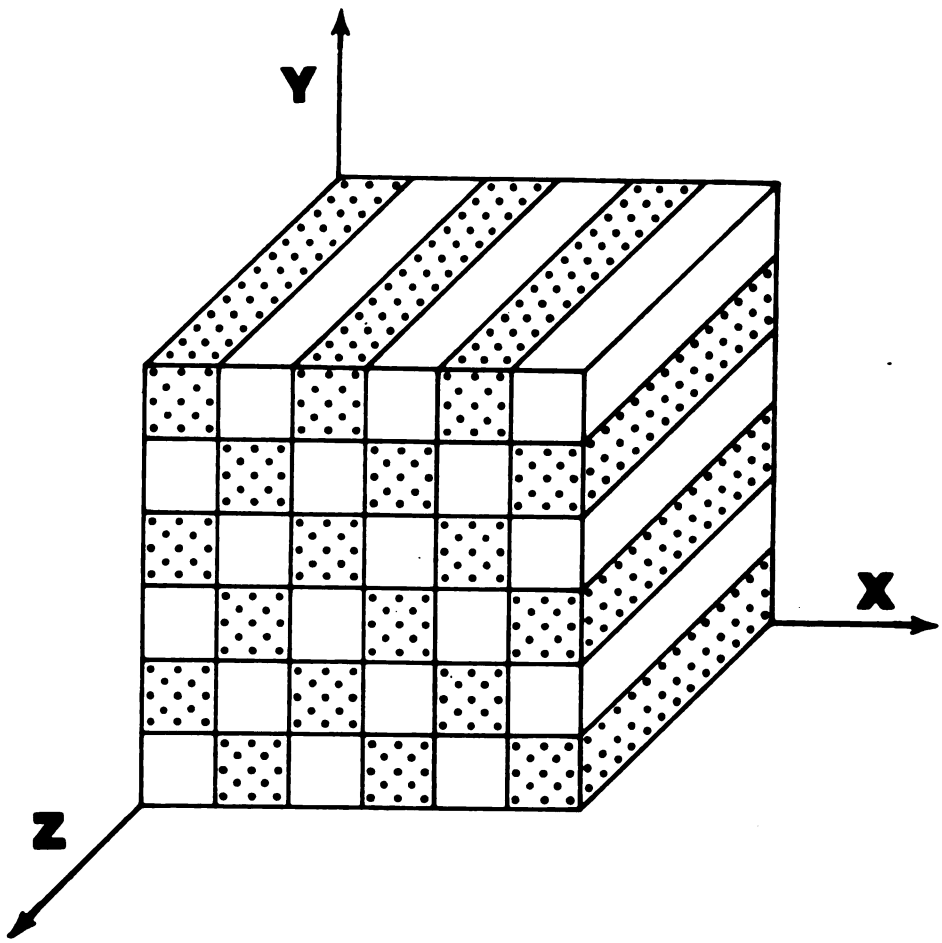


FIGURE 46: Elemental volume of theoretical model material.

probable that the layering of snow and sastrugi is repetitive to at least the 40 feet depth of penetration of the short spread seismic lines.

The following notation, adapted from Love (1944), is used in the equations on the following pages to derive the elastic moduli of an elemental volume of the material:

Xx= the normal component of the stress across a surface element perpendicular to the X-axis (Normal stress)

Yz= the tangential component parallel to the Y-axis of the stress across a surface element perpendicular to the Z-axis (Shear stress)

exx = the linear dilatation of line elements in the direction of the X-axis in the unstrained state (Normal strain)

eyz = the decrease of the angle between two line elements which are parallel to the Y and Z axes in the unstrained state (Shear strain)

Cij = elastic moduli of isotropic material number one

C'ij = elastic moduli of isotropic material number two

Subscripts attached to the end of stress and strain variables denote the stresses and strains for isotropic materials one and two, respectively.

The stress-strain relationships in a homogeneous transversely isotropic material are as follows:

$$Xx = C11\ exx + C12\ eyy + C13\ ezz + \ldots$$

$$Yy = C21\ exx + C22\ eyy + C23\ ezz + \ldots$$

$$Zz = C31\ exx + C32\ eyy + C33\ ezz + \ldots$$

$$Yz = \ldots + C44\ eyz \ldots$$

$$Zx = \ldots + \ldots + C55\ ezx$$

$$Xy = \ldots + \ldots + \ldots + C66\ exy$$

For a transversely isotropic material the elastic parameters are reduced to five independent elastic moduli that are arranged into the following array:

$$\begin{bmatrix} C11 & C12 & C13 & 0 & 0 & 0 \\ C12 & C11 & C13 & 0 & 0 & 0 \\ C13 & C13 & C33 & 0 & 0 & 0 \\ 0 & 0 & 0 & C44 & 0 & 0 \\ 0 & 0 & 0 & 0 & C44 & 0 \\ 0 & 0 & 0 & 0 & 0 & \frac{C11 - C12}{2} \end{bmatrix}$$

For isotropic material there are only two independents elastic moduli, where C11= C33, C12= C13, and C44= $\frac{C11-C12}{2}$.

To derive the elastic moduli for the model material of Figure 46 the normal stress-strain relationships are first established. It is required that the normal stress on the Z face of the elemental volume (Zz), vary in such a way that the normal strains are the same for the two different isotropic materials. The other two normal stresses, Xx and Yy, do not vary, so the normal strains for these stresses are not equal for the two different isotropic materials. Using these requirements the normal stress-strain relationships are as follows:

(1) Xx1 = C11 exx1 + C12 eyy1 + C12 ezz1

(2) Xx2 = C'11 exx2 + C'12 eyy2 + C'12 ezz2

(3) Yy1 = C12 exx1 + C11 eyy1 + C12 ezz1

(4) Yy2 = C'12 exx2 + C'11 eyy2 + C'12 ezz2

(5) $Zz1 = C12\ exx1 + C12\ eyy1 + C11\ ezz1$

(6) $Zz2 = C'12\ exx2 + C'12\ eyy2 + C'11\ ezz2$

Where,

(7) $Xx = Xx1 = Xx2$

(8) $Yy = Yy1 = Yy2$

(9) $Zz = \frac{Zz1 + Zz2}{2}$ ; $Zz1 \neq Zz2$

(10) $exx = \frac{exx1 + exx2}{2}$ ; $exx1 = 2exx - exx2$

(11) $eyy = \frac{eyy1 + eyy2}{2}$ ; $eyy1 = 2eyy - eyy2$

(12) $ezz = ezz1 = ezz2$

Substituting the equivalents for exx1 and eyy1, from equations 10 and 11 respectively, into equations 1-4, and reducing the equations, the following values for exx2 and eyy2 are obtained:

(13) $$exx2 = \frac{[(C11 + C'11) - (C12 + C'12)]\ (C12 - C'12)ezz}{D} + \frac{2[C11(C11 + C'11) - C12(C12 + C'12)]exx}{D} + \frac{2[C12(C11 + C'11) - C11(C12 + C'12)]eyy}{D}$$

(14) $$eyy2 = \frac{[(C11 + C'11) - (C12 + C'12)]\ (C12 - C'12)ezz}{D} + \frac{2[C12(C11 + C'11) - C11(C12 + C'12)]exx}{D} + \frac{2[(C11(C11 + C'11) - C12(C12 + C'12)]eyy}{D}$$

Where $D = (C11 + C'11)^2 - (C12 + C'12)^2$

Substituting the values obtained in equations 13 and 14

into equations 5 and 6, and then solving for equation 9, the following equation is obtained after collecting terms:

$$(15)\quad Zz = ezz\left(\frac{C11 + C'11}{2} - \frac{(C'12 - C12)^2}{C11 + C'11 + C12 + C'12}\right) + (exx + eyy)\left(\frac{C11\ C'12 + 2C12\ C'12 + C'11\ C12}{C11 + C'11 + C12 + C'12}\right)$$

Substituting equations 13 and 14 into equations 2,4 and collecting terms produces the following equations:

$$(16)\quad Xx = ezz\left(\frac{C11\ C'12 + 2C12\ C'12 + C'11\ C12}{C11 + C'11 + C12 + C'12}\right) + exx\left(2\left(\frac{(C11\ C'11 + C12\ C'12)\ (C11 + C'11)}{D}\right)\right) - exx\left(2\left(\frac{(C'11\ C12 + C11\ C'12)\ (C12 + C'12)}{D}\right)\right) + eyy\left(2\left(\frac{(C'11\ C12 + C11\ C'12)\ (C11 + C'11)}{D}\right)\right) - eyy\left(2\left(\frac{(C11\ C'11 + C12\ C'12)\ (C12 + C'12)}{D}\right)\right)$$

$$(17)\quad Yy = ezz\left(\frac{(C11\ C'12 + 2C12\ C'12 + C'11\ C12)}{C11 + C'11 + C12 + C'12)}\right) + exx\left(2\left(\frac{(C'11\ C12 + C11\ C'12)\ (C11 + C'11)}{D}\right)\right) - exx\left(2\left(\frac{(C11\ C'11 + C12\ C'12)\ (C12 + C'12)}{D}\right)\right) + eyy\left(2\left(\frac{(C11\ C'11 + C12\ C'12)\ (C11 + C'11)}{D}\right)\right) - eyy\left(2\left(\frac{(C'11\ C12 + C11\ C'12)\ (C12 + C'12)}{D}\right)\right)$$

The formulas in equations 15-17 were verified for the isotropic case by letting $C11 = C'11$, and $C12 = C'12$.

The shear stress-strain relationships must now be developed to obtain the remaining elastic moduli. On the face of the elemental volume perpendicular to the Z-axis it is required that the stress vary across the face in order to insure constant strain. This leads to the following equations:

(18) $Yz1 = C44 \; eyz$

(19) $Yz2 = C'44 \; eyz$

Where,

(20) $Yz1 \neq Yz2 \quad ; \; Yz = \frac{Yz1 + Yz2}{2}$

(21) $eyz = eyz1 = eyz2$

Substituting equations 18 and 19 into equation 20 the following equation is obtained:

(22) $Yz = \left( \frac{C44 + C'44}{2} \right) \; eyz$

Proceeding for the other shear stress, Xy, on the face of the elemental volume perpendicular to the Y-axis, the strain varies across the face and stress remains constant and the following results are obtained:

(23) $Xy = Xy1 = C44 \; exy1 = Xy2 = C'44 \; exy2$

Where,

(24) $exy \neq exy1 \neq exy2 \quad ; \quad exy = \frac{exy1 + exy2}{2}$

(25) $Xy = \left( \frac{2C44 \; C'44}{C44 + C'44} \right) \; exy$

Using the results obtained in equations 15, 16, 17, 22 and 29, we can determine the elastic moduli for the

transversely isotropic model material. The elastic moduli are as follows:

$$(26)\quad \bar{C}33 = \frac{C11 + C'11}{2} - \frac{(C'12 - C12)^2}{C11 + C'11 + C12 + C'12}$$

$$(27)\quad \bar{C}13 = \frac{C11\ C'12 + 2C12\ C'12 + C'11\ C12}{C11 + C'11 + C12 + C'12}$$

$$(28)\quad \bar{C}11 = 2\left(\frac{(C11\ C'11 + C12\ C'12)\ (C11 + C'11)}{D} - \frac{(C'11\ C12 + C11\ C'12)\ (C12 + C'12)}{D}\right)$$

$$(29)\quad \bar{C}12 = 2\left(\frac{(C'11\ C12 + C11\ C'12)\ (C11 + C'11)}{D} - \frac{(C11\ C'11 + C12\ C'12)\ (C12 + C'12)}{D}\right)$$

$$(30)\quad \bar{C}44 = \frac{C44 + C'44}{2} = \bar{C}55$$

$$(35)\quad \bar{C}66 = \frac{2C44\ \ C'44}{C44\ + C'44} = \frac{\bar{C}11 - \bar{C}12}{2}$$

Where $\bar{C}ij$ = elastic moduli of component model.

In order to compare the theoretical model to the anisotropy observed in the study the velocity surfaces for the theoretical model must be obtained. This can be done by selecting values for the elastic moduli of the two different isotropic materials in the model and using the velocity equations derived for transversely isotropic material by Bennett (1968). The velocity equations are as follows:

$$(32)\quad V_{1,2}^2 = \left(\frac{(\bar{C}11 + \bar{C}44)}{2p}\right)\sin^2 @ + \left(\frac{(\bar{C}33 + \bar{C}44)}{2p}\right)\cos^2 @ + \left[\left(\left(\frac{(\bar{C}11 - \bar{C}44)}{2p}\right)\sin^2 @ - \left(\frac{(\bar{C}33 - \bar{C}44)}{2p}\right)\cos^2 @\right)^2 + \left(\frac{(\bar{C}13 + \bar{C}44)}{p}\right)^2 \sin^2 @ \cos^2 @\right]^{1/2}$$

$$(33)\quad V_3^2 = \left(\frac{\bar{C}66}{p}\right)\sin^2 @ + \left(\frac{\bar{C}44}{p}\right)\cos^2 @$$

$V_1$ = P wave velocity

$V_2$ = SH wave velocity

$V_3$ = SV wave velocity

$p$ = density

$@$ = angle between propagating wave and the Z-axis

For P wave propagation parallel to the Z-axis equation 32 reduces to this:

$$(34)\quad V_1^2 = \frac{\bar{C}33}{p}$$

For SV wave propagation parallel to the Z-axis equation 33 reduces to this:

$$(35)\quad V_3^2 = \frac{\bar{C}44}{p}$$

Equations 34 and 35 hold for isotropic material, with

$$\bar{C}66 = \frac{\bar{C}11 - \bar{C}12}{2}$$

It is assumed that the density for both materials in

the model is equal to one in order to eliminate this variable from the equations. The Poisson's ratio can be determined from the equations below using the ratio of P wave to SH velocity at the 40 feet depth in the 090 direction of the survey:

$$R^2 = \frac{2\,(P - 1)}{2P - 1} \quad ; \quad P = \text{Poisson's Ratio}$$

Where,

$$R = \frac{Vp}{Vs} = 1.65 \quad ; \quad P = .21$$

A ratio of the velocities between the two different isotropic materials which composes the model were determined by iterative modeling. The Basic program listed in Appendix V was used to find the ratio which gave the model a percent anisotropy similar to the observed P wave anisotropy of the study. A ratio of 1.83 yielded a P wave percent anisotropy of 15.6% for the model. Therefore,

$$\frac{Vp'}{Vp} = \frac{Vs'}{Vs} = 1.83$$

Where,

Vp' = P wave velocity for material one

Vs' = SH wave velocity for material one

Vp = P wave velocity for material two

Vs = SH wave velocity for material two

The velocities for each isotropic material in the model were again determined by iterative modeling. The

velocities which yielded the closest match to the fastest P wave velocities observed in the study are listed below:

| | | | |
|---|---|---|---|
| Material One: | Vp' | = 12,290 | ft./sec. |
| | Vs' | = 7,446 | ft./sec. |
| Material Two: | Vp | = 6,716 | ft./sec. |
| | Vs | = 4,069 | ft./sec. |

The faster velocity for material one approximate the velocities determined for ice crystals and ice sheets, and the slower velocity of material two approximate the velocities for snow layers (Bennett, 1968; Bentley, 1972).

The computer program takes the above input and determines the independent elastic moduli for each istropic material using equations 34 and 35. The program then substitutes these elastic moduli into equations 26-31, and then determines the elastic moduli of the transversely isotropic model material. Substituting these values into equations 32 and 33, the velocity surfaces for the three types of seismic body waves are determined.

The velocities for each type of seismic wave for the model are listed in Appendix VI, Table 42. The velocities are determined for different angles of propagation relative to the Z-axis of the model. The theoretical and observed velocity surfaces are compared by aligning the Z-axis of the model with the north-south (090) orientation of the survey and then plotting.

The P wave velocity surfaces for the model and those observed in the study are plotted in Figure 47 and show good correlation. The 090 direction is the maximum on both velocity surfaces with the other directions being lower. This indicates that the 090 direction, or north-south orientation in the survey, is parallel to the axis of symmetry of a transversely isotropic material. The Z-axis is horizontal and north-south in orientation. This is the direction which is parallel to the major axis of the sastrugi in the area. The percent anisotropy of the observed and theoretical P wave velocity surfaces are both 15.6%. The P wave arrivals in the survey are the most reliable of the three wave types due to the strength and high velocity of the P waves.

The SH wave velocity surfaces are plotted in Figure 48 and do not show a good correlation between the observed and the model. The model velocity surface is more cuspate than the observed surface. The percent anisotropy of the model is also higher than the observed at 7.4% and 3.9%, respectively. The SH arrivals are not as reliable as the P wave arrivals due to the weaker strength and slower velocities of the SH waves.

The SV wave theoretical and the observed SV(+) wave velocity surfaces are plotted in Figure 49 and also show a poor correlation. The observed velocity surface is more cuspate than the model velocity surface. As a result the

percent velocity anisotropy for the observed is much higher than the model at 15.6% and 1.8% respectively. The SV wave arrivals are probably the least reliable arrival of the three wave types. This is due to the SV wave weaker strength, slower velocity, and the large amount of P wave energy generated by the SV source.

The results of this section indicate a good correlation between the theoretical transversely isotropic model and the observed P wave velocity surfaces. The poor correlation between the Shear wave velocity surfaces of the model and the observed is probably due to unreliable Shear arrivals interpreted from the survey and differences between the theoretical model material and the material within the study area.

The P waves appear to be the most reliable of the three wave types due to the strong P wave arrivals observed in the survey and the good correlation of observed and theoretical velocity surfaces. Therefore, based on the P wave analysis, the near surface layers within the study area are consistent with a homogeneous transversely isotropic material that has a north-south, horizontally oriented axis of symmetry. This transverse isotropy is probably due to the north-south oriented ridges of hard sastrugi interlayered with snow in this area.

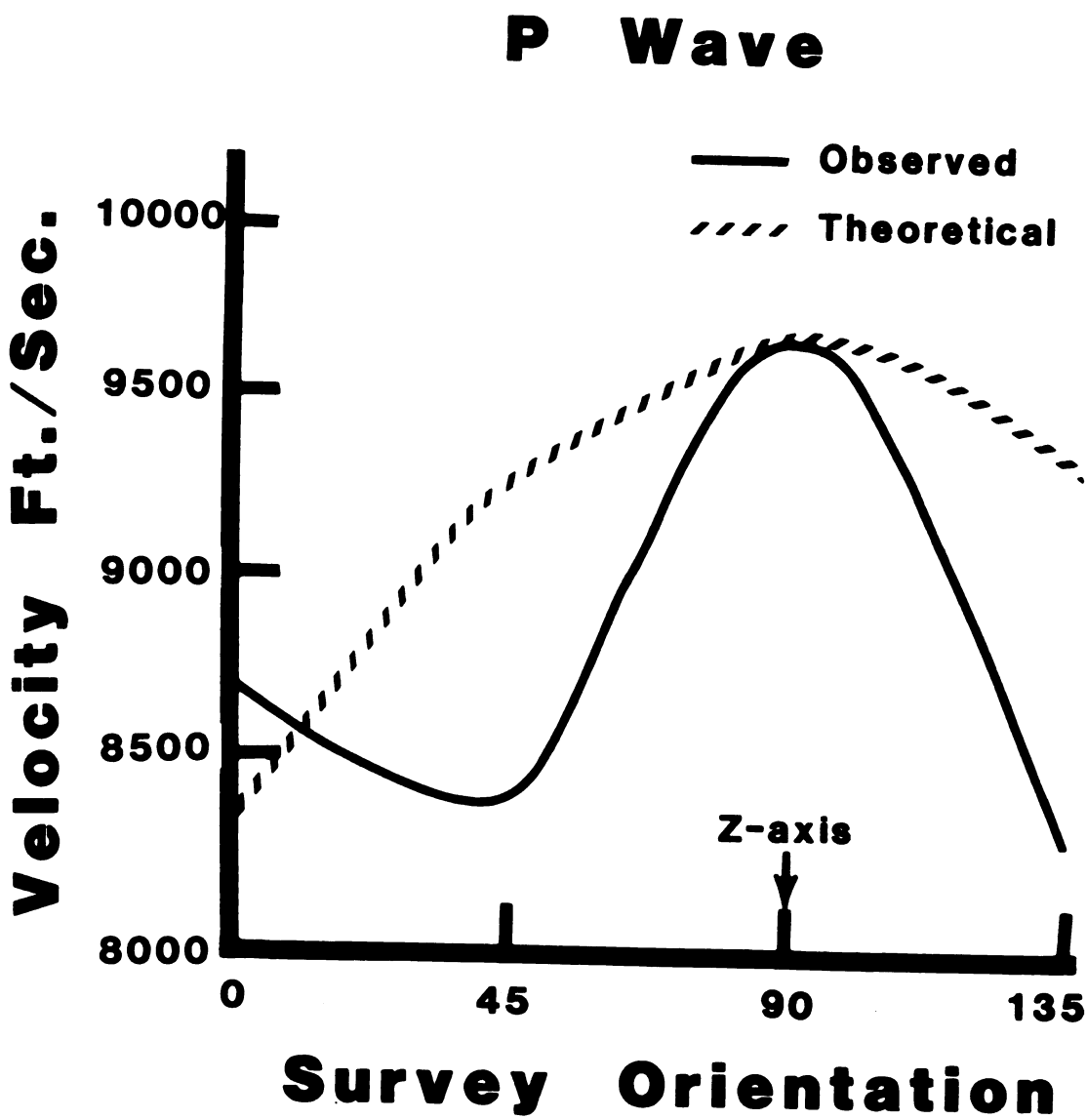


FIGURE 47: Velocity surfaces for P waves.

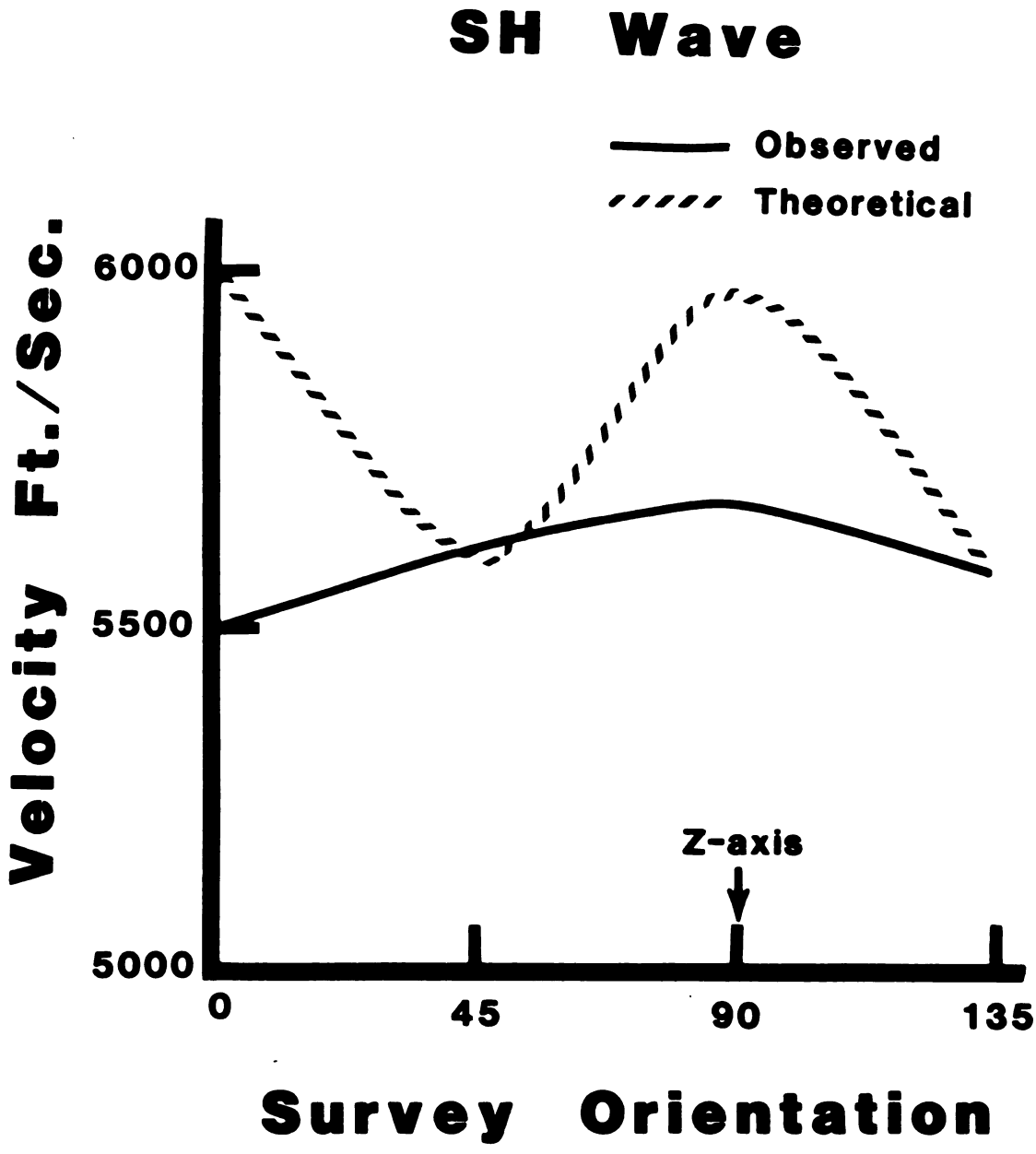


FIGURE 48: Velocity surfaces for SH waves.

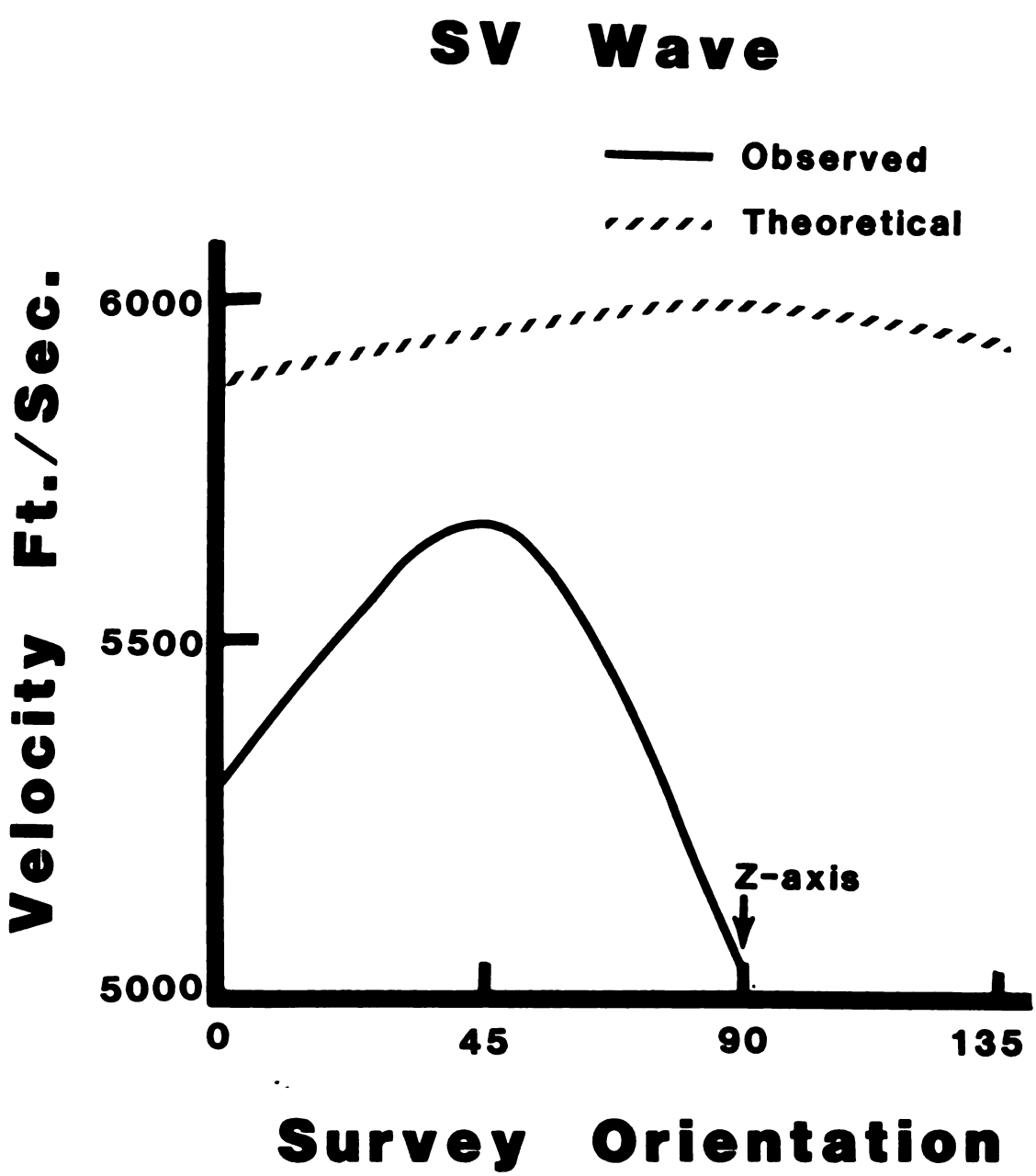


FIGURE 49: Velocity surfaces for SV waves.

# Chapter 8

# CONCLUSIONS

Velocity anisotropy in the surface layers of the study area is observed for P, SH, and SV waves. The development of patterns in the velocity surfaces with increasing depth is the best indicator of this anisotropy. The correlation between velocity surfaces and energy radiation patterns further supports the presence of anisotropy as opposed to directional heterogeneity.

The anisotropy of the surface layers in the study area differs from the anisotropy observed by others in the deeper zones of the ice shelf (Bennett et al., 1979). The surface layers exhibit strong P wave velocity anisotropy of 15.6% . The deeper zones, which are believed to be anisotropic due to crystal orientation, exhibit a small variation in P wave velocity with no pattern being apparent. Also, maximum P wave velocity anisotropy is 7% for a single ice crystal (Bennett, 1968). Therefore, the observed anisotropy of the surface layers in the study area is not due to crystal orientation but is probably structurally related.

A theoretical model composed of alternating prisms of two elastically different, but isotropic materials, is

developed to test the idea that the observed anisotropy is structural in origin. The model is based on the presence of abundant ridges of hard sastrugi oriented north-south, alternating with softer snow or hoarefrost between the ridges in the study area. The model is shown to be transversely isotropic and velocity surfaces for the model are determined. The good correlation between the observed and the theoretical P wave velocity surfaces indicate that the surface layers in the study area behave as a homogeneous, transversely isotropic material, in so far as elastic waves are concerned.

A 360 degree survey is needed to definitely conclude that the complete centrosymmetry associated with transverse isotropy is present. However, within the limits of this study it is concluded that the surface layers are probably transversely isotropic with a horizontally oriented, north-south axis of symmetry. This anisotropy appears to be structurally related to the oriented sastrugi interlayered with snow in the study area. The axis of symmetry for the transverse isotropic surface layers is parallel to the north-south major axis of the sastrugi.

# RECOMMENDATIONS

The first recommendation for any seismic survey that is conducted for the purpose of detecting anisotropy is to do a complete 360 degree survey at a minimum of 45 degree intervals. This is necessary in order to demonstrate complete centrosymmetry of the seismic data, which is important in determining the presence and type of anisotropy. A certain degree of centrosymmetry may be demonstrated without the benefit of a 360 degree survey, as shown in this study.

More information and statistics on the exact orientation and dimensions of any observable surface features, such as the sastrugi in this study, would aid the study of structural anisotropy and theoretical modeling.

An analysis of dispersion of surface waves would also be useful in the study of anisotropy. Dispersion of surface waves has been demonstrated to occur in multilayered anisotropic media (Crampin, 1970). An attempt was made in this study to determine if dispersion of surface waves had occurred, but the results were inconclusive and are not presented.

# APPENDICES

# APPENDIX I

## Time - Distance Data

TABLE 1: P WAVE TIME-DISTANCE DATA

| X | 000° | 045° | 090° | 135° |
|---|---|---|---|---|
| 5 | 2.3 | 2.3 | - | 2.7 |
| 10 | 4.7 | 4.7 | 4.0 | 4.7 |
| 15 | 6.7 | 7.0 | 6.2 | 6.7 |
| 20 | 8.5 | 8.7 | 8.0 | 8.6 |
| 30 | 10.7 | 10.7 | 10.7 | 12.2 |
| 40 | 13.3 | 13.3 | 12.7 | 15.2 |
| 50 | 14.7 | 16.0 | 14.5 | 17.0 |
| 60 | 16.7 | 17.3 | 16.7 | 18.7 |
| 70 | 18.5 | 19.3 | 18.3 | 20.0 |
| 80 | 21.0 | 21.2 | 19.5 | 21.3 |
| 90 | 22.0 | 23.0 | - | 23.7 |
| 100 | 22.8 | 24.0 | 21.3 | 25.2 |

X= Distance from geophone to source in feet.

All arrival times are in milliseconds.

TABLE 2: SH (+) WAVE TIME-DISTANCE DATA

| X | 000° | 045° | 090° | 135° |
|---|---|---|---|---|
| 5 | 4.1 | 4.0 | 4.4 | 3.7 |
| 10 | 7.5 | 8.5 | 8.9 | 7.3 |
| 15 | 10.8 | 12.3 | 12.4 | 10.3 |
| 20 | 14.0 | 15.7 | 15.2 | 13.8 |
| 30 | 18.7 | 20.3 | 20.7 | 19.3 |
| 40 | 22.8 | 24.3 | 25.0 | 23.5 |
| 50 | 26.7 | 27.8 | 28.6 | 26.5 |
| 60 | 29.3 | 30.3 | 31.0 | 29.2 |
| 70 | 32.0 | 32.8 | 33.1 | 31.8 |
| 80 | 34.3 | 34.7 | 35.1 | 34.0 |
| 90 | 36.3 | 36.6 | 36.9 | 36.1 |
| 100 | 38.2 | 38.5 | 39.0 | 38.0 |

X= Distance from geophone to source in feet.

All arrival times in milliseconds.

TABLE 3: SH (-) WAVE TIME-DISTANCE DATA

| X | 000° | 045° | 090° | 135° |
|---|---|---|---|---|
| 5 | 4.1 | 4.0 | 4.5 | 5.0 |
| 10 | 7.8 | 8.1 | 8.7 | 8.7 |
| 15 | 11.0 | 11.9 | 11.2 | 12.3 |
| 20 | 14.4 | 15.0 | 14.7 | 15.0 |
| 30 | 19.3 | 19.9 | 19.5 | 20.5 |
| 40 | 23.3 | 24.1 | 23.7 | 24.3 |
| 50 | 26.8 | 27.0 | 26.8 | 27.2 |
| 60 | 29.5 | 29.7 | 29.6 | 29.7 |
| 70 | 32.0 | 32.1 | 32.0 | 32.2 |
| 80 | 34.3 | 34.7 | 33.8 | 34.5 |
| 90 | - | 37.0 | 35.8 | 36.7 |
| 100 | 38.6 | 39.2 | 38.0 | 39.3 |

X= Distance from geophone to source in feet.

All arrival times in milliseconds.

TABLE 4: SV (+) WAVE TIME-DISTANCE DATA

| X | 000° | 045° | 090° |
|---|---|---|---|
| 5 | - | 3.4 | - |
| 10 | 3.8 | 5.8 | 4.9 |
| 15 | 7.8 | 9.0 | 7.3 |
| 20 | 10.0 | 11.9 | 9.7 |
| 30 | 14.2 | 16.8 | 14.3 |
| 40 | 18.0 | 21.0 | 18.7 |
| 50 | 21.8 | 24.5 | 22.2 |
| 60 | 25.3 | 27.0 | 25.2 |
| 70 | 28.5 | 29.3 | 28.0 |
| 80 | 30.5 | 31.3 | 31.0 |
| 90 | 32.3 | 33.5 | 33.8 |
| 100 | 34.5 | 35.2 | 36.3 |

X= Distance from geophone to source in feet.

All arrival times are in milliseconds.

TABLE 5: SV (-) WAVE TIME-DISTANCE DATA

| X | 000° | 045° | 090° | 135° |
|---|---|---|---|---|
| 5 | 5.7 | 4.2 | 6.5 | 4.8 |
| 10 | 8.3 | 5.8 | 7.8 | 8.0 |
| 15 | 9.7 | 8.5 | 9.3 | 10.1 |
| 20 | 11.8 | 10.6 | 12.3 | 11.8 |
| 30 | 15.5 | 14.7 | 16.5 | 14.7 |
| 40 | 18.8 | 18.5 | 20.0 | 18.3 |
| 50 | 21.9 | 21.0 | 22.2 | 20.7 |
| 60 | 23.8 | 23.2 | 24.3 | 23.0 |
| 70 | 25.8 | 25.3 | 26.5 | 25.1 |
| 80 | 27.3 | 27.2 | 28.3 | 27.0 |
| 90 | 29.0 | 29.0 | 30.2 | 29.6 |
| 100 | 30.5 | 30.7 | 31.8 | 31.0 |

X= Distance from geophone to source in feet.

All arrival times are in milliseconds.

TABLE 6: SH WAVE AVERAGE TIME-DISTANCE DATA

| X | 000° | 045° | 090° | 135° |
|---|---|---|---|---|
| 5 | 4.1 | 4.0 | 4.5 | 4.4 |
| 10 | 7.7 | 8.3 | 8.8 | 8.0 |
| 15 | 10.9 | 12.1 | 11.8 | 11.3 |
| 20 | 14.2 | 15.4 | 15.0 | 14.4 |
| 30 | 19.0 | 20.1 | 20.1 | 19.9 |
| 40 | 23.1 | 24.2 | 24.4 | 23.9 |
| 50 | 26.8 | 27.4 | 27.7 | 26.9 |
| 60 | 29.4 | 30.0 | 30.3 | 29.5 |
| 70 | 32.0 | 32.5 | 32.6 | 32.0 |
| 80 | 34.3 | 34.7 | 34.5 | 34.3 |
| 90 | 36.3 | 36.8 | 36.4 | 36.4 |
| 100 | 38.4 | 38.9 | 38.5 | 38.7 |

X= Distance from geophone to source in feet.

All arrival times are in milliseconds.

## APPENDIX II

### Power and Log Curve Statistics

TABLE 7: POWER CURVE STATISTICS P WAVE 000°

| X | a | b | $R^2$ |
|---|---|---|---|
| 5-20 | .712658223 | .797354222 | .984870292 |
| 30 | 1.011783336 | .691214517 | .992823854 |
| 40 | 1.199506653 | .644657076 | .996988701 |
| 50 | 1.233088758 | .639791967 | .995602373 |
| 60 | 1.149851049 | .656722991 | .994593573 |
| 70-100 | 1.281259094 | .629824736 | .994372872 |

TABLE 8: POWER CURVE STATISTICS P WAVE 045°

| | | | |
|---|---|---|---|
| 5-20 | .689876559 | .815747246 | .985296078 |
| 30 | .979334980 | .709189401 | .991108293 |
| 40 | 1.188297463 | .656440282 | .996485635 |
| 50 | 1.196013120 | .655090162 | .995249457 |
| 60 | 1.062076762 | .684078129 | .995892901 |
| 70-100 | 1.258755148 | .643131813 | .994631391 |

TABLE 9: POWER CURVE STATISTICS P WAVE 090°

| | | | |
|---|---|---|---|
| 5-30 | .746936462 | .767617137 | .987256241 |
| 40 | .995869188 | .688309387 | .996525647 |
| 50 | 1.172715564 | .645253164 | .998295918 |
| 60-100 | 1.436387484 | .593654704 | .992437967 |

TABLE 10: POWER CURVE STATISTICS P WAVE 135°

| | | | |
|---|---|---|---|
| 5-20 | .726396056 | .819105900 | .998129476 |
| 30 | .805514795 | .783446468 | .992963874 |
| 40 | 1.007915978 | .717756238 | .986410030 |
| 50 | 1.330216395 | .643396038 | .980324647 |
| 60 | 1.820739529 | .567180729 | .990208766 |
| 70-100 | 2.024549775 | .5433894-1 | .990474957 |

X= Distance between source and geophones.

a & b = Regression coefficients.

$R^2$ = Correlation coefficient.

TABLE 11: POWER CURVE STATISTICS SH WAVE 000°

| X | a | b | $R^2$ |
|---|---|---|---|
| 5-15 | 1.040080752 | .863651901 | .998305050 |
| 20 | 1.263309265 | .794811213 | .996437059 |
| 30 | 1.515373996 | .738444498 | .996406864 |
| 40 | 1.932789965 | .669465463 | .997643294 |
| 50 | 2.366544972 | .615781125 | .996220868 |
| 60 | 2.907047418 | .564525791 | .996876421 |
| 70 | 3.498293293 | .520455886 | .999641907 |
| 80-100 | 3.516233967 | .519234005 | .999511874 |

TABLE 12: POWER CURVE STATISTICS SH WAVE 045°

| | | | |
|---|---|---|---|
| 5-15 | .973950078 | .911332580 | .991273923 |
| 20 | 1.485088538 | .765314577 | .992221286 |
| 30 | 1.995824241 | .674606861 | .996004819 |
| 40 | 2.490912424 | .611863081 | .997356949 |
| 50 | 2.989057248 | .563726895 | .996778930 |
| 60 | 3.586696353 | .518549391 | .999432078 |
| 70 | 3.833369882 | .502751000 | .999932560 |
| 80-100 | 3.784978876 | .505751052 | .999870096 |

TABLE 13: POWER CURVE STATISTICS SH WAVE 090°

| | | | |
|---|---|---|---|
| 5-15 | 1.225097718 | .832802738 | .995505323 |
| 20 | 1.597794738 | .742100733 | .999135394 |
| 30 | 1.763547685 | .709704960 | .996686839 |
| 40 | 2.211081150 | .644948668 | .995144391 |
| 50 | 2.946752681 | .569072671 | .994078255 |
| 60 | 3.897517586 | .499402298 | .997047718 |
| 70 | 4.540336680 | .463053129 | .999216924 |
| 80-100 | 4.564106730 | .462235607 | .998840311 |

TABLE 14: POWER CURVE STATISTICS SH WAVE 135°

| | | | |
|---|---|---|---|
| 5-15 | 1.138262110 | .844763092 | .999753417 |
| 20 | 1.301622797 | .796082269 | .997710551 |
| 30 | 1.616119436 | .727205894 | .993669473 |
| 40 | 2.106242804 | .651320992 | .990070315 |
| 50 | 3.037058964 | .555825081 | .997352223 |
| 60 | 3.509250342 | .520239314 | .999952278 |
| 70 | 3.565922667 | .516393423 | .999942652 |
| 80-100 | 3.404684512 | .527256048 | .999620029 |

TABLE 15: POWER CURVE STATISTICS SV(+) WAVE 000°

| X | a | b | $\hat{R^2}$ |
|---|---|---|---|
| 5-30 | .460861991 | .994278730 | .974229731 |
| 40 | .798837799 | .843760509 | .999823712 |
| 50 | .876409966 | .817656683 | .998043451 |
| 60 | 1.078491297 | .764171024 | .992985117 |
| 70-100 | 1.382063464 | .704083341 | .988383503 |

TABLE 16: POWER CURVE STATISTICS SV(+) WAVE 045°

| | | | |
|---|---|---|---|
| 5-20 | .814808913 | .880476561 | .997002185 |
| 30 | .868452080 | .856143933 | .991429114 |
| 40 | 1.179581001 | .768727709 | .991464101 |
| 50 | 1.548789999 | .695881721 | .989182077 |
| 60 | 2.137442271 | .615581921 | .991657550 |
| 70-100 | 2.756820081 | .555007438 | .996636592 |

TABLE 17: POWER CURVE STATISTICS SV(+) WAVE 090°

| | | | |
|---|---|---|---|
| 5-30 | .598390527 | .924542718 | .997837064 |
| 40 | .697135078 | .879619990 | .995758820 |
| 50 | .836255583 | .830970787 | .994660246 |
| 60 | 1.079754449 | .767542008 | .996693518 |
| 70-100 | 1.310712735 | .721691888 | .999728532 |

TABLE 18: POWER CURVE STATISTICS SV(-) WAVE 000°

| X | a | b | $R^2$ |
|---|---|---|---|
| 5-20 | 2.129022074 | .585340323 | .992332190 |
| 30 | 1.902081804 | .618396897 | .994010621 |
| 40 | 1.720469959 | .643677013 | .997535282 |
| 50 | 1.933684555 | .611474131 | .994096163 |
| 60 | 2.341073455 | .563336004 | .991851930 |
| 70-100 | 2.876030866 | .514340791 | .994590001 |

TABLE 19: POWER CURVE STATISTICS SV(-) WAVE 045°

| | | | |
|---|---|---|---|
| 5-20 | 1.188614370 | .734045743 | .990758806 |
| 30 | 1.017472349 | .776174814 | .994949335 |
| 40 | 1.249567627 | .717259518 | .994270958 |
| 50 | 1.467062562 | .673821668 | .990737815 |
| 60 | 1.946985449 | .603385750 | .993427184 |
| 70-100 | 2.416871293 | .552303596 | .999932805 |

TABLE 20: POWER CURVE STATISTICS SV(-) WAVE 090°

| | | | |
|---|---|---|---|
| 5-20 | 2.252072751 | .576283925 | .962363632 |
| 30 | 1.636623809 | .668098344 | .991174987 |
| 40 | 1.638277683 | .664740546 | .986548134 |
| 50 | 2.167616655 | .591402449 | .992173907 |
| 60 | 2.696399042 | .537577845 | .997063093 |
| 70-100 | 3.013743094 | .511415315 | .999348339 |

TABLE 21: POWER CURVE STATISTICS SV(-) WAVE 135°

| | | | |
|---|---|---|---|
| 5-20 | 1.829572645 | .622032044 | .996800897 |
| 30 | 2.015753177 | .593585864 | .998223062 |
| 40 | 1.958580770 | .601161944 | .998083070 |
| 50 | 1.913338347 | .606422061 | .997741374 |
| 60 | 1.854370764 | .614453368 | .996451077 |
| 70-100 | 2.128746617 | .581849339 | .998442715 |

TABLE 22: LOG CURVE STATISTICS P WAVES

| EVENT | a | b | c | $R^2$ |
|---|---|---|---|---|
| P 000° | -60.19555771 | 16.93815095 | 36 | .9968273832 |
| P 045° | -66.04290443 | 18.27424715 | 38 | .9977331136 |
| P 090° | -36.24888239 | 12.11525068 | 18 | .9984717190 |
| P 135° | -50.64644613 | 15,62046596 | 25 | .9972357891 |

TABLE 23: LOG CURVE STATISTICS SH WAVES

| | | | | |
|---|---|---|---|---|
| SH 000° | -69.18200250 | 22.43262792 | 21 | .999786073 |
| SH 045° | -52.98719266 | 19.33007445 | 14 | .999808036 |
| SH 090° | -54.10215801 | 19.50654268 | 15 | .999504995 |
| SH 135° | -61.66946683 | 20.97148297 | 18 | .999401828 |

TABLE 24: LOG CURVE STATISTICS SV WAVES

| | | | | |
|---|---|---|---|---|
| SV(+) 000° | -95.52275447 | 26.66818215 | 32 | .998501353 |
| SV(+) 045° | -70.99645479 | 22.12059965 | 23 | .998789422 |
| SV(+) 090° | -152.37948543 | 37.24211816 | 58 | .999694795 |
| SV(-) 000° | -66.20504628 | 19.85069509 | 32 | .998465210 |
| SV(-) 045° | -70.14081758 | 20.73168646 | 30 | .998598657 |
| SV(-) 090° | -72.42353287 | 21.30139303 | 34 | .996483254 |
| SV(-) 135° | -88.58476191 | 24.00830956 | 45 | .998622312 |

a & b = Regression coefficients.

c= Constant.

$R^2$= Correlation coefficient.

## APPENDIX III

### Velocities and WHB Depths

TABLE 25: VELOCITIES AND WHB DEPTHS P WAVE 000°

| X | V(ft/sec) | V(m/sec) | D(ft) | D(m) |
|---|---|---|---|---|
| 5 | 2421 | 738 | 0.8 | 0.25 |
| 10 | 2716 | 828 | 1.9 | 0.59 |
| 15 | 3011 | 918 | 3.2 | 0.98 |
| 20 | 3306 | 1007 | 4.7 | 1.42 |
| 30 | 3897 | 1187 | 7.8 | 2.38 |
| 40 | 4487 | 1367 | 11.3 | 3.43 |
| 50 | 5077 | 1547 | 14.9 | 4.54 |
| 60 | 5668 | 1727 | 18.7 | 5.70 |
| 70 | 6258 | 1907 | 22.6 | 6.90 |
| 80 | 6848 | 2087 | 26.7 | 8.13 |
| 90 | 7439 | 2267 | 30.8 | 9.38 |
| 100 | 8029 | 2447 | 35.0 | 10.65 |

TABLE 26: VELOCITIES AND WHB DEPTHS P WAVE 045°

| | | | | |
|---|---|---|---|---|
| 5 | 2353 | 717 | 0.8 | 0.25 |
| 10 | 2627 | 800 | 1.9 | 0.58 |
| 15 | 2900 | 884 | 3.2 | 0.96 |
| 20 | 3174 | 967 | 4.6 | 1.39 |
| 30 | 3721 | 1134 | 7.7 | 2.33 |
| 40 | 4268 | 1301 | 11.1 | 3.37 |
| 50 | 4816 | 1467 | 14.7 | 4.46 |
| 60 | 5363 | 1634 | 18.4 | 5.61 |
| 70 | 5910 | 1801 | 22.3 | 6.79 |
| 80 | 6457 | 1968 | 26.3 | 8.01 |
| 90 | 7004 | 2134 | 30.4 | 9.25 |
| 100 | 7552 | 2301 | 34.5 | 10.51 |

X= Distance from source to geophones in feet.

V= Velocity at distance X in feet/sec. and meters/sec.

D= Depth of penetration.

TABLE 27: VELOCITIES AND WHB DEPTHS P WAVE 090°

| X | V(ft/sec) | V(m/sec) | D(ft) | D(m) |
|---|---|---|---|---|
| 5 | 1898 | 579 | 1.2 | 0.35 |
| 10 | 2311 | 704 | 2.6 | 0.80 |
| 15 | 2724 | 830 | 4.3 | 1.31 |
| 20 | 3137 | 956 | 6.1 | 1.86 |
| 30 | 3962 | 1207 | 9.9 | 3.03 |
| 40 | 4787 | 1459 | 14.0 | 4.27 |
| 50 | 5613 | 1710 | 18.2 | 5.55 |
| 60 | 6438 | 1962 | 22.6 | 6.87 |
| 70 | 7264 | 2213 | 27.0 | 8.22 |
| 80 | 8089 | 2465 | 31.4 | 9.58 |
| 90 | 8914 | 2717 | 36.0 | 10.96 |
| 100 | 9740 | 2968 | 40.5 | 12.35 |

TABLE 28: VELOCITIES AND WHB DEPTHS P WAVE 135°

| | | | | |
|---|---|---|---|---|
| 5 | 1921 | 585 | 1.0 | 0.30 |
| 10 | 2241 | 683 | 2.3 | 0.70 |
| 15 | 2561 | 780 | 3.8 | 1.15 |
| 20 | 2881 | 878 | 5.4 | 1.64 |
| 30 | 3521 | 1073 | 8.9 | 2.72 |
| 40 | 4161 | 1268 | 12.7 | 3.87 |
| 50 | 4801 | 1463 | 16.7 | 5.08 |
| 60 | 5442 | 1658 | 20.8 | 6.33 |
| 70 | 6082 | 1853 | 25.0 | 7.61 |
| 80 | 6722 | 2048 | 29.3 | 8.91 |
| 90 | 7362 | 2243 | 33.6 | 10.24 |
| 100 | 8002 | 2438 | 38.0 | 11.58 |

X= Distance from source to geophones in feet.

V= Velocity at distance X in feet/sec. and meters/sec.

D= Depth of penetration.

TABLE 29: VELOCITIES AND WHB DEPTHS SH WAVE 000°

| X | V(ft/sec) | V(m/sec) | D(ft) | D(m) |
|---|---|---|---|---|
| 5 | 1159 | 353 | 1.1 | 0.34 |
| 10 | 1382 | 421 | 2.5 | 0.75 |
| 15 | 1605 | 489 | 4.1 | 1.25 |
| 20 | 1828 | 557 | 5.8 | 1.77 |
| 30 | 2274 | 693 | 9.5 | 2.89 |
| 40 | 2719 | 829 | 13.4 | 4.08 |
| 50 | 3105 | 946 | 17.0 | 5.18 |
| 60 | 3611 | 1100 | 21.8 | 6.64 |
| 70 | 4057 | 1236 | 26.1 | 7.95 |
| 80 | 4502 | 1372 | 30.5 | 9.29 |
| 90 | 4948 | 1508 | 34.9 | 10.64 |
| 100 | 5394 | 1644 | 39.4 | 12.01 |

TABLE 30: VELOCITIES AND WHB DEPTHS SH WAVE 045°

| | | | | |
|---|---|---|---|---|
| 5 | 983 | 300 | 1.3 | 0.40 |
| 10 | 1242 | 378 | 2.9 | 0.88 |
| 15 | 1500 | 457 | 4.7 | 1.43 |
| 20 | 1759 | 536 | 6.7 | 2.04 |
| 30 | 2276 | 694 | 10.7 | 3.26 |
| 40 | 2794 | 851 | 15.0 | 4.57 |
| 50 | 3311 | 1009 | 19.4 | 5.91 |
| 60 | 3828 | 1167 | 23.8 | 7.25 |
| 70 | 4346 | 1324 | 28.4 | 8.65 |
| 80 | 4863 | 1482 | 33.0 | 10.06 |
| 90 | 5380 | 1639 | 37.6 | 11.46 |
| 100 | 5898 | 1797 | 42.3 | 12.89 |

X= Distance from source to geophones in feet.

V= Velocity at distance X in feet/sec. and meters/sec.

D= Depth of penetration in feet and meters.

TABLE 31: VELOCITIES AND WHB DEPTHS SH WAVE 090°

| X | V(ft/sec) | V(m/sec) | D(ft) | D(m) |
|---|---|---|---|---|
| 5 | 1025 | 312 | 1.3 | 0.40 |
| 10 | 1282 | 391 | 2.9 | 0.88 |
| 15 | 1538 | 469 | 4.6 | 1.40 |
| 20 | 1794 | 547 | 6.5 | 1.98 |
| 30 | 2307 | 703 | 10.5 | 3.20 |
| 40 | 2820 | 859 | 14.7 | 4.48 |
| 50 | 3332 | 1015 | 19.1 | 5.82 |
| 60 | 3845 | 1172 | 23.5 | 7.16 |
| 70 | 4358 | 1328 | 28.0 | 8.53 |
| 80 | 4870 | 1484 | 32.6 | 9.93 |
| 90 | 5383 | 1640 | 37.2 | 11.34 |
| 100 | 5896 | 1797 | 41.8 | 12.74 |

TABLE 32: VELOCITIES AND WHB DEPTHS SH WAVE 135°

| | | | | |
|---|---|---|---|---|
| 5 | 1097 | 334 | 1.2 | 0.37 |
| 10 | 1335 | 407 | 2.6 | 0.79 |
| 15 | 1574 | 480 | 4.3 | 1.31 |
| 20 | 1812 | 552 | 6.1 | 1.86 |
| 30 | 2289 | 698 | 9.3 | 2.83 |
| 40 | 2766 | 843 | 14.0 | 4.27 |
| 50 | 3243 | 988 | 18.2 | 5.55 |
| 60 | 3719 | 1133 | 22.6 | 6.89 |
| 70 | 4196 | 1279 | 27.0 | 8.23 |
| 80 | 4673 | 1424 | 31.4 | 9.58 |
| 90 | 5150 | 1569 | 36.0 | 10.97 |
| 100 | 5627 | 1715 | 40.5 | 12.34 |

X= Distance from source to geophones in feet.

V= Velocity at distance X in feet/sec. and meters/sec.

D= Depth of penetration in feet and meters.

TABLE 33: VELOCITIES AND WHB DEPTHS SV(+) WAVE 000°

| X | V(ft/sec) | V(m/sec) | D(ft) | D(m) |
|---|---|---|---|---|
| 5 | 1387 | 423 | 0.8 | 0.27 |
| 10 | 1575 | 480 | 2.1 | 0.62 |
| 15 | 1762 | 537 | 3.4 | 1.04 |
| 20 | 1950 | 594 | 4.9 | 1.49 |
| 30 | 2325 | 709 | 8.2 | 2.49 |
| 40 | 2700 | 823 | 11.7 | 3.57 |
| 50 | 3075 | 937 | 15.5 | 4.72 |
| 60 | 3450 | 1051 | 19.4 | 5.91 |
| 70 | 3825 | 1166 | 23.4 | 7.13 |
| 80 | 4200 | 1280 | 27.5 | 8.39 |
| 90 | 4575 | 1394 | 31.7 | 9.66 |
| 100 | 4950 | 1508 | 33.8 | 10.31 |

TABLE 34: VELOCITIES AND WHB DEPTHS SV(+) WAVE 045°

| | | | | |
|---|---|---|---|---|
| 5 | 1266 | 386 | 1.0 | 0.31 |
| 10 | 1492 | 455 | 2.4 | 0.72 |
| 15 | 1718 | 524 | 3.9 | 1.19 |
| 20 | 1944 | 592 | 5.6 | 1.70 |
| 30 | 2396 | 730 | 9.2 | 2.80 |
| 40 | 2848 | 868 | 13.0 | 3.97 |
| 50 | 3300 | 1006 | 17.1 | 5.20 |
| 60 | 3752 | 1143 | 21.2 | 6.47 |
| 70 | 4204 | 1281 | 25.5 | 7.77 |
| 80 | 4656 | 1419 | 29.8 | 9.09 |
| 90 | 5108 | 1557 | 34.2 | 10.43 |
| 100 | 5560 | 1694 | 38.7 | 11.78 |

TABLE 35: VELOCITIES AND WHB DEPTHS SV(+) WAVE 090°

| | | | | |
|---|---|---|---|---|
| 5 | 1692 | 516 | 0.7 | 0.20 |
| 10 | 1826 | 556 | 1.6 | 0.46 |
| 15 | 1966 | 599 | 2.6 | 0.80 |
| 20 | 2094 | 638 | 3.8 | 1.16 |
| 30 | 2363 | 720 | 6.5 | 1.97 |
| 40 | 2631 | 802 | 9.4 | 2.88 |
| 50 | 2900 | 884 | 12.6 | 3.85 |
| 60 | 3169 | 966 | 16.0 | 4.88 |
| 70 | 3437 | 1047 | 19.5 | 5.95 |
| 80 | 3706 | 1129 | 23.2 | 7.05 |
| 90 | 3974 | 1211 | 26.9 | 8.19 |
| 100 | 4243 | 1293 | 30.7 | 9.36 |

X= Distance from source to geophones in feet.

V= Velocity at distance X in feet/sec. and meters/sec.

D= Depth of penetration in feet and meters.

TABLE 36: VELOCITIES AND WHB DEPTHS SV(-) WAVE 000°

| X | V(ft/sec) | V(m/sec) | D(ft) | D(m) |
|---|---|---|---|---|
| 5 | 1864 | 568 | 0.9 | 0.27 |
| 10 | 2116 | 645 | 2.1 | 0.62 |
| 15 | 2368 | 722 | 3.4 | 1.04 |
| 20 | 2620 | 798 | 4.9 | 1.49 |
| 30 | 3123 | 952 | 8.2 | 2.49 |
| 40 | 3627 | 1105 | 11.7 | 3.57 |
| 50 | 4131 | 1259 | 15.5 | 4.72 |
| 60 | 4635 | 1412 | 19.4 | 5.91 |
| 70 | 5138 | 1566 | 23.4 | 7.13 |
| 80 | 5642 | 1719 | 27.5 | 8.39 |
| 90 | 6146 | 1873 | 31.7 | 9.66 |
| 100 | 6650 | 2026 | 36.0 | 10.96 |

TABLE 37: VELOCITIES AND WHB DEPTHS SV(-) WAVES 045°

| | | | | |
|---|---|---|---|---|
| 5 | 1688 | 514 | 0.9 | 0.28 |
| 10 | 1929 | 588 | 2.1 | 0.64 |
| 15 | 2171 | 662 | 3.5 | 1.07 |
| 20 | 2412 | 735 | 5.0 | 1.53 |
| 30 | 2894 | 882 | 8.4 | 2.55 |
| 40 | 3377 | 1029 | 12.0 | 3.65 |
| 50 | 3859 | 1176 | 15.8 | 4.81 |
| 60 | 4341 | 1323 | 19.8 | 6.02 |
| 70 | 4824 | 1470 | 23.8 | 7.26 |
| 80 | 5306 | 1617 | 28.0 | 8.53 |
| 90 | 5788 | 1764 | 32.2 | 9.82 |
| 100 | 6271 | 1911 | 36.5 | 11.13 |

X= Distance from source to geophones in feet.

V= Velocity at distance X in feet/sec. and meters/sec.

D= Depth of penetration in feet and meters.

TABLE 38: VELOCITIES AND WHB DEPTHS SV(-) WAVE 090°

| X | V(ft/sec) | V(m/sec) | D(ft) | D(m) |
|---|---|---|---|---|
| 5 | 1831 | 558 | 0.9 | 0.26 |
| 10 | 2066 | 630 | 2.0 | 0.61 |
| 15 | 2300 | 701 | 3.3 | 1.01 |
| 20 | 2535 | 773 | 4.8 | 1.45 |
| 30 | 3005 | 916 | 8.0 | 2.43 |
| 40 | 3474 | 1059 | 11.5 | 3.50 |
| 50 | 3943 | 1202 | 15.2 | 4.63 |
| 60 | 4413 | 1345 | 19.0 | 5.80 |
| 70 | 4882 | 1488 | 23.0 | 7.01 |
| 80 | 5352 | 1631 | 27.1 | 8.25 |
| 90 | 5821 | 1774 | 31.2 | 9.52 |
| 100 | 6291 | 1917 | 35.5 | 10.80 |

TABLE 39: VELOCITIES AND WHB DEPTHS SV(-) WAVE 135°

| | | | | |
|---|---|---|---|---|
| 5 | 2083 | 635 | 0.7 | 0.23 |
| 10 | 2291 | 698 | 1.8 | 0.53 |
| 15 | 2499 | 762 | 2.9 | 0.89 |
| 20 | 2707 | 825 | 4.2 | 1.29 |
| 30 | 3124 | 952 | 7.2 | 2.18 |
| 40 | 3540 | 1097 | 10.4 | 3.17 |
| 50 | 3957 | 1206 | 13.8 | 4.21 |
| 60 | 4374 | 1333 | 17.4 | 5.31 |
| 70 | 4790 | 1460 | 21.2 | 6.45 |
| 80 | 5207 | 1587 | 25.0 | 7.63 |
| 90 | 5623 | 1622 | 29.0 | 8.83 |
| 100 | 6040 | 1841 | 33.0 | 10.06 |

X= Distance from source to geophones in feet.

V= Velocity at distance X in feet/sec. and meters/sec.

D= Depth of penetration in feet and meters.

# APPENDIX IV

## Log of Energy Radiation Values

TABLE 40: LOGS OF ENERGY RADIATION VALUES P WAVES

| X | 000° | 045° | 090° | 135° |
|---|---|---|---|---|
| 10 | 10.6987 | 11.0137 | 11.4508 | 11.5236 |
| 20 | 10.6196 | 10.3854 | 10.8729 | 10.4827 |
| 40 | 10.4710 | 9.5492 | 10.0200 | 10.0684 |
| 60 | 9.3871 | 8.9045 | 9.5863 | 9.5927 |
| 80 | 8.6906 | 8.4748 | 8.9586 | 8.8813 |
| 100 | 8.4865 | 9.0437 | 9.3887 | 9.2580 |

TABLE 41: LOGS OF ENERGY RADIATION VALUES SH WAVES

| | | | | |
|---|---|---|---|---|
| 10 | 12.6939 | 13.2402 | 13.2924 | 13.0981 |
| 20 | 12.4726 | 11.8509 | 12.8379 | NA |
| 40 | 12.1141 | 12.0334 | 12.4672 | 12.1049 |
| 60 | 10.1092 | 11.1936 | 10.8206 | 11.0021 |
| 80 | 9.5929 | 9.8939 | 10.0273 | 9.6636 |
| 100 | 9.2400 | 9.8849 | 9.7721 | 9.7081 |

X= Distance from source to geophones in feet.

# APPENDIX V

## Basic Program for Determining Model Velocities

```
100 'THIS PROGRAM WILL COMPUTE THE ELASTIC CONTSTANTS FOR TWO DIFFERENT ISOTROPIC MATERIALS.
110 'THE USER MUST INPUT ONE POISSON'S RATIO FOR THE MATERIALS, THE RATIO OF P WAVE VELOCITIES
120 'FOR THE MATERIALS, AND THE P WAVE VELOCITY OF THE FASTER OF THE TWO.
130 'THE PROGRAM WILL THEN DETERMINE THE ELASTIC CONSTANTS FOR A TRANSVERSELY ISOTROPIC MATERIAL
140 'COMPOSED OF ALTERNATING PARALLEL PRISMS OF THE TWO MATERIALS DEFINED.  VELOCITIES FOR
150 'P, SV, AND SH WAVES ARE THEN COMPUTED.  THE VELOCITIES ARE COMPUTED FOR WAVES TRAVELING
160 'AT VARYING AZIMUTH TO THE Z-AXIS OF THE TRANSVERSELY ISOTROPIC MATERIAL.  THEY ARE
170 'COMPUTED FROM 0 TO 135 DEGREES IN 5 DEGREE INCREMENTS.  MAXIMUM AND MINIMUMVELOCITIES FOR
180 'EACH TYPE OF WAVE ARE USED TO COMPUTE PERCENT ANISOTROPY.
190 CLS
200 PI=3.141593
210 INPUT "ENTER YOUR POISSON'S RATIO:",PO
220 INPUT "ENTER THE RATIO BETWEEN PWAVE VELOCITIES OF THE TWO DIFFERENT MATERIALS:",RAT
230 INPUT "ENTER THE PWAVE VELOCITY OF THE FASTER MATERIAL:",VP
240 R=SQR((2*(PO-1))/(2*PO-1))
250 VS=VP/R
260 VP1=VP/RAT
270 VS1=VP1/R
280 C11=VP^2
290 C44=VS^2
300 C12=VP^2-(2*(VS^2))
310 D11=VP1^2
320 D44=VS1^2
330 D12=VP1^2-(2*(VS1^2))
340 K33=(C11+D11)/2-(((D12-C12)^2)/(C11+D11+C12+D12))
350 K13=(C11*D12+2*C12*D12+D11*C12)/(C11+D11+C12+D12)
360 K12=K13
370 K21=K12
380 FK11=((C11*D11+C12*D12)*(C11+D11))/((C11+D11)^2-(C12+D12)^2)
390 SK11=((D11*C12+C11*D12)*(C12+D12))/((C11+D11)^2-(C12+D12)^2)
400 K11=2*(FK11-SK11)
410 FK12=((D11*C12+C11*D12)*(C11+D11))/((C11+D11)^2-(C12+D12)^2)
420 SK12=((C11*D11+C12*D12)*(C12+D12))/((C11+D11)^2-(C12+D12)^2)
430 K12=2*(FK23-SK23)
440 K31=K12
450 K32=K13
460 K44=(C44+D44)/2
470 K55=(2*C44*D44)/(C44+D44)
480 K66=(K11-K12)/2
490 CLS
500 PRINT "THIS IS A TABLE OF BODY WAVE VELOCITIES FOR THE FOLLOWING"
510 PRINT
520 PRINT "A TRANSVERSELY ISOTROPIC MATERIAL WITH"
```

## Basic Program Continued

```
530 PRINT "POISSON'S RATIO=",PO
540 PRINT "PWAVE VELOCITY RATIO BETWEEN MATERIALS=",RAT
550 PRINT "PWAVE VELOCITY OF MATERIAL ONE=",VP
560 PRINT "SHWAVE VELOCITY OF MATERIAL ONE=",VS
570 PRINT "PWAVE VELOCITY OF MATERIAL TWO= ",VP1
580 PRINT "SHWAVE VELOCITY OF MATERIAL TWO=",VS1
590 PRINT
600 PRINT
610 PRINT
620 PRINT "DEGREES","P VELOCITY","SH VELOCITY","SV VELOCITY"
630 PVELMAX=0
640 PVELMIN=100000!
650 SVVELMAX=0
660 SVVELMIN=100000!
670 SHVELMAX=0
680 SHVELMIN=100000!
690 FOR X=0 TO 135 STEP 5
700 Y=X*PI/180
710 W=(COS(Y)^2)
720 Z=(SIN(Y)^2)
730 VI1=((K11+K44)/2)*Z+((K33+K44)/2)*W
740 VI21=(((K11-K44)/2)*Z-(((K33-K44)/2)*W))^2
750 VI22=(K13+K44)^2*Z*W
760 VI2F=SQR(VI21+VI22)
770 PVEL=SQR(VI1+VI2F)
780 SHVEL=SQR(VI1-VI2F)
790 SVVEL=SQR(Z*K66+W*K44)
800 PRINT X,PVEL,SHVEL,SVVEL
810 IF PVEL>PVELMAX THEN PVELMAX=PVEL
820 IF PVEL<PVELMIN THEN PVELMIN=PVEL
830 IF SVVEL>SVVELMAX THEN SVVELMAX=SVVEL
840 IF SVVEL<SVVELMIN THEN SVVELMIN=SVVEL
850 IF SHVEL>SHVELMAX THEN SHVELMAX=SHVEL
860 IF SHVEL<SHVELMIN THEN SHVELMIN=SHVEL
870 NEXT
880 PANISO=100*(2*(PVELMAX-PVELMIN))/(PVELMAX+PVELMIN)
890 SVANISO=100*(2*(SVVELMAX-SVVELMIN))/(SVVELMAX+SVVELMIN)
900 SHANISO=100*(2*(SHVELMAX-SHVELMIN))/(SHVELMAX+SHVELMIN)
910 PRINT
920 PRINT
930 PRINT "WAVE TYPE","VEL MAX","VEL MIN","% ANISOTROPY"
940 PRINT
950 PRINT "P WAVE",PVELMAX,PVELMIN,PANISO
960 PRINT "SV WAVE",SVVELMAX,SVVELMIN,SVANISO
970 PRINT "SH WAVE",SHVELMAX,SHVELMIN,SHANISO
980 END
Ok
```

## APPENDIX VI

TABLE 42: VELOCITIES FROM ANISOTROPIC MODEL

| @ | P WAVE | SH WAVE | SV WAVE |
|---|---|---|---|
| 0 | 9741 | 6000 | 6000 |
| 5 | 9737 | 5989 | 5999 |
| 10 | 9727 | 5959 | 5997 |
| 15 | 9708 | 5910 | 5993 |
| 20 | 9679 | 5850 | 5988 |
| 25 | 9639 | 5782 | 5981 |
| 30 | 9585 | 5715 | 5974 |
| 35 | 9516 | 5654 | 5965 |
| 40 | 9431 | 5607 | 5956 |
| 45 | 9330 | 5579 | 5947 |
| 50 | 9214 | 5573 | 5938 |
| 55 | 9086 | 5592 | 5929 |
| 60 | 8948 | 5636 | 5920 |
| 65 | 8805 | 5699 | 5913 |
| 70 | 8664 | 5776 | 5906 |
| 75 | 8536 | 5858 | 5901 |
| 80 | 8430 | 5930 | 5897 |
| 85 | 8359 | 5982 | 5894 |
| 90 | 8334 | 6000 | 5893 |
| 95 | 8359 | 5982 | 5894 |
| 100 | 8430 | 5930 | 5897 |
| 105 | 8536 | 5858 | 5901 |
| 110 | 8664 | 5776 | 5906 |
| 115 | 8805 | 5699 | 5913 |
| 120 | 8948 | 5636 | 5920 |
| 125 | 9086 | 5592 | 5929 |
| 130 | 9214 | 5573 | 5938 |
| 135 | 9330 | 5579 | 5947 |

@ = Angle between direction of propagating wave and the Z-axis

All velocities are in feet/second.

# LIST OF REFERENCES

# LIST OF REFERENCES


Anderson, D.L., 1961. Elastic Wave Propagation in Layered Anisotropic Media: Journal of Geophysical Research, Vol.66, pp.2953-2963.

Backus, G.E., 1962. Long-wave Elastic Anisotropy Produced by Horizontal Layering: Journal of Geophysical Research, Vol.67, pp.4427-4440.

Bennett, H.F., 1968. An Investigation into Velocity Anisotropy through Measurements of Ultrasonic Wave Velocities in Snow and Ice Cores from Greenland and Antarctica: PH.D. Thesis, University of Wisconsin.

Bennett, H.F., Prather, B.W., Wanslow, J.B., Turpening, R.M., Adams, J., 1978. Seismic Velocity Anisotropy Measurements in a Rock (Ice) Undergoing Shear Metamorphism: EOS Transactions, American Geophysical Union, Abstracts Spring Meeting, 1978.

_____, _____, _____, _____, _____, 1979. Seismic Shear Wave Velocity Anisotropy in a Zone of High Shear Strain: Abstracts Seismological Society of America Spring Meeting,1979.

Bentley, C.R., 1972. Seismic Wave Velocities in Anisotropic Ice: A Comparison of Measured and Calculated Values in and around the Deep Drill Hole at Byrd Station: Journal of Geophysical Research, Vol.77, pp.4406-4420.

Berryman, J.G., 1979. Long-wave Anisotropy in Transversely Isotropic Media: Geophysics, Vol.44, pp.896-917.

Buchwald, V.T., 1959. Elastic Waves in Anisotropic Media: Proceedings of the Royal Society of London, A, Vol. 253, pp.563-580.

Cholet, J., Richard, H., 1954. A Test on Elastic Anisotropy Measurements at Berriane (North Sahara): Geophyscal Prospecting, Vol.2, pp.232-246.

Crampin, S., 1970. The Dispersion of Surface Waves in Multilayered Anisotropic Media: Geophysical Journal of the Royal Astronomical Society, Vol.21,pp.387-402.

_____, 1977. A Review of the Effects of Anisotropic Layering on the Propagation of Seismic Waves: Geophysical Journal of the Royal Astronomical Society, Vol.49, pp.9-27.

_____, 1978. Seismic Wave Propagation Through a Cracked Solid: Polarization as a Possible Dilatency Diagnostic: Geophysical Journal of the Royal Astronomical Society, Vol.53, pp.467-496.

Crampin, S., Bamford, D., 1977. Inversion of P-Wave Velocity Anisotropy: Geophysical Journal of the Royal Astronomical Society, Vol.49, pp.123-132.

Crary, A.P., Robinson, E.S., Bennett, H.F., Boyd, W.B., 1962. Glaciological Studies of the Ross Ice Shelf Antarctica,1957-1960: IGY Glaciological Report No.6.

_____, _____, _____, _____, 1962. Glaciological Regime of the Ross Ice Shelf: Journal of Geophysical Research, Vol.67,pp.2791-2806.

Daley, P.F., Hron, F., 1977. Reflection and Transmission Coefficients for Transversely Isotropic Media: Bulletin Seismological Society of America, Vol.67, pp.661-675.

_____, _____, 1979. Reflection and Transmission Coeefficients for Seismic Waves in Ellipsoidally Anisotropic Media: Geophysics, Vol.44, pp.27-38.

Dewart, G., 1968. Seismic Investigation of Ice Properties and Bedrock Topography at the Confluence of Two Glaciers, Kaskawulsh Glacier, Yukon Territory, Canada: Institute of Polar Studies, Report No.37, The Ohio State University.

Hagedoorn, J.G., 1954. A Practical Example of an Anisotropic Velocity Layer: Geophysical Prospecting, Vol.2, pp.52-60.

Jolly, R.N., 1956. Investigation of Shear Waves: Geophysics, Vol.21, pp.905-938.

Keith, C.M., Crampin, S., 1977. Seismic Body Waves in Anisotropic Media: Reflection and Refraction at a Plane Interface: Geophysical Journal of the Royal Astronomical Society, Vol.49, pp.181-208.

Krey, Th., Helbig, K., 1956. A Theorem Concerning Anisotropy of Stratified Media and it'Significance for Reflection Seismics: Geophysical Prospecting, Vol.4, pp.294-302.

Levin, F.K., 1978. The Reflection, Refraction, and Diffraction of Waves in Media with an Elliptical Velocity Dependence: Geophysics, Vol.43, pp.528-537.

_____, 1979. Seismic Velocities in Transversely Isotropic Media: Geophysics, Vol.44, pp.920-938.

Love, A.E.H., 1944. A Treatise on the Mathematical Theory of Elasticity: Dover Publications, New York.

Nur, A., 1971. Effects of Stress on Velocity Anisotropy in Rocks with Cracks: Journal of Geophysical Research, Vol.76, pp.2022-2034.

Nur, A., Simmons, C., 1969. Stress Induced Velocity Anisotropy in Rocks: An Experimental Study: Journal of Geophysical Research, Vol.74, pp.6667-6674.

Officer, C.B., 1958. Introduction to the Theory of Sound Transmission: McGraw Hill Book Company, Inc.

Postma, G.W., 1955. Wave Propagation in Stratified Media: Geophysics, Vol.20, pp.780-806.

Sato, R., Lapwood, E.R., 1968. Shear Waves in Transversely Isotropic Medium: Geophysical Journal of the Royal Astronomical Society, Vol.14, pp.463-470.

Slichter, L.B., 1932. The Theory of the Interpretation of Seismic Travel-time Curves in Horizontal Structures: Physics, Vol.3, pp.273-295.

Tillman, J., Bennett, H.F., 1973. Ultrasonic Shear Wave Birefringence as a Test of Homogeneous Elastic Anisotropy: Journal of Geophysical Research, Vol.78, No. 32, pp.7223-7229.

Uhrig, L.F., Van Melle, F.A., 1955. Velocity Anisotropy in Stratified Media: Geophysics, Vol.20, pp.774-779.

Wanslow, J., 1981. Seismic Compressional and Shear Wave Velocities in an Anisotropic Area of the Ross Ice Shelf, 18 Kilometers East of Minna Bluff, Antarctica: M.S. Thesis, Michigan State University.

## GENERAL REFERENCES


Bender, J.A., 1957. Air Permeability of Snow: U.S. Army Snow Ice and Permafrost Research Establishment, Corps of Engineers, Research Report No.37.

Brace, W.F., 1960. Orientation of Anisotropic Minerals in a Stress Field: Geological Society of America, Memoir 79, pp.9-20.

_____, 1965. Relation of Elastic Properties of Rocks tc Fabric: Journal of Geophysical Research, Vol.70, pp.5657-5667.

Dix, C.H., 1955. Seismic Velocities from Surface Measurements: Geophysics, Vol.20, pp.68-86.

Dobrin, M.B., 1976. Introduction to Geophysical Prospecting: Third Edition, McGraw Hill Book Company, Inc.

Ewing, W.M., Wencelas, S., Press, F., 1957. Elastic Waves in Layered Media: McGraw Hill Book Company, Inc.

Grant, F.C., and West, C.F., 1965. Interpretation Theory in Applied Geophysics: McGraw Hill Book Company, Inc.

Gutenburg, B., 1952. SV and SH: Transactions, American Geophysical Union, Vol.33, pp.573-584.

Helbig, K., 1964. Refraction Seismics with an Anisotropic Overburden: Geophysical Prospecting, Vol.12, pp.383-396.

Kohnen, H., Gow, A.J., 1979. Ultrasonic Investigations of Crystal Anisotropy in Deep Ice Cores from Antarctica: Journal of Geophysical Research, Vol.84,pp.4865-4874.

Musgrave, M.J.P., 1954. On the Propagation of Elastic Waves in Aeolotropic Media: Proceedings of the Royal Society of London, A, Vol.226, pp.339-366.

Prather, B.W., 1972. Seismic Anisotropy in the Vaughn Lewis Glaceir Juneau Icefield, Alaska, 1969: M.S. Thesis, Michigan State University.

Press, F., Ewing, W.M., 1951. Propagation of Elastic Waves in a Floating Ice Sheet: Transaction, American Geophysical Union, Vol.32, pp.673-678.

Ricker, N., 1953. The Form and Laws of Propagation of Seismic Wavelets: Geophysics, Vol.18, pp.10-40.

Sclue, J.W., 1977. A Physical Model for Surface Wave Azimuthal Anisotropy: Bulletin Seismological Society of America, Vol.67, pp.1515-1519.

Thiel, E., Ostenso, N., 1961. Seismic Studies on Antarctic Ice Shelves: Geophysics, Vol.26, pp.319-343.

Vlaar, N.J., 1968. Ray Theory for an Anisotropic Inhomogeneous Media: Bulletin Seismological Society of America, Vol.56, pp.527-559.